OECD DIVINE Element 1:
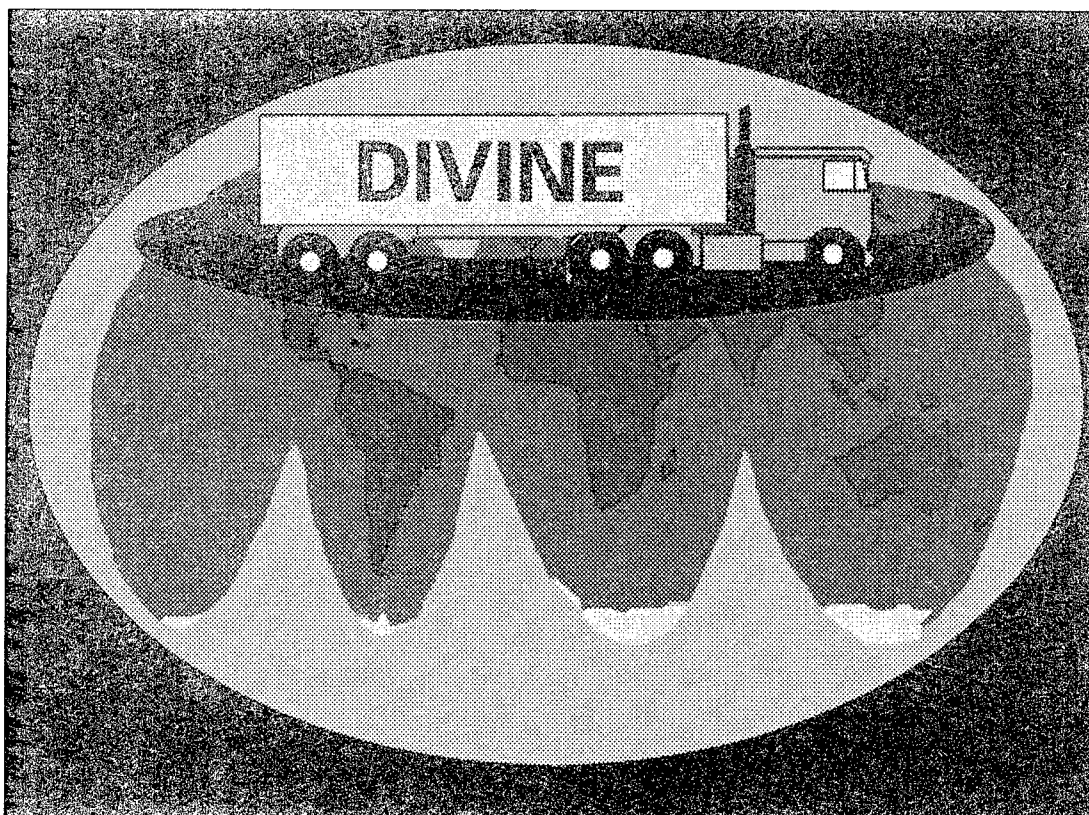
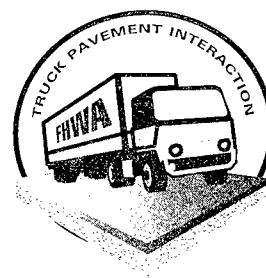# Accelerated Dynamic Pavement

Testing

PUBLICATION NO. FHWA-RD-97-138

SEPTEMBER 1998

U.S. Department of Transportation

Federal Highway Administration

Research and Development
Turner-Fairbank Highway Research Center
6300 Georgetown Pike
McLean, VA 22101-2296

FOREWORD

This report is one of the final reports prepared for the Organisation for Economic Co-operation and Development (OECD) Dynamic Interaction Vehicle-INfrastructure Experiment (DIVINE) project by the Federal Highway Administration, Office of Engineering Research and Development. This report describes Element 1—Accelerated Dynamic Pavement Testing—of the DIVINE project, which consists of the design of the experiment, testing method and data collection, results of the data analysis, and major findings and recommendations.

The findings in this report provide new and useful information to answer many questions regarding the nature and influence of different vehicle suspension-generated dynamic loading, pavement structural variability, and interactions between the vehicle and pavements.

Charles J. Nemmers, P.E.
Director, Office of Engineering
Research and Development

NOTICE

LIST OF TABLES

LIST OF FIGURES (Continued)

LIST OF FIGURES

TABLE OF CONTENTS

1. Report No. FHWA-RD-97-138	2. ⎪⎪⎪⎪⎪⎪⎪⎪⎪⎪⎪⎪⎪⎪ PB99-107401	3. Recipient's Catalog No.
4. Title and Subtitle OECD DIVINE ELEMENT 1: ACCELERATED DYNAMIC PAVEMENT TESTING		5. Report Date September 1998
		6. Performing Organization Code HNR-30
7. Author(s) William J. Kenis and Weijun Wang		8. Performing Organization Report No.
9. Performing Organization Name and Address Pavement Performance Division, HNR-30 Turner-Fairbank Highway Research Center 6300 Georgetown Pike McLean, Virginia 22101-2296		10. Work Unit No. (TRAIS) 3C4A
		11. Contract or Grant No.
12. Sponsoring Agency Name and Address Office of Engineering Research and Development Federal Highway Administration 6300 Georgetown Pike McLean, Virginia 22101-2296		13. Type of Report and Period Covered Final Report October 1994 - September 1997
		14. Sponsoring Agency Code

15. Supplementary Notes

16. Abstract

The loads that trucks impose on pavements and bridges have an important effect on the life of the infrastructure and, therefore, on total national road costs. The Organisation for Economic Co-operation and Development (OECD) Road Transport Research Programme has found that dynamic pavement loading is increasing in OECD countries, resulting in an increased rate of road wear. Although the importance of the relationship between the magnitude of dynamic loading and road wear is being recognized, many questions remain regarding the nature and influence of dynamic loading, and the interaction between the vehicle and pavements and bridges.

In an attempt to address some of these issues, the OECD Road Transport Research Programme launched a major 2-year study into the relationship between heavy vehicle dynamic loading and pavement and bridge wear, known as the Dynamic Interaction of the Vehicle and INfrastructure Experiment (DIVINE) project. The project consisted of the following six interrelated research projects:

Element 1: Accelerated Pavement Dynamic Testing
Element 2: Pavement Primary Response Testing
Element 3: Road Simulator Testing
Element 4: Computer Simulation of Heavy Vehicles
Element 5: Spatial Repeatability of Dynamic Loads
Element 6: Bridge Dynamic Loads

Element 1 of the DIVINE project is an accelerated pavement testing project undertaken at the Canterbury (New Zealand) Accelerated Pavement Testing Indoor Facility (CAPTIF) to determine the effect of the quality of two different suspensions -- airbag with shock absorber and multi-leaf steel spring suspensions, based on measurements of primary pavement response and the rates of damage progression in a flexible pavement subjected to accelerated loadings.

This report describes Element 1 of the program, which consists of the design of the experiment, testing method, method of data collection, results of the data analysis, and major findings and recommendations.

17. Key Words Accelerated pavement loading test, pavement performance, vehicle dynamic load, structural variability, OECD DIVINE project.	18. Distribution Statement No restrictions. This document is available to the public through the National Technical Information Service, Springfield, Virginia 22161.

19. Security Classif. (of this report) Unclassified	20. Security Classif. (of this page) Unclassified	21. No. of Pages 110	22. Price

Form DOT F 1700.7 (8-72)   Reproduction of completed page authorized

SI* (MODERN METRIC) CONVERSION FACTORS

APPROXIMATE CONVERSIONS TO SI UNITS

Symbol	When You Know	Multiply By	To Find	Symbol
LENGTH				
in	inches	25.4	millimeters	mm
ft	feet	0.305	meters	m
yd	yards	0.914	meters	m
mi	miles	1.61	kilometers	km
AREA				
in²	square inches	645.2	square millimeters	mm²
ft²	square feet	0.093	square meters	m²
yd²	square yards	0.836	square meters	m²
ac	acres	0.405	hectares	ha
mi²	square miles	2.59	square kilometers	km²
VOLUME				
fl oz	fluid ounces	29.57	milliliters	mL
gal	gallons	3.785	liters	L
ft³	cubic feet	0.028	cubic meters	m³
yd³	cubic yards	0.765	cubic meters	m³

NOTE: Volumes greater than 1000 l shall be shown in m³.

Symbol	When You Know	Multiply By	To Find	Symbol
MASS				
oz	ounces	28.35	grams	g
lb	pounds	0.454	kilograms	kg
T	short tons (2000 lb)	0.907	megagrams (or "metric ton")	Mg (or "t")
TEMPERATURE (exact)				
°F	Fahrenheit temperature	5(F-32)/9 or (F-32)/1.8	Celcius temperature	°C
ILLUMINATION				
fc	foot-candles	10.76	lux	lx
fl	foot-Lamberts	3.426	candela/m²	cd/m²
FORCE and PRESSURE or STRESS				
lbf	poundforce	4.45	newtons	N
lbf/in²	poundforce per square inch	6.89	kilopascals	kPa

APPROXIMATE CONVERSIONS FROM SI UNITS

Symbol	When You Know	Multiply By	To Find	Symbol
LENGTH				
mm	millimeters	0.039	inches	in
m	meters	3.28	feet	ft
m	meters	1.09	yards	yd
km	kilometers	0.621	miles	mi
AREA				
mm²	square millimeters	0.0016	square inches	in²
m²	square meters	10.764	square feet	ft²
m²	square meters	1.195	square yards	yd²
ha	hectares	2.47	acres	ac
km²	square kilometers	0.386	square miles	mi²
VOLUME				
mL	milliliters	0.034	fluid ounces	fl oz
L	liters	0.264	gallons	gal
m³	cubic meters	35.71	cubic feet	ft³
m³	cubic meters	1.307	cubic yards	yd³
MASS				
g	grams	0.035	ounces	oz
kg	kilograms	2.202	pounds	lb
Mg (or "t")	megagrams (or "metric ton")	1.103	short tons (2000 lb)	T
TEMPERATURE (exact)				
°C	Celcius temperature	1.8C + 32	Fahrenheit temperature	°F
ILLUMINATION				
lx	lux	0.0929	foot-candles	fc
cd/m²	candela/m²	0.2919	foot-Lamberts	fl
FORCE and PRESSURE or STRESS				
N	newtons	0.225	poundforce	lbf
kPa	kilopascals	0.145	poundforce per square inch	lbf/in²

* SI is the symbol for the International System of Units. Appropriate rounding should be made to comply with Section 4 of ASTM E380.

(Revised September 1993)

CHAPTER 1. BACKGROUND

1.1 INTRODUCTION

The loads that trucks impose on pavements and bridges have an important effect on the life of the infrastructure and, therefore, on total national road costs. There is also a worldwide emphasis on improving road freight productivity through the use of higher payloads, which have a large potential payoff through reductions in total vehicle operating costs and transport costs, which typically represent 10 percent of the Gross National Product in countries having advanced economies.

The pressure on existing and aging road systems is increasing. The Organisation for Economic Co-operation and Development (OECD) Road Transport Research has found that dynamic pavement loading is increasing in OECD countries, resulting in an increased rate of road wear. The importance of the relationship between the magnitude of dynamic loading and road wear is only just being recognized as a result of the increasing attention being paid to addressing the problems associated with infrastructure and vehicle operating costs brought about by:

- Increasing rate of traffic growth.
- Increasing rate of pavement deterioration.
- Vehicle innovations in axle configurations, suspensions, and tires.
- Increased economic pressures and the need to optimize available resources.

Although dynamic loading is the subject of increasing attention, many questions remain regarding the nature and influence of dynamic loading, and the interaction between the vehicle and pavements and bridges.

In an attempt to address some of these issues, the OECD's Road Transport Research Programme launched a major 2-year study into the relationship between heavy vehicle dynamic loading and pavement and bridge wear, known as the **D**ynamic Interaction of the **V**ehicle and **IN**frastructure **E**xperiment (DIVINE) Project. The objectives of DIVINE were to:

- Provide a means for identifying and assessing "road-friendly" vehicles.
- Quantify the improvements in road and bridge life possible through the use of "road-friendly" vehicles.
- Determine whether vehicle and suspension configurations that are "road-friendly" are also "bridge-friendly."

The DIVINE project involved more than 20 OECD member countries and included specialists in vehicles, pavements, bridges, road management, and transport policy.

The project consisted of the following six interrelated research projects:

Element 1: Accelerated Pavement Dynamic Testing
Element 2: Pavement Primary Response Testing
Element 3: Road Simulator Testing
Element 4: Computer Simulation of Heavy Vehicles

Element 5: Spatial Repeatability of Dynamic Loads
Element 6: Bridge Dynamic Loads

This report describes Element 1 of the program—the design of the experiment, testing method, method of data collection, results of the data analysis, and major findings and recommendations. The work was carried out by the University of Canterbury, New Zealand; Industrial Research Ltd. (IRL), New Zealand; Transport New Zealand; Australia Road Research Board and Transport Research (ARRBTR), Australia; and the Federal Highway Administration (FHWA), U.S.A. Several reports describing the various aspects of this study have been published by these organizations, and all details, figures, and tables of contents described in this DIVINE Element 1 report should be referenced to these specific reports (see references).

1.2 OBJECTIVE

Element 1 of the DIVINE programme is an accelerated pavement testing project undertaken at the Canterbury Accelerated Pavement Testing Indoor Facility (CAPTIF) to determine the effect of the quality of two different suspensions—airbag with shock absorber and multi-leaf steel spring suspensions, based on measurements of primary pavement response and the rates of damage progression in a flexible pavement subjected to accelerated loadings. The suspensions selected were to possess performance characteristics representing the extremes of the range likely to be encountered in practice.

The research was to involve the following four phases:

(1)   Application of known levels of accelerated dynamic loading to nominally identical instrumented flexible pavements using CAPTIF.

(2)   Collection of test data that include response of the pavement to load, structural condition, surface profile, and magnitude of applied dynamic load at various intervals during trafficking.

(3)   Determination of the extent to which the initial condition of the pavement, its deterioration over time, and the extent to which dynamic loads associated with different types of suspension affect the life of road pavements.

(4)   Evaluation of the results in terms of current pavement design and analysis procedures.

CHAPTER 2. DESIGN OF THE EXPERIMENT

This chapter summarizes the overall design of the Element 1 experiment. Topics discussed include: selection of test facility, design of test pavement, the traffic loading programme, and the measurement programme.

2.1 SELECTION OF THE TEST FACILITY

Accelerated pavement tests are conducted to compare the performance of different pavements or pavement materials under controlled conditions. The tests are usually run until there is sufficient cracking, rutting, or other deterioration of the pavement according to the criteria specified for the experiment. In the case of Element 1, other particular requirements needed to be satisfied, namely that the accelerated loading facility required the ability to simultaneously test two different suspensions that operate on identical test pavements and under identical environmental conditions.

A variety of different accelerated facilities throughout OECD member countries were evaluated in terms of their potential to serve this research objective. In general, it was found that all accelerated facilities evaluated were designed mainly for studying pavement behavior under one given suspension type that is designed to keep dynamic loadings as small as possible. Only one of those examined was able to simulate the loading of real vehicles with the ability of loading pavements through different suspension types. This testing facility was the Canterbury Accelerated Pavement Testing Indoor Facility (CAPTIF) located in Christchurch, New Zealand.

CAPTIF is housed in a hexagon-shaped building that is 26 m wide and 6 m high. An annular concrete tank of 4 m wide and 1.5 m deep confines the bottom and sides of the track. The track has a median diameter and circumference of 18.5 m and 58.1 m, respectively. The decision to use CAPTIF for the test was based on the fact that loading could be applied by the two Simulated Loading and Vehicle Emulators (SLAVEs), and that the radii of the loading arms did not have to be the same. The primary characteristics of the SLAVE are summarized in table 2.1.[6] The two loading arms rotate about a fixed center and are fixed by hinges to either end of a sliding frame that can be moved radially. The SLAVE's position on the pavement can be moved laterally through a 1-m range (±500 mm about the mid-point) in 1-cm increments by a hydraulically controlled sliding frame that connects the two vehicle arms at the center pedestal. Because there is a solid connection between the vehicles, as one moves closer to the center of the track, the other moves equally in the opposite direction. The lateral movement can be set manually from the control room or by programming an automatic distribution pattern on the control computer. This feature allows multiple wheelpaths to be used to represent different trafficking situations of a road in service. For the DIVINE study, one path would be loaded by a steel spring suspension and the other path would be loaded by an airbag suspension. The cross section of the test track and elevation view of the SLAVE are illustrated in figures 2.1 and 2.2, respectively. If all other parameters (pavement thickness, material type and strength, load, tire pressure, etc.) were identical, then any difference in performance could be directly related to the suspension type.
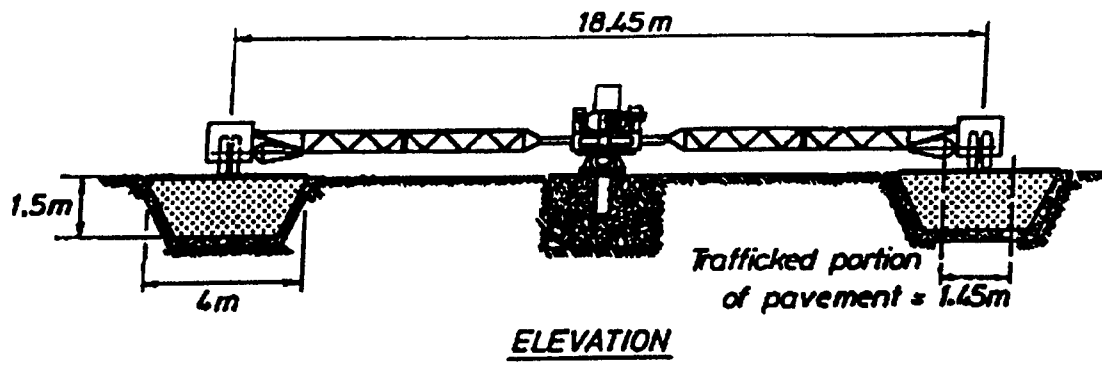
Figure 2.1. Cross section of CAPTIF test track.
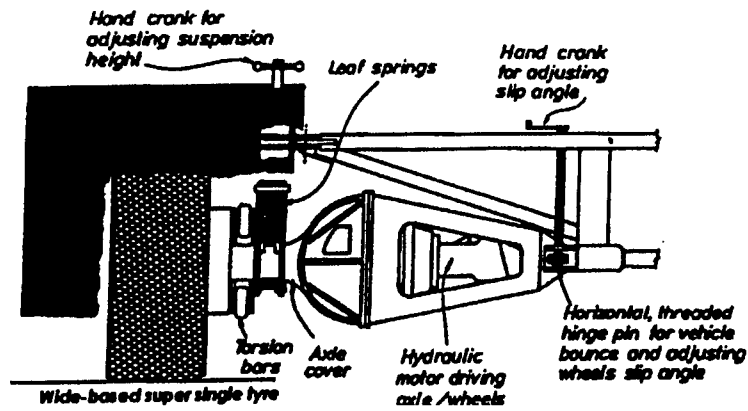
Figure 2.2. Elevation view of a SLAVE vehicle (steel suspension).

Table 2.1. Characteristics of SLAVE.

Item	Characteristic
Test Wheels	Dual or single tires; standard or wide base; bias or radial ply; tube or tubeless; maximum overall tire diameter of 1.06 m
Mass of Each Vehicle	21 kN to 60 kN, in 2.75-kN increments
Suspension	Airbag; multi-leaf spring; single or double parabolic
Power Drive to Wheel	Controlled variable hydraulic power to axle; bi-directional
Transverse Movement of Wheels	1.0 m center-to-center; programmable for any distribution of wheelpaths
Speed	0 to 50 km/h, programmable, accurate to 1 km/h
Radius of Travel	9.2 m

2.2 SELECTION OF SUSPENSION TYPES

In order to meet the objectives of the experiment, it was necessary to configure the loading on each pavement with suspensions that would represent the traditional and the more recently developed types. It was, therefore, proposed that one of the loading vehicles on CAPTIF be equipped with a commonly used suspension unit, namely a two-stage trapezoidal multi-leaf steel spring. Damping on this type of spring is generated by the inter-leaf friction of the spring without viscous dampers. The second loading vehicle was equipped with dual airbags and a Koni hydraulic shock absorber operated by a bell crank linkage with equal-length arms from the axle (the ratio of deflections at either end of the bell crank is 1.0). Because of limitations on space, it was not possible to use a standard, as-supplied, air-spring assembly; however, all components of the air-suspension system were standard, and the stiffness and damping characteristics of the system were identical to those of the standard.

Plots of the responses of the two suspension systems obtained from the standard 80-mm European Community (EC) bump tests conducted after 250,000 (250k) load cycles are given in figures 2.3a and 2.3b. The air suspension had a natural frequency of 1.41 Hz and damping of 17 percent, while the steel spring had a natural frequency of 1.93 Hz and damping of 21 percent. These data suggest that the air suspension was very similar in frequency and damping to typical heavy-vehicle air suspensions, while the steel suspension had a somewhat lower frequency and higher damping than would be expected for typical truck leaf-spring mechanical suspensions (these results are also summarized in table 6.1). Although drop tests indicated that there was perhaps less difference in the "road-friendliness" of the two generic suspension types than would occur in practice, there was a substantial difference in the actual dynamic wheel forces [measured as dynamic load coefficients (DLCs)] for the two test wheels and it appears that the dynamic behavior of the test steel suspension, when attached to the CAPTIF rotating arm, produced dynamic wheel forces similar to an actual truck steel suspension. These characteristics are presented in chapter 6.

2.3 SELECTION OF VEHICLE TIRES

Each vehicle was equipped with a 385/65 R22.5 Bridgestone wide-base tire having a mean radius of 0.5 m and inflated to 700 kPa. Wheel camber and toe in on each assembly were both set to zero.

2.4 DESIGN OF TEST PAVEMENT

The design of the test pavement was based on the principle that the fatigue and deformation performance of the pavement, under loads of typical heavy vehicles operating worldwide, would be nominally equal, i.e., deformation and cracking would occur at about the same time. In accordance with the New Zealand (NZ) pavement design method that accounts for classical fatigue cracking of the asphalt concrete (AC) layer and rutting of the subgrade, the CAPTIF pavement was designed for equal cracking and rutting under the designed load; a flexible pavement consisting of an 88-mm-thick asphaltic layer over a prepared 200-mm average thickness granular base and a selected subgrade of California Bearing Ratio (CBR) 12 percent was thus constructed. The design of the AC mix was based on the Marshall design method with top size aggregate of 16 mm. The performance of the designed pavement was predicted using several methods from different OECD countries, and it was expected that the pavement would carry between 450k and 600k repetitions of a 49-kN wide-base single-tire load before failure. It was also hoped that one wheelpath would fail first and loading would continue on the other wheelpath.
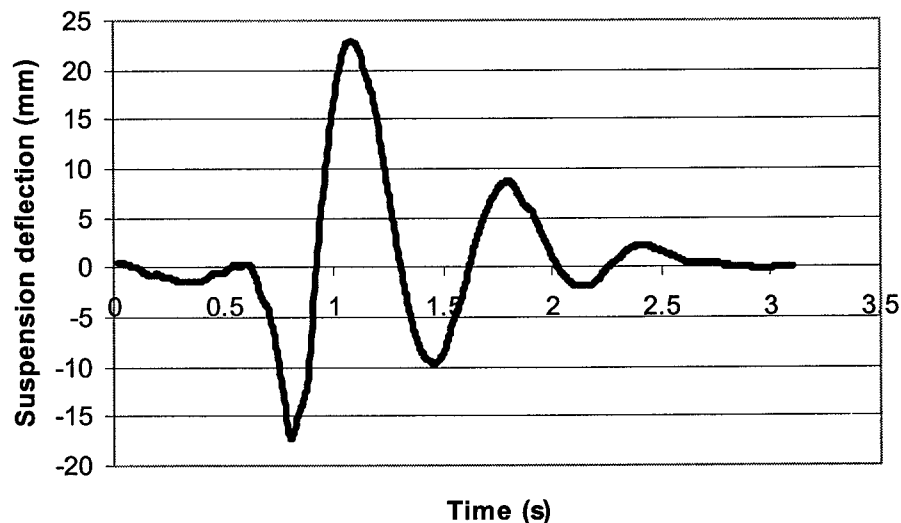
Figure 2.3a. Typical air-suspension bump test response.

6
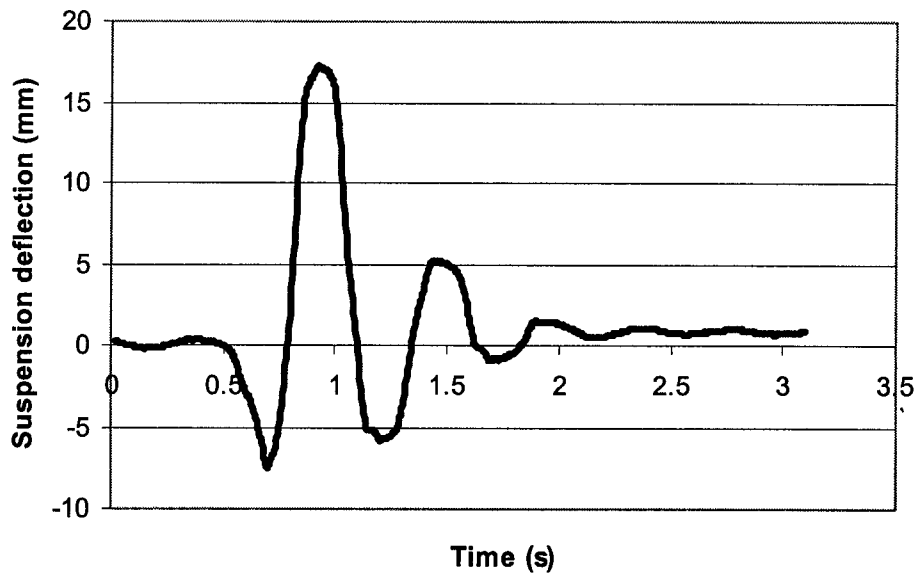
Figure 2.3b. Typical steel-suspension bump test response.

Although the pavement was designed to carry between 450k and 600k repetitions of the 49-kN wide-base single-tire load, loading was halted at 1700k repetitions without major failure. Listed below are those factors that would have tended to reduce damage:

- NZ flexible pavement design method inherently compensates for adverse environmental factors that were absent in the controlled environment in CAPTIF. The test track is protected from direct sunlight and rainfall, and the concrete pavement tank completely isolates the pavement from groundwater influences. Thus, the water content of the pavement layers did not fluctuate during the test as might normally be expected on in-service pavements, e.g., water is not available to enter asphalt concrete even when surface cracking occurs. Thus, this pavement lasted more than three times longer than expected.

- Reduced stress in AC layer for thin AC-layered pavements because of larger tire footprint-to-thickness ratio under dynamic loading.

- Relatively stiff subgrade (CBR 12).

- Relatively high uniformity.

Those factors that would have had a tendency to increase damage are given below:

- Smaller unloading period between repetitions (about 4.6 s) accelerates accumulative permanent deformations in all layers.

- Tire horizontal shear (scrubbing forces) that were accentuated by the circular track.

- Thin AC layer causes higher AC underside-layer tensile strain and/or sublayer permanent deformations.

- Relatively channelized trafficking.

7

- High degree of spatial repeatability.

- Use of wide-base tires in lieu of dual tires.

Given the fact that little damage occurred to the pavements, despite the large numbers of load repetitions, it would appear that the lack of environmental influences tended to prevail in limiting the amount of pavement damage generated during testing. Although the DIVINE pavement is considered clearly structurally weaker than typical U.S. or Canadian flexible pavements, the authors compared falling weight deflectometer (FWD) deflections from CAPTIF with that from the Long Term Pavement Performance (LTPP) program in the United States and Canada on General Pavement Study (GPS) pavement sections. The LTPP FWD deflection had a mean center surface deflection of 0.7 mm/kPa, while the mean center surface deflection was 0.92 mm/kPa, reported from FWDs at CAPTIF (see table 6.1). Note that the CAPTIF deflection is only slightly higher than the above-mentioned value.

All of the above factors cited are well understood by most pavement design engineers, except for those effects dealing with tire scrubbing and tire footprint; therefore, a brief discussion of these two phenomena are presented in appendixes A and B.

In appendix A, it is suggested that because of the combination of angular velocity of the CAPTIF arm relative to the ground and the angular velocity of the wheel relative to the arm, radial "scrubbing" forces were applied to the road surface (in the outwards direction) by the tires, continuously throughout the experiment. The inevitable consequence of these continuous large transverse forces would be a circumferential, top-down crack in the wheelpath. Since the fatigue properties of asphalt are sensitive to stress level, then it is sufficient to expect that much of the cracking would have been affected by this stress mode. Because the difference in the scrubbing forces between the tracks is small, then the influence of these forces is negligible in the comparative sense.

In appendix B, it is shown that the tire footprint on pavement increases under larger loads; thus, the strains occurring in the pavement will be reduced nonlinearily with load, depending on the rate of change of footprint with load. For thick AC-layered pavements, the reduction in strain on the bottom of the pavement because of increased footprint area will be much less than that for thin AC-layered pavements because of increased footprint area. For wide-base single tires, this pseudo-nonlinearity effect is greater than that for dual tires. This does not mean, however, that strains are smaller for thin pavements, it only suggests that the rate of change of strain is reduced with dynamic loading.

2.5 TRAFFIC LOADING AND MEASUREMENT PROGRAM

Each vehicle was loaded to 49 kN. Lateral distribution of load in each wheelpath was designed to allow a reasonable wheelpath wander, while maintaining a satisfactory separation between the wheelpaths. The distribution program moved the vehicles to the next centimeter wheelpath increment every 10 laps.

8

The airbag suspension was placed on one arm (the inner arm), with the steel-spring suspension on the other (outer) arm and the sliding frame used to ensure that the two wheelpaths did not overlap during trafficking. In order to maximize the separation between the two wheelpaths, wide-based single tires were used with a separation of 800 mm between the centerline of the wheelpaths. The wheelpaths are about 400 mm wide, including wander of about ±100 mm. This provides a 0.2-m separation of wheelpaths without overlapping (0.2 m of untrafficked pavement at all times).

Vehicle speed was set to a constant mean speed of 45 km/h. The mean radii of wheelpaths of these vehicles were 9.6 m and 8.8 m, respectively; thus, mean speeds of the steel and air suspensions were 47 km/h and 43 km/h, respectively. At these speeds, unloading time between loading pulses is about 4.6 s. This rate is somewhat higher than might be expected on in-service roads, but lower than that usually used in laboratory tests.

The coordinates of measurements at CAPTIF are based on radial and circumferential position. The circumferential position is measured as a distance around the centerline wheelpath in meters from a reference point. These metrics are referred to as "stations." The circumference of the track was divided into 58 stations, and these divisions were radial. Thus, station 10 refers to a position on a radial line that intersects the centerline wheelpath at 10 m from the starting point, which is at station zero. Station locations were then used to define other measurement locations, the placement of pavement instrumentation, the occurrence of pavement deterioration, etc. Their position remained unchanged throughout the test.

Pavement condition and response, and vehicle load data were collected throughout the test. Because the rate of pavement deterioration was slower than expected, the interval between measurements was increased from that initially planned. The number of load cycles (in thousands) at measurements were 20, 30, 40, 60, 80, 100, 150, 200, 250, 300, and then increments of 100 thereafter. To reduce the time and cost of collecting and processing the data, the complete set of measurements was collected every third measurement interval, with a subset of the most critical data collected every measurement cycle.

Between 27 October 1994 and 17 August 1995, SLAVE applied 1.7 million loads to each wheelpath while traveling 98,000 km. Twenty-four sets of pavement condition measurements were completed and 182 Mb of raw data were collected. Several new data systems were commissioned in addition to those in regular use at CAPTIF.

CHAPTER 3. CONSTRUCTION OF TEST PAVEMENTS

Construction at CAPTIF commenced on 28 February 1994. The pavement consisted of clay subgrade, crushed rock base, and AC surface layers. During construction, FWD tests were conducted on each wheelpath of each natural layer at 1-m intervals around the track.

3.1 SUBGRADE

The imported clay material was stockpiled and covered with a polythene cover to prevent the moisture content of the material from changing. Marks were placed on the sidewall of the tank, using a laser level, in order to guide the placement of each lift of the subgrade installation. The marks were located 200 mm above the mean reduced level of the previous layer. A small, six-wheeled tip truck was used to move the material from the stockpile to the correct location in the tank, and a bulldozer and flat rakes were then used to level the material. This method of construction ensured that the correct amount of material could be placed where it was required and minimized the amount of compaction due to trafficking by construction vehicles and plant. An 8-tonne (t) tandem steel-wheeled roller was used to compact each lift of the subgrade. Each lift received one dead-weight pass to level the surface of the material; the subsequent passes for that particular lift were vibratory.

The first lift of the subgrade was placed, leveled, and compacted on 28 February 1994. Wet weather delayed construction until 3 March, when Lift 2 was placed. Rain prevented the completion of Lift 2 in 1 day; it was completed on 4 March. Lifts 3 to 7 inclusive were placed, leveled, and compacted, and densities were measured at a rate of one lift per day over the period 7 to 11 March inclusive. Lift 8, the final lift of the subgrade, was placed on 14 March and was leveled and compacted on 15 March 1994. A steel frame (2 m by 4 m) towed behind a tractor was used to remove any localized high spots in the subgrade surface following placement and compaction of all lifts. The surface produced by this technique was very even in both the longitudinal and transverse directions.

For each lift of the subgrade and for the crushed rock base course, the material densities were measured using a nuclear density meter (NDM). Measurements were taken in the inner and outer wheelpaths and on the centerline of the track at each station (174 readings per lift). The NDM was operated in backscatter mode, so that there was no penetration of the radioactive probe into the material. When the NDM operates in backscatter mode, the density of the top 150 mm of material is determined. The laser level was used to measure the thickness of the lift at the same locations that density measurements were made.

FWD tests were conducted at both 25 and 40 kN in the outer and inner wheelpaths at each station (116 locations). At that stage, the density of the top 300 mm of the subgrade was measured by inserting the NDM probe into the subgrade to a depth of 300 mm. The density in the top 300 mm of the subgrade was very uniform, the mean density being 1.932 t/m^3 (175 values) with a standard deviation of 0.038 t/m^3. The values ranged between 1.814 and 2.021 t/m^3. At each station, a manual surface profile was taken, the material height being measured every 200 mm across the width of the track.

On 18 March, dynamic cone penetrometer (DCP) tests were performed at each of the locations where density measurements were carried out. The number of blows required to penetrate from 0 to 90 mm, 90 to 190 mm, and 190 to 290 mm below the surface was recorded. The results of the DCP tests showed that the strength of the subgrade was also uniform around the track. The results of the DCP and moisture content tests indicated that the strength of the subgrade may have been stronger than that specified in the project brief. On 22 March, the in situ CBR was determined at three locations, at 50, 150, and 250 mm below the surface of the subgrade, and the mean CBR was 12 percent (higher than the design value of 10 percent). The in situ CBR results agreed with the FWD and resilient modulus test results.

FWD deflection bowl data were collected on the subgrade under the 25-kN load for purposes of backcalculating subgrade moduli.[9]

3.2 CRUSHED ROCK BASE

The first lift of the crushed rock was placed, leveled, and compacted on 25 March 1994. Densities and laser level heights were measured using the same procedure as that used for the subgrade. The second lift of crushed rock was placed and leveled on 29 March and compaction was completed on 30 March. The surface was then left to cure (1 to 5 April).

FWD testing was conducted on the inner and outer wheelpaths at each station on 6 April, at loads of 16, 25, and 40 kN. Densities and transverse profiles were also measured at this stage. In situ densities were high, ranging between 97 percent and 103 percent modified. Backcalculation was conducted by ARRBTR on samples of the data collected at loads of 16 and 25 kN. The backcalculated moduli of the crushed rock varied between about 250 and 400 MPa, and there was no obvious relationship between the backcalculated modulus and in situ moisture content determined from NDM testing.

Repeated-load triaxial testing conducted by the University of Canterbury showed that there was no optimum moisture content of the crushed rock (density values being about the same for moisture contents greater than about 2.5 percent). The results of triaxial testing at a moisture content of 2.5 percent (approximately equal to the in situ values) showed that the moduli were about the same as those backcalculated from the FWD data; however, they were generally higher at a moisture content of 2.5 percent than that at moisture contents of 1.2 percent and 4.2 percent.

3.3 ASPHALT CONCRETE

A uniform application of 0.67 L/m^2 of slow-break cationic emulsion was applied to the track surface on 8 April, and the asphaltic concrete was placed on 9 April. At this stage, 40 H-bar strain gauges were secured to the surface of the crushed rock with adhesive tape.

The asphalt concrete was hand placed in two lifts on 11 April. The first lift was leveled using flat rakes and a pedestrian roller was used to compact the asphalt. A thin-lift NDM was used to monitor compaction levels. At the completion of the first lift, the surface was sprayed with an emulsion tack coat to ensure a bond between the two lifts. The second lift was leveled using a screed bar to ensure that the surface was as level as practical across the track. The asphalt temperature during placement ranged from 148 to 105°C.

The density of the asphalt was measured on 12 April using the thin-lift gauge. Twelve cylindrical cores were removed from the track for further testing. FWD testing also commenced on 12 April at the same locations as the previous tests, under loads of 15, 20, 25, 40, and 60 kN. A limited number of tests were also conducted at 50 kN.

Longitudinal profiles were measured in both wheelpaths, the track centerline, and 400 mm on either side of the wheelpaths. Transverse profiles were measured at each station.

3.4 CONSTRUCTION STATISTICS

Plots of spatial variation of layer thickness, FWD unit deflection (deflection per unit applied pressure on the loading plate during the FWD tests), and layer moduli at construction and at 20k load repetitions are given in figures 3.1 through 3.6. Some basic statistics of these variables are given in tables 3.1, 3.2, and 3.3.[11]

The variation in layer thickness for the two top layers in both paths is small—between 4.3 percent and 7.7 percent. Mean thickness values, standard deviation (std.), and coefficient of variation (V) between the inner and outer tracks are similar. For both wheelpaths, the variation of AC thickness is about 75 percent greater than the variation of the base thickness, as might normally be expected. Unit load deflections for all layers seem to vary quite randomly. Basic statistics show that the variation of unit deflections for all layers in both wheelpaths is about 10 percent. Although mean deflection on top of the AC layer of the outer path is about 7 percent less than that of the inner path (outer wheelpath is stiffer), mean deflections at the top of the base and subgrade for inner and outer wheelpaths are about the same. All other statistics between inner and outer tracks are similar.

Subgrade deflection is, in general, 34 percent larger than base course deflection, indicating that the base course does, in fact, tend to stiffen the overall pavement (except at stations 16 and 37, where subgrade deflections on the outer wheelpath were less than the base course deflections), indicating either a weaker base course in this area or data error. The overall findings, except for the reverse deflections found between subgrade and base at stations 16 and 37, indicate that the pavement structural conditions for both inner and outer wheelpaths at construction were similar.

13
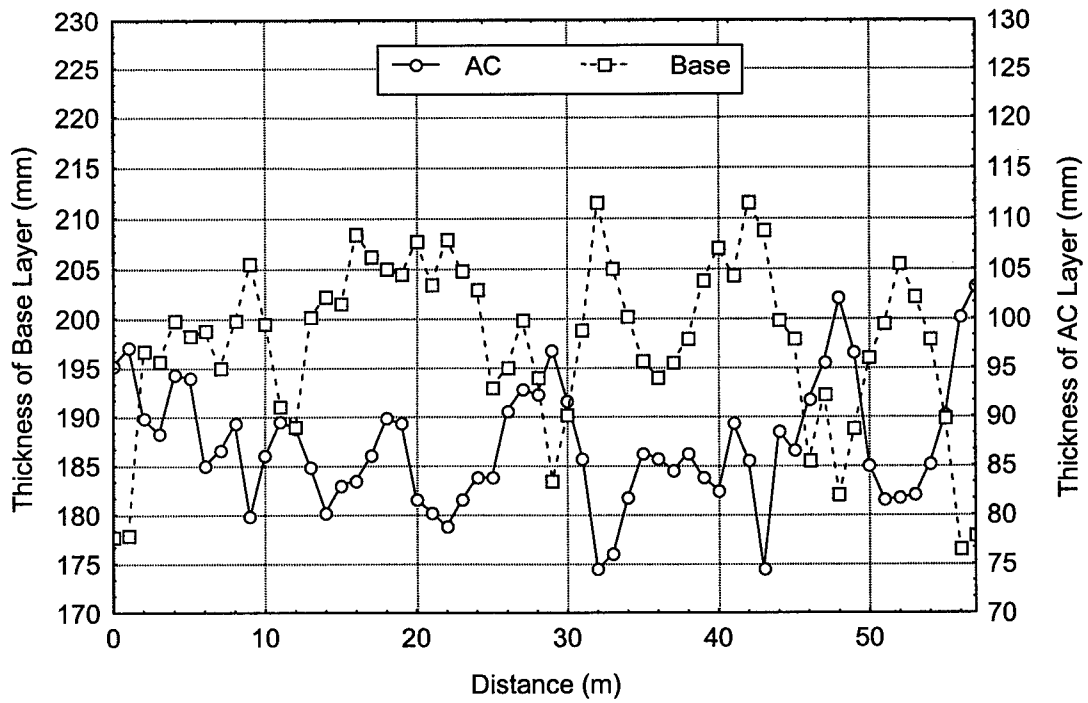
Figure 3.1. Layer thickness, inner track.
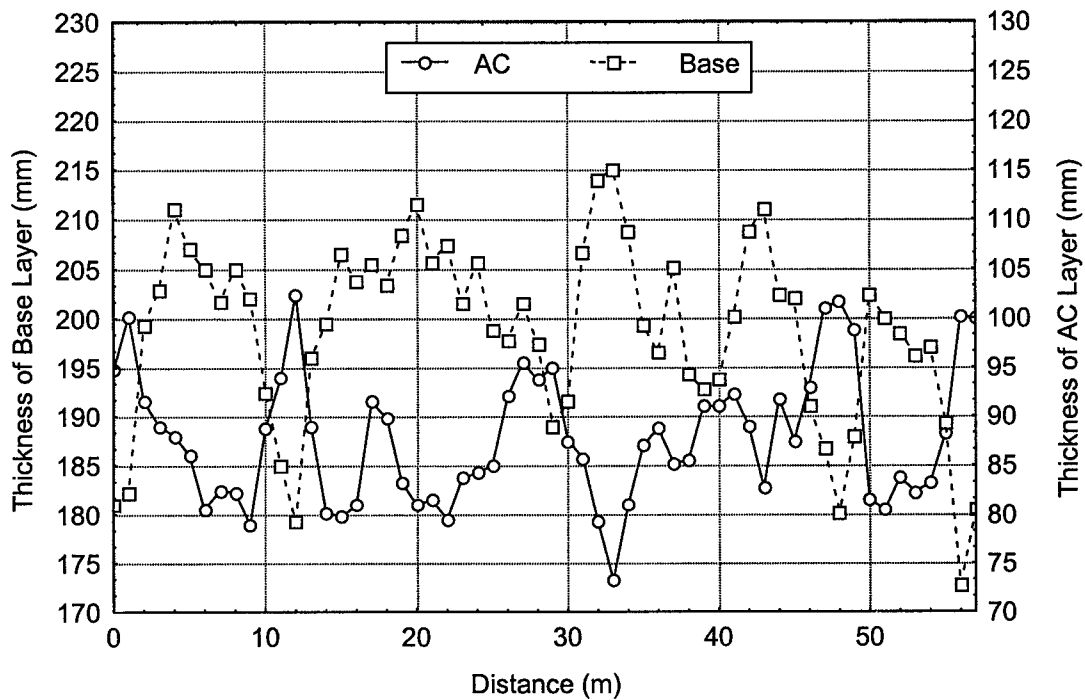
Figure 3.2. Layer thickness, outer track.

14
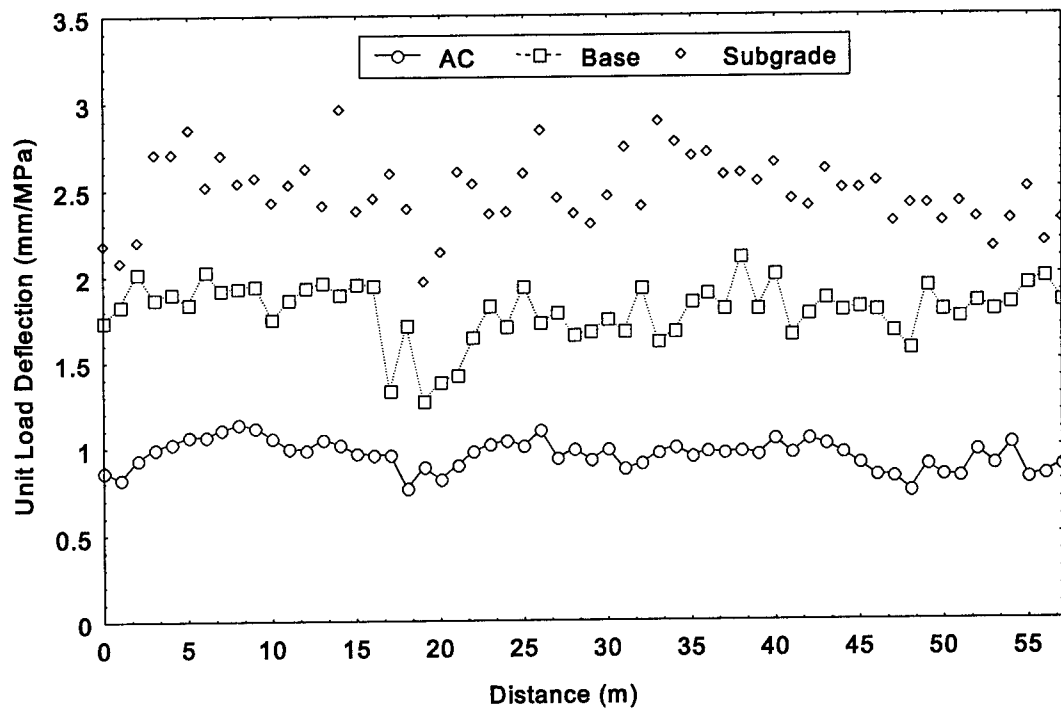
Figure 3.3. Unit load layer deflection at construction, inner track.
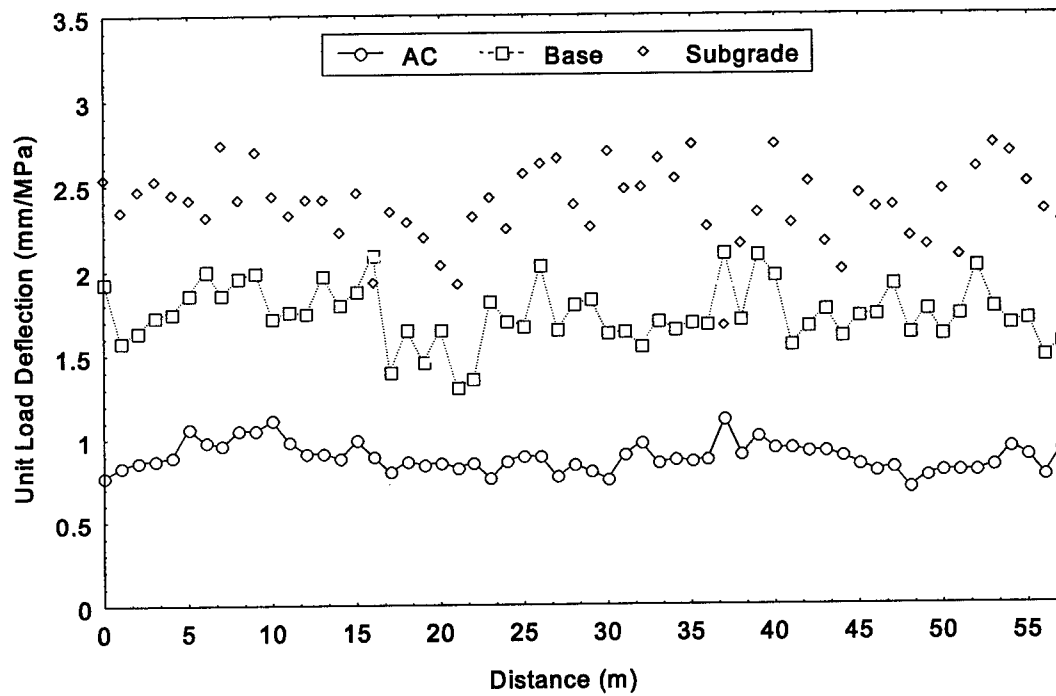
Figure 3.4. Unit load layer deflection at construction, outer track.
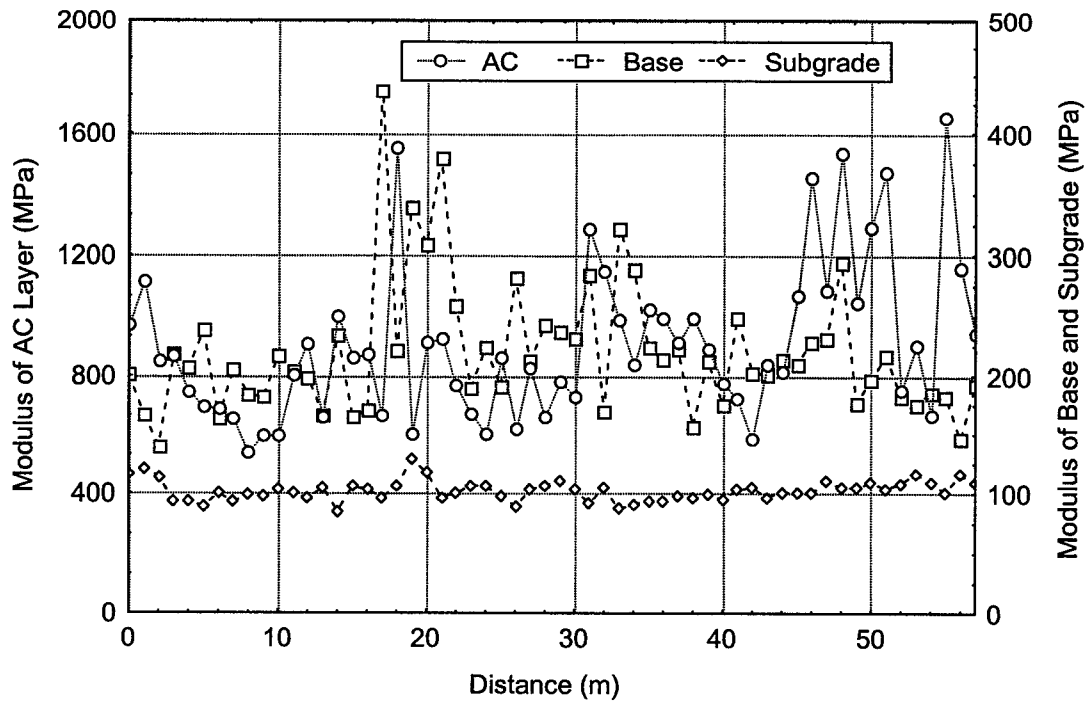
Figure 3.5. Layer moduli, inner track (initial).
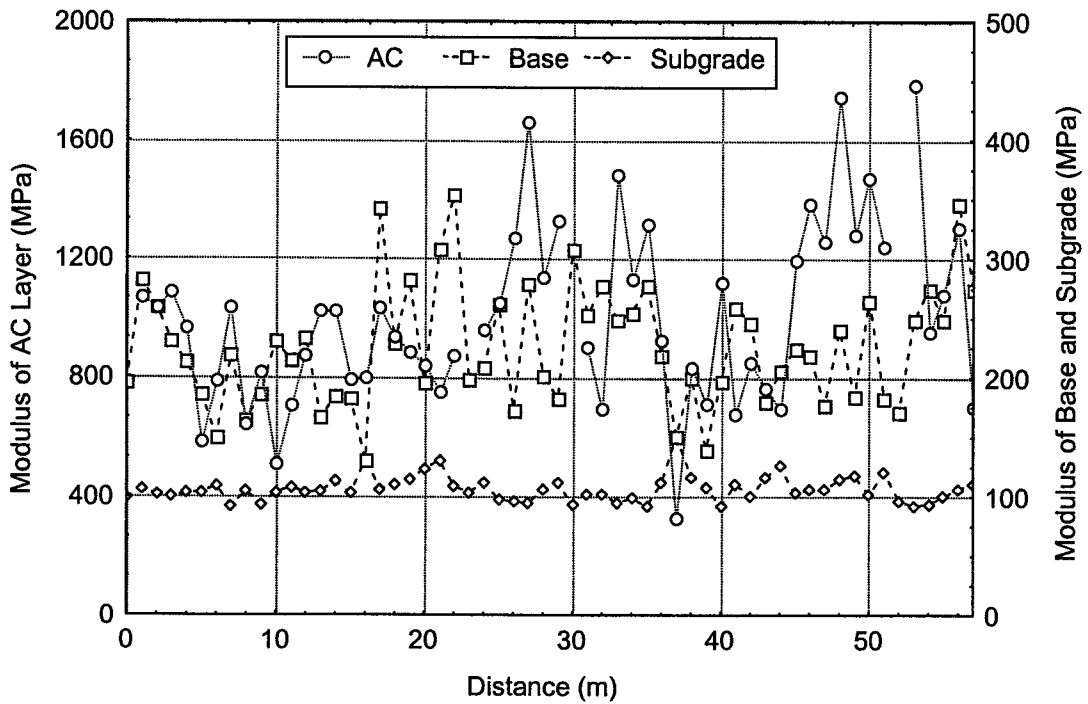
Figure 3.6. Layer moduli, outer track (initial).

16

Table 3.1. Statistics of CAPTIF pavement layer thickness.

	MEAN	MINIMUM	MAXIMUM	std.	V
Outer Track					
H_{AC} (mm)	88	73	103	6.808	0.077
H_{base} (mm)	199	173	215	9.496	0.048
Inner Track					
H_{AC} (mm)	87	75	103	6.333	0.073
H_{base} (mm)	198	177	212	8.580	0.043

Table 3.2. Statistics of CAPTIF pavement unit layer deflection at construction (FWD data).

	MEAN	MINIMUM	MAXIMUM	std.	V
Outer Track					
AC (mm/MPa)	0.888	0.703	1.121	0.090	0.101
Base (mm/MPa)	1.742	1.309	2.099	0.179	0.103
Subgrade (mm/MPa)	2.383	1.674	2.737	0.224	0.094
Inner Track					
AC (mm/MPa)	0.954	0.748	1.135	0.089	0.093
Base (mm/MPa)	1.793	1.267	2.105	0.169	0.094
Subgrade (mm/MPa)	2.478	1.959	2.954	0.205	0.083

Table 3.3. Statistics of CAPTIF pavement unit surface deflection at beginning of test (at 20k, FWD data).

	MEAN	MINIMUM	MAXIMUM	std.	V
Inner Track					
All Data (mm/MPa)	0.949	0.768	1.095	0.089	0.094
Select Data (mm/MPa)	0.953	0.768	1.095	0.091	0.095
Outer Track					
All Data (mm/MPa)	0.965	0.796	1.258	0.111	0.115
Select Data (mm/MPa)	0.945	0.796	1.131	0.092	0.098

Table 3.4. Statistics of CAPTIF pavement layer modulus.

	MEAN	MINIMUM	MAXIMUM	std.	V
Outer Track					
E_{AC} (MPa)	1081.810	330.000	2183.000	404.780	0.374
E_{base} (MPa)	226.020	131.000	354.000	51.260	0.227
$E_{subgrade}$ (MPa)	106.710	92.000	151.000	11.120	0.100
Inner Track					
E_{AC} (MPa)	904.900	538.000	1658.000	262.550	0.290
E_{base} (MPa)	220.350	140.000	437.000	55.810	0.253
$E_{subgrade}$ (MPa)	102.340	85.000	129.000	8.680	0.085

CHAPTER 4. MATERIALS CHARACTERIZATION

Characterization of the asphalt concrete used in the test pavements was carried out under contract by ARRBTR for OECD.

The design of the AC mix was based on the Marshall mix design method, with a top-size aggregate of 16 mm. The bulk density of the Marshall specimens varied between 2.363 and 2.321 t/m^3, with little difference between Lift 1 and Lift 2 specimens, but slightly lower than the density of the pre-trial mix. Flexural fatigue tests were carried out on samples removed from the pavement after the completion of trafficking.

Resilient modulus and dynamic creep tests were carried out on cores removed from the pavement at construction and on Marshall specimens prepared by the contractor during construction. The densities of the cores varied between 2.244 and 2.211 t/m^3.

4.1 ASPHALT CONCRETE RESILIENT MODULUS/DYNAMIC CREEP TEST

Resilient modulus tests and dynamic creep tests were conducted on pavement cores taken from the CAPTIF pavement without sample preparation.

Twelve untrimmed and unpolished AC core samples were used for resilient modulus tests and the tests were performed on Australia Road Research Board's (ARRB's) Materials Testing Apparatus (MATTA) in line with the procedure in the draft Australian Standard for materials testing.[14] All samples used in the test were nominally 80 mm thick and 100 mm in diameter. The test results are given in table 4.1. The tests show variation in the average resilient modulus with temperature and rise time. The average modulus of the cores was between 50 and 60 percent of the moduli determined in a similar manner on Marshall specimens. Of direct relevance to the CAPTIF loading tests are the moduli obtained at a rise time of 30 ms (this loading time is closest to the CAPTIF test vehicle speed of 45 km/h).

The dynamic creep core samples were prepared for testing by trimming their height and polishing their ends. One gram of Dow Corning insulating compound was applied to the sample faces. The samples used for the dynamic creep test were trimmed so that their mean height was as close as possible to half of the mean diameter (this is in line with the procedures recommended in the draft Australian Standard[15] and in line with current practice elsewhere). It should be pointed out that the dynamic creep test is a repeated-load test and not a creep test in the classical sense. The tests were conducted on the MATTA, with the load applied uniaxially. During the test, square pulse loads are applied with a loading duration of 0.5 s and a cycle time of 2 s. Table 4.2 presents a summary of the dynamic creep test results, including the number of cycles to 1 percent and 3 percent strain and the minimum creep slope (the point of inflection of the creep curve). The minimum creep slopes (not really creep slope, but slope of the plot of accumulated compressive versus load repetitions) for the CAPTIF Marshall specimens were found to be similar to other AC materials used in the Australian Accelerated Loading Facility (ALF) test pavement at 50°C. The minimum creep slopes for the CAPTIF cores, however, were much higher than other AC materials, suggesting that at 50°C, the mix is not very rut-resistant.

Table 4.1. Summary of results: resilient modulus testing.

Temperature (°C)	Rise Time (ms)	Res. Modulus (Marshall) (MPa)*	Res. Modulus (Cores) (MPa)*	E(cores)/ E(Marshall) (percent)
10	30	7310	4590	63
	50	6700	4170	62
	70	6160	3760	61
	90	5800	3420	59
	110	5400	3160	58
15	30	5140	2930	57
	50	4620	2660	58
	70	4230	2380	56
	90	3860	2120	55
	110	3570	1930	54
25	30	2390	1400	59
	50	2110	1120	53
	70	1810	920	51
	90	1580	790	50
	110	1370	660	48

* Results rounded to nearest 10 MPa.

This large difference between core and Marshall specimen might be because the mix, as placed, was not as well compacted as the Marshall specimens.

4.2 ASPHALT CONCRETE FATIGUE TEST

The fatigue test was based on Strategic Highway Research Program (SHRP) Test Protocol M-009, as modified by the NARC Fatigue Project Group for use in Australia. Rectangular beam specimens of 400 mm by 50 mm (depth) by 63.5 mm (width) were prepared from the rough-cut beams and tested using the IPC Beam Fatigue Apparatus (UTM 176). This four-point flexural beam fatigue test was conducted in third-point haversine tension loading at a frequency of 10 Hz without rest period. One sample each at three strain levels, 300, 500, and 700 microstrain, in the controlled strain mode was tested at a temperature of 20°C ±0.5°C. The fatigue life was determined when the flexural stiffness of the sample reached 50 percent of the initial flexural stiffness measured at 50 cycles. For comparative purposes, a standard Australian asphalt mix (C1) was also tested.

20

Table 4.2. Summary of results: dynamic creep testing.

Sample	Air Voids (Percent)	Cycles to 1 Percent Strain	Cycles to 3 Percent Strain	Min. Creep Slope (50°C)	Min. Creep Slope (35°C)
CAPTIF: Marshall					
G94/138-1		2510	23472	0.5	
G94/138-2		747	3165	5.7	
G94/138-3		527	3470	4.5	
CAPTIF: Cores					
G94/101-1		67	473	41.4	
G94/101-2		66	307	78.1	
G94/101-4		38	220	98.3	
ALF Cores					
C1	3.7	127	1458	13.3	0.8
C3	3.5	65	2233	5.1	1.7
C4	2.9	85	5987	2.8	0.1
C6	5.3	203	4708	4.0	0.2
C7	3.8	78	1744	8.6	0.4

The initial flexural stiffness at 50 cycles and the number of cycles to failure at 50 percent of the initial flexural stiffness at the three strain levels for the CAPTIF and C1 mixes are given in table 4.3. The initial flexural stiffness values of the CAPTIF mix were significantly lower than that of the C1 mix. As the "void from bulk density" values for the CAPTIF mix were not known, air voids of the individual beams could not be estimated.

The fatigue relationship between the fatigue life (N_F) and the initial strain amplitude (e) is generally represented by the following equation:

$$N_F = K \cdot (e)^{-n}$$

where K and n are a mix-dependent constant and exponent, respectively.

The laboratory fatigue performance of the CAPTIF mix appeared to be better than the C1 mix, particularly at low strain levels, possibly because of low initial flexural stiffness values. However, when the results of both mixes are combined, the strain-fatigue relationship fits in a single straight line ($r^2 = 0.97$ and the corresponding exponent n is -5.25, see figure 4.1), suggesting that their performance can be considered similar. The difference in their initial flexural stiffness values and possible differences in the compaction levels (air voids) in the mixes should also be considered.

Table 4.3. Flexural stiffness and fatigue life.

Strain Level (10^{-6})	Initial Flexural Stiffness at 50 Cycles (MPa)	Number of Cycles to Fatigue, N_F	Bulk Density (t/m^3)	Air Voids (%)
CAPTIF Mix				
300	2228	3686950	2.361	
500	1575	199550	2.141	
700	1527	26450	2.119	
ALF C1 Mix				
400	6015	348075		3.7
600	5991	55658		3.0
800	5719	12892		2.8
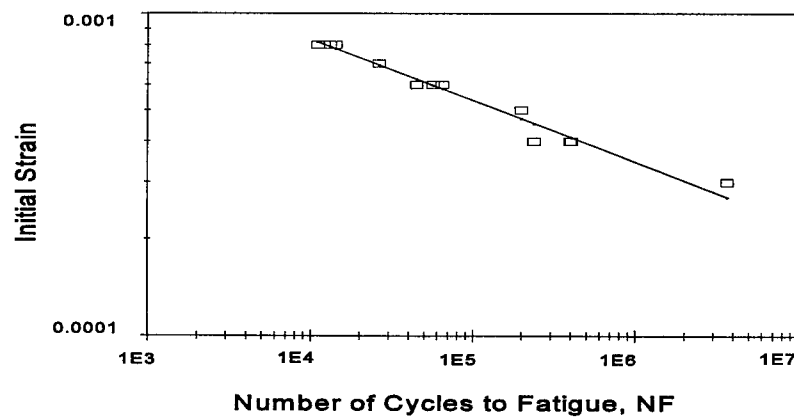
Figure 4.1. Initial strain versus fatigue life for CAPTIF and C1 mixes (combined).

22

CHAPTER 5. MEASUREMENT SYSTEMS

A number of measurement systems were deployed during the accelerated loading tests. The descriptions of these measurement systems follow.

5.1 DYNAMIC LOAD

The dynamic wheel force loading of the SLAVE vehicles was measured by a pair of accelerometers—one on the chassis and the other, in the same vertical plane, on the axle of the test wheel. Direct measurement of chassis/axle movement was monitored by a Linear Variable Displacement Transducer (LVDT) fitted between the two components. An infrared trigger beam was aimed at a revolution marker strip on the inner perimeter of the pavement. The three gauges on each vehicle were connected to a six-channel power supply and signal conditioning unit. This unit, together with the trigger beam, was connected to a high-speed HP3852A data acquisition computer, via a plug-in 24-channel multiplexer. The HP3852A, mounted on the SLAVE instrumentation cabinet, was controlled by the same laptop computer as the laser profiler and was operated remotely via the radio frequency modem link to the HP Vectra PC in the control room.

The data acquisition system served two purposes: (1) to monitor the dynamic behavior of the vehicle itself under different suspension and loading configurations and (2) to check that the dynamic characteristics did not change during the project because of age or usage.

A "steady" speed test was used to monitor the pavement forces. SLAVE was run at both a steady normal speed of 45 km/h and a low speed of 6 km/h. Measurement parameters were entered into the software, including vehicle configuration, speed, and wheelpath position. The software monitored the vehicle speed and, when it settled to a speed within the specified tolerance, readings were automatically triggered. Two complete laps of data were sampled at 1024 samples/lap for each vehicle, in both the normal loading wheelpath and the reverse wheelpath.

A "bump" test was used to check the vehicle characteristics. The SLAVE vehicles were moved to a central transverse position and a wooden ramp with an 80-mm vertical drop at the trailing edge was placed in the wheelpath. Measurement parameters were entered into the software and the SLAVE vehicles were run over the bump at 6 km/h. Measurements were triggered by a threshold value set on the axle accelerometer output and 1024 samples were taken for each pass. Each vehicle was measured over two passes of the bump for each run.

5.2 PROFILES

Transverse Profile

Transverse profiles were measured using the CAPTIF profilometer and digital output was captured on a Psion Organizer hand-held computer. The profilometer consists of an aluminum beam, 4.4 m long, supported at each end on aluminum legs. A machined aluminum carriage is driven along the beam by a mains-powered electric motor and drive chain. The carriage supports a jockey wheel that is free to move in a vertical direction. Connected to this wheel is an LVDT to

give a vertical displacement reading at any point along the path of the carriage. The transverse position is given by an optical sensor attached to the idler sprocket.

In use, the pavement was swept to remove any extraneous material that might have caused an erroneous reading, appropriate station data were fed into the Psion computer, and then the wheel was lowered and a control switch at the motor end set the machinery in motion. Electronic measurement data were input directly to the Psion computer as the profilometer wheel traversed the track. When the carriage reached the end of its path, a micro-switch stopped the motor. The operator then reversed the control switch to return the carriage to the start point, where the wheel was lifted into its traveling position. The operator and assistant then moved the beam to the next station to be measured. During the test, the transverse profile was measured every 25 mm horizontally along the pavement section.

The electronic data were collected in one ASCII format file for each station in the Psion computer. The memory capacity of the Psion computer is sufficient to hold 12 to 15 profiles and the Psion computer, therefore, needed to be cleared by down-loading to the HP Vectra PC, via serial link, up to four times for each set of profile measurements.

Longitudinal Profile

At first, a Dipstick profiler was used to record longitudinal profiles around the track circumference. Although the experiments began by using this device, better accuracy was desirable and this was achieved by the use of a laser-based device that was subsequently commissioned in March 1995 and used regularly in testing intervals from 500k laps. As a back-up to the new laser system, Dipstick profiles continued to be measured until the completion of the test. Each of these measurement systems is described below.

Dipstick profiler. The original CAPTIF Dipstick was a manually operated device designed to measure the slope between adjacent points on the road spaced 250 mm apart and then calculate elevation changes from this. Thus, the profile is built up by adding elevation changes. The closure error for one track circuit was typically about 38 mm. This was treated as a uniform linear shift that was subtracted from data points. The process was essentially a numerical integration and thus a very small constant error term in each reading will cause this type of error. The 38-mm amount was reasonably consistent for all measurement sets. The datum for profile was referenced back to the concrete tank wall at station zero using the transverse profile measurement at this station. Thus, there is an absolute datum. (The original device used a spherical foot with spacing of the feet at 300 mm, but the spherical feet were replaced with flat discs spaced at 250 mm.)

The centerlines to be measured were marked out by an apparatus attached to the rear of the steel suspension vehicle. This pressed a chalk stick against the pavement surface via a spring-loaded arm that could be adjusted transversely across the full width of the track. The SLAVE vehicles were driven around the track at a low speed until the marking was complete (these centerlines of wheelpaths were also used as a reference for the deflectometer readings).

Before each measurement run, the Dipstick was placed across two calibration marks on the top of the test track wall. The zeroing software on the palmtop computer was run and the instrument was then rotated 180°. The software compared the two readings and adjusted the calibration of the gauge. To begin the first measurement, the backward foot on the Dipstick was placed on the intersection of the station 00 mark and the centerline, and the operator ran the data capture software. When the computer signaled that the reading was complete, the operator rotated the instrument 180° to the next point on the centerline and held the instrument steady for the next reading. This continued until the entire centerline had been traversed back to the start point where the operator closed the data reading program. Three runs were taken on each centerline for greater accuracy.

Laser profiler. The CAPTIF laser profiler system uses an ARRBTR laser profilometer to measure longitudinal pavement profiles from a radial beam fitted to the rear of a steel-suspension vehicle. The transverse position of the laser beam is adjusted by moving the laser carriage along the radial beam. Vehicle speed is measured by a rotorpulser fitted to the wheel hub and profile readings are triggered every 50 mm of vehicle travel. An integrated accelerometer in the laser camera assembly compensates for vertical vehicle chassis movement. Double integration of the vertical distance and acceleration gives the longitudinal surface shape.

The laser camera and the rotorpulser are connected to an interface unit, containing a power supply and signal conditioner, on the SLAVE instrumentation box at the inner end of the steel-suspension vehicle arm. Also connected to the interface unit is an infrared revolution marker that is aimed at a reflective strip on the surface of the inner perimeter of the track.

To begin data acquisition, the rotorpulser, radial beam, and camera carriage are fitted to the SLAVE vehicle. The height of the camera is set to a fixed range and the horizontal position of the carriage is adjusted to line up with the pavement centerline to be measured. The SLAVE is run up to a minimum speed of 25 km/h and the measurement parameters are entered into the laptop computer via the modem link from the control room. Readings are taken over 10 laps, after which SLAVE is stopped so that the carriage can be moved to the next transverse position. At the completion of all runs, data are down-loaded to the HP Vectra.

5.3 LOAD DEFLECTION DEVICES

Pavement deflections have traditionally been measured in the CAPTIF facility with use of the deflectometer, a refinement of the Geobeam developed by Tonkin and Taylor.[6] It was decided at an early stage that the FWD should also be used during pavement construction and loading. The deflectometer was used both at FWD testing intervals and at intermediate intervals to economically achieve a more complete set of data.

A	Optical sensor	F	Signal wire support
B	Lifting handle	G	Chain Drive
C	Carriage	H	Drive motor
D	LVDT	I	Electronics box
E	Jockey wheel	J	Cradle for Psion computer
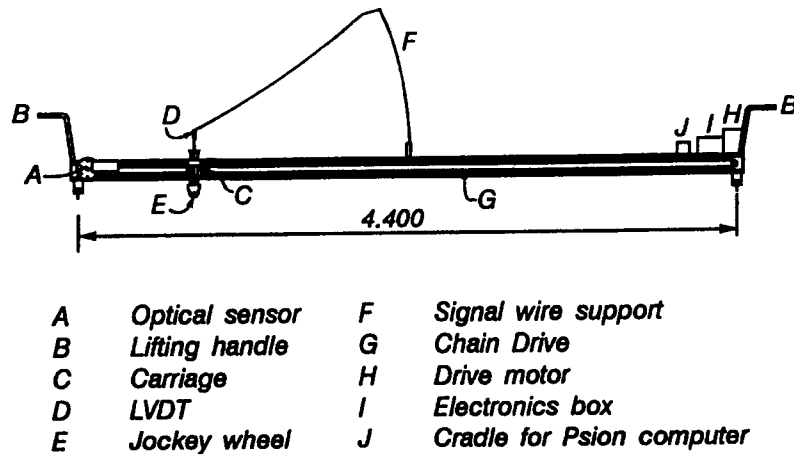
Figure 5.1. CAPTIF profilometer.

CAPTIF Deflectometer

The purpose of the deflectometer is to measure the elastic response of a pavement under the passage of a moving wheel load. The deflectometer, in normal field operation, is positioned between dual stationary tires and, as the vehicle is moved away, readings are taken of the vertical pavement rebound at 50-mm intervals up to 5 m distance, then every 500 mm up to a maximum of 15 m. The method used at CAPTIF is described below.

The deflectometer comprises two instruments—the deflection beam itself and a distance-measuring device. The deflection beam is fabricated from box-section aluminum, with the only moving parts being a lockable hinge section for easier transportation and a height-adjusting wheel for vertical alignment. The beam rests on three feet, two at the midpoint and one at the operator's end. The beam is weighted to balance on these feet to allow a vertical gap-measuring sensor to be suspended above a target disc placed on the pavement surface between the vehicle's tires. The electronic components are contained within the aluminum box section. The distance-measuring device consists of a revolving drum, supported on a stand and damped by a friction screw, attached by a wound length of thin nylon cord to the vehicle. Around the flanges of the drum are drilled a series of equally spaced holes, and an optical sensor counts the passage of the holes as the drum is rotated by the vehicle moving away. The sensor is wired to the electronic data capture system in the beam and thence to the Psion storage computer. The drum is rewound by a free-wheeling crank handle after each set of readings. Figure 5.1 shows the CAPTIF deflectometer.

Because the DIVINE project required the SLAVE to be fitted with single wheels, the wheels on the test vehicles had to be changed to standard 10.00R20 dual wheels before each deflectometer testing. The deflectometer operator controls the position of the SLAVE vehicles using a cordless remote control throughout the testing. This control allows vehicle speeds up to a brisk walking pace in both directions.

Deflections were measured at each station for each wheelpath. The transverse position of the SLAVE vehicle was set to correspond to the wheelpath to be measured. The SLAVE was then stopped and the deflectometer apparatus was moved onto the track.

After positioning the target disk on the centerline at the station to be measured, the deflectometer was placed tangentially to the centerline, with the gap sensor over the target, and an initial gap of 2 to 3 mm was set using the foot-adjusting wheel. Using a safety stop to prevent running over the beam or the operator, the vehicle was reversed over the target and gap sensor so that they were between the dual tires, 100 mm ahead of the axle. The distance-measuring device was then connected by the operator's assistant and the data corresponding to the station were entered into the Psion computer. When ready, the vehicle was moved away slowly, but steadily. Deflection readings were taken at 50-mm intervals up to a distance of 4 m to conserve memory in the Psion computer. The 4-m distance was sufficient to capture the full deflection bowl. When readings were completed, data captured by the Psion computer were downloaded to the HP Vectra via the Psion communication link in the same manner as the CAPTIF profilometer data.

After one wheelpath was complete, the deflectometer was moved off the track and the SLAVE was run up to speed from the control room so that the test vehicle could be repositioned on the other centerline.

Falling Weight Deflectometer (FWD)

The Dynatest FWD is a computer-controlled, hydraulically operated deflectometer towed behind a vehicle that carries the data acquisition and computing equipment. A circular foot of a set size is placed on the surface of the pavement and a known weight is then dropped from a known height. The weight and the height are adjustable. The reaction to the weight is measured with a load cell, and the deflection waveform is measured by velocity sensors (geophones - integrated to obtain displacement) set at given distances from the point of impact. The correlation of the amplitude of the waveforms and the time taken to travel to the distant sensors can be backcalculated to give the equivalent deflection bowls and moduli of the pavement layers.

After the first FWD tests, a method of towing the FWD behind the SLAVE vehicle was developed that allowed more accurate placement of the FWD plate as the FWD trailer followed exactly along the centerline to be measured. Safety was also improved by removing the possibility of a collision between SLAVE and the FWD vehicle and trailer. Data were captured on a floppy disk on the FWD computer and subsequently copied to the HP Vectra at the end of a testing interval.

5.4 PAVEMENT STRAIN RESPONSE INSTRUMENTS

The deflections of each layer of the pavement were measured by two methods. The Bison coil transducers, normally used at CAPTIF, were supplemented by partial deflection gauges (PDG) supplied and installed by ARRBTR. H-bar strain gauges supplied by ARRB were used to measure horizontal strain at the bottom of the AC layer. A plan view of the layout of the various gauges is shown in figure 5.2.

27
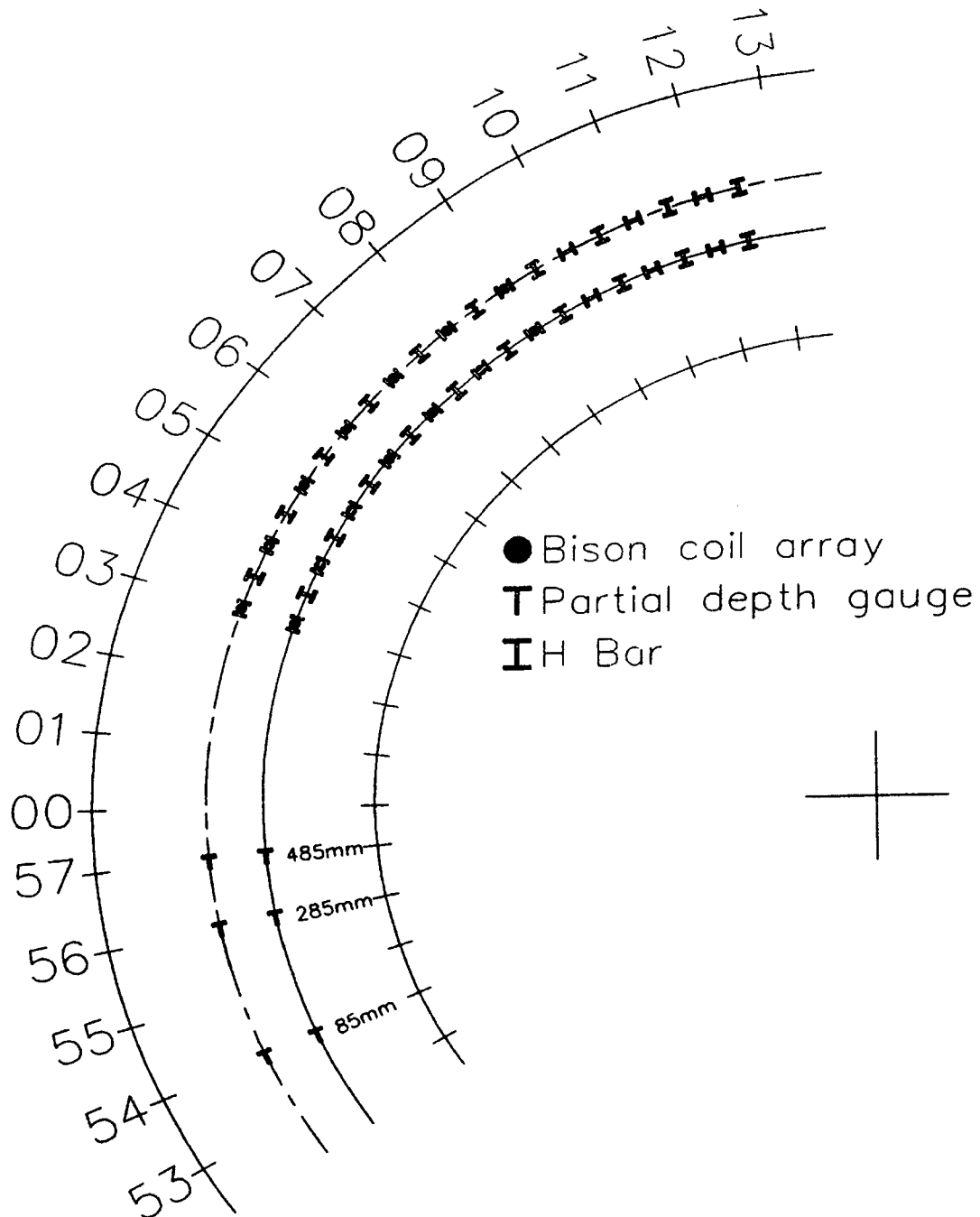
Figure 5.2. Layout of gauges.

Bison Strain Coils

Bison strain gauges were installed in all three layers at each of the six stations (stations 04, 05, 06, 07, 08, and 09). For both inner and outer wheelpaths, there were a total of 36 Bison coil strain measurement locations. The Bison strain coil sensors work on the principle of inductive coupling of free-floating wire-wound disks. The signal conditioning and data capture system has been refined at CAPTIF over several years from a prototype Canadian system. The signal

28

conditioning boards are housed in two cabinets at the side of the track adjacent to the sensors, and a multi-core cable runs back to an interface board in the HP Vectra PC. An infrared trigger beam detects the approach of the vehicle to be measured, assists in data capture, and monitors vehicle speed.

The data acquisition software can capture the output of six coil pairs at one time. The SLAVE was run up to the test speed of 45 km/h and measurement parameters were entered into the Vectra PC. Data were collected over 10 laps and were averaged.

During trafficking, pavement deformation moved some of the coils out of range and their readings were invalid. However, 26 of the 34 coil pairs installed performed correctly until the end of loading.

Partial Deflection Gauges (PDGs)

PDGs were inserted to measure displacements in the pavement layers and the top 200 mm of the subgrade.

PDGs measure deflections relative to the surface at one depth within the pavement. The PDG is a displacement transducer placed in a loose plastic tube that is installed in a drilled hole in the pavement. One end of the transducer, with a light spring-loaded core, is fixed to the surface anchor and the other end is anchored at the bottom of the tube sitting at the desired depth. ARRBTR initially supplied two PDGs and signal conditioning modules to be attached to three locations in each wheelpath, measuring deflections in the asphalt and basecourse layers, and in the complete pavement to the top of the subgrade. Later, additional gauges and conditioning modules were supplied to enable simultaneous measuring of the PDGs in each wheelpath without having to stop SLAVE and move the gauges. The gauges were fixed in place only for the duration of the measurements because permanently installing the cables under the asphalt may have compromised the pavement performance.

The ARRBTR data acquisition software was installed on the HP Vectra that was connected to the signal conditioning modules by serial cable. The gauges were calibrated before each test and measurements were triggered manually as the SLAVE vehicles passed over the gauges at both 45-km/h and 6-km/h speeds. Data were viewed graphically after each run and, if invalid, the data were rejected and the run repeated.

Horizontal Strain Gauges

ARRBTR supplied 40 H-bar strain gauges that were placed at the top of the base course at intervals of 500 mm along each wheelpath centerline over 10 stations (from station 3 to 13) of the track. The gauges were orientated to measure, alternately, transverse and longitudinal strains. The survival rate of the gauges during construction was expected to be about 50 percent, but, in the event, all the gauges survived.

ARRBTR's data acquisition system was supplied with six channels only, for economic and logistical reasons. To allow quicker and easier monitoring of the gauges, IRL and CAPTIF staff subsequently developed a system based on CAPTIF's HP3852A data acquisition computer.

When this system was fully commissioned it could monitor 20 H-bars simultaneously (one complete wheelpath) and had the advantage of being automatically triggered by an infrared beam detecting the approach of Vehicle A or Vehicle B, respectively. Data capture was controlled by an HP-IB link between the HP3852A and the HP Vectra PC.

The SLAVE was run at steady speeds of 45 km/h and 6 km/h and measurement parameters were entered into the HP Vectra. The software monitored the vehicle speed and, when it settled to a speed within the specified tolerance, readings were automatically triggered. The captured data were filtered and graphed to check for erroneous readings before being saved. Once readings for one wheelpath were complete, the second wheelpath was connected to the HP3852A.

The gauges began to fail from the beginning of pavement loading. As each gauge failed, its circuit had to be bridged out to prevent erroneous readings on the remaining gauges. By 300k cycles all the H-bars had failed.

5.5 PAVEMENT TEMPERATURE

Thirteen temperature sensors were used to measure pavement temperature. Five sensors were placed at the top of the basecourse and another five above them between the two asphalt lifts. They were equally spaced around the track just inside the inner wheelpath. Three sensors were placed on the surface of the inner perimeter of the track at equal spacing to measure air temperature. These sensors were fitted with shrouds to minimize temperature fluctuations caused by air movement from the passing of the SLAVE vehicles. The temperature was set at 20°C during the test.

Temperature readings from all the sensors were logged hourly by a Taupo field data logger located at the center of the track. Two of the temperature sensors failed toward the end of pavement loading.

5.6 CRACKING

High-quality draughting film proved to be the best medium for recording the cracks: it had exceptional clarity; it was very tough; and it was stable at different temperatures and over time. The film was cut into 58 sheets, each dedicated to a particular station on the track. A clear Perspex template board was placed across both wheelpaths at each station and the appropriate sheet of film placed over the board. Visible cracks were traced onto the sheet and marked with the current date and load cycle. The cracks did not show through to the sheet unless they were first highlighted on the pavement with crayon.

Once marked, the sheets were hung on a wall, measured with a cartometer for both transverse and longitudinal cracking in each wheelpath, then carefully photographed using black and white film, camera tripod, and halogen lighting. The photographic film was digitized at the end of the project for computer storage.

CHAPTER 6. MEASUREMENTS AND DATA COLLECTION

The DIVINE Element 1 test data set collected at CAPTIF is one of the most comprehensive data sets ever assembled for the purpose of addressing the hypotheses and questions related to vehicle dynamics and pavement performance.

Because the objective of the experiment was to establish the relative deterioration of nominally identical pavements under different suspension types, it was necessary to carry out a number of different measurements in the course of the experiment to monitor deterioration. Similarly, in order to make suitable and relevant comparisons, it was necessary to ensure that the initial condition of each of the pavements tested was also well known. From these data, the similarity of the pavements at the outset of the test could be determined, as well as changes in the absolute condition of each pavement. This chapter provides a summary of the limitations, validity, and meaning of the data collected. Measurements are presented in terms of "zero measurements" (measured before the commencement of trafficking), the measurements made during the loading tests, and the data collected at the end of tests (post-mortem tests).

6.1 ZERO MEASUREMENTS

A summary of the outcomes of the measurements taken before trafficking of the pavements (zero measurements) is listed in table 6.1 and briefly described below.

Profiles

The longitudinal profile appeared uniform when plotted against angular position; however, as the radius decreased, so did the wavelength of any unevenness. This would then correspond to a higher frequency, which would generate a higher International Roughness Index (IRI). In the test, it was proposed that this would be offset by the inner vehicle operating at a lower speed. The level of IRI values observed is relatively high for a new pavement. It is thought that this is due to the hand-screening used during construction, which caused the unevenness to have shorter wavelengths than would be the case when using a paving machine.

Transverse profiles were measured at each station across the pavement.

Tire Stiffness and Imprint

The tire deflections and imprints, measured as incremental loadings, were applied statically to the vehicles. The imprints showed the classic expected shape change from approximately circular at low loads to rectangular at high loads (however, the authors do not know if these will be made available for distribution). A simple linear regression on the tire-deflection data gave a tire stiffness value of 1.28 kN/mm. This value of stiffness is in line with typical values for wide single tires.

Table 6.1. Comparative trafficking conditions of the two suspension systems (during or after construction).

Key Dynamic Characteristics	Air-Suspended Test Wheel (inner wheelpath)	Steel-Suspended Test Wheel (outer wheelpath)	Comment
Pavement mechanical & structural properties at construction:			
- surfacing thickness			
(mean)	87 mm	88 mm	no sig. diff.
(std)	6.3 mm	6.8 mm	no sig. diff.
- base course thickness			
(mean)	198 mm	199 mm	no sig. diff.
(std)	8.6 mm	9.5 mm	no sig. diff.
- surfacing FWD deflections (expressed as deflection per unit loading)			
(mean)	0.95 mm/kPa	0.89 mm/kPa	no sig. diff.
(std)	0.089 mm/kPa	0.090 mm/kPa	no sig. diff.
- base course FWD deflections			
(mean)	1.79 mm/kPa	1.74 mm/kPa	no sig. diff.
(std)	0.17 mm/kPa	0.18 mm/kPa	no sig. diff.
- subgrade FWD deflections			
(mean)	2.48 mm/kPa	2.38 mm/kPa	no sig. diff.
(std)	0.20 mm/kPa	0.22 mm/kPa	no sig. diff.
- equivalent pavement stiffness			Mean combined stiffness of two layers was 10 percent higher in outer wheelpath.
(mean)	7.69×10^8 MPa.mm^3	8.54×10^8 MPa.mm^3	
(std)	1.47×10^8 MPa.mm^3	1.87×10^8 MPa.mm^3	
Pavement surface properties			Outer wheelpath was smoother at the start of the test.
- IRI (initial)	4.8	4.1	
Dynamic wheel forces			Frequency of steel suspension was relatively low and damping relatively high DLC in outer wheelpath was relatively high.
- suspension frequency	1.41 Hz	1.93 Hz	
- suspension damping	17 percent	21 percent	
- DLC (initial)	0.05	0.17	

The tire deflections were as tabulated below:

Vehicle Load (kN)	Tire Deflection (mm)
31	21.0
40	28.1
49	35.3
58	42.0

Suspension Stiffness

The suspension stiffness was measured by recording the displacements as load increments were applied to the vehicles. The results of these measurements are tabulated in table 6.2 and shown in figure 6.1. Note that for air suspension, it was necessary to measure off the shock absorber bell crank, which moves in the opposite direction.

Table 6.2. Suspension deflection versus vehicle load.

Vehicle load (kN)	Vehicle A - steel suspension deflection (mm)	Vehicle B - air suspension deflection (mm)
31	21.0	-130
40	28.1	-114
49	35.3	-82
58	42.0	-55

Suspension Characterization

The vehicle suspensions were characterized by monitoring the accelerations of each vehicle while that vehicle was driven at crawl speed over the standard 80-mm ramp defined in EC Directive 90/486/EEC. The resulting computed wheel force signal was then analyzed to determine the fundamental bounce frequency of the suspension and its damping, as previously reported in section 2.2 (air suspension of 1.41 Hz with damping of 17 percent, and a steel suspension of 1.93 Hz with damping of 21 percent). The accelerometers used had a linear response in the 1- to 5000-Hz frequency range with an accuracy of ±5 percent.
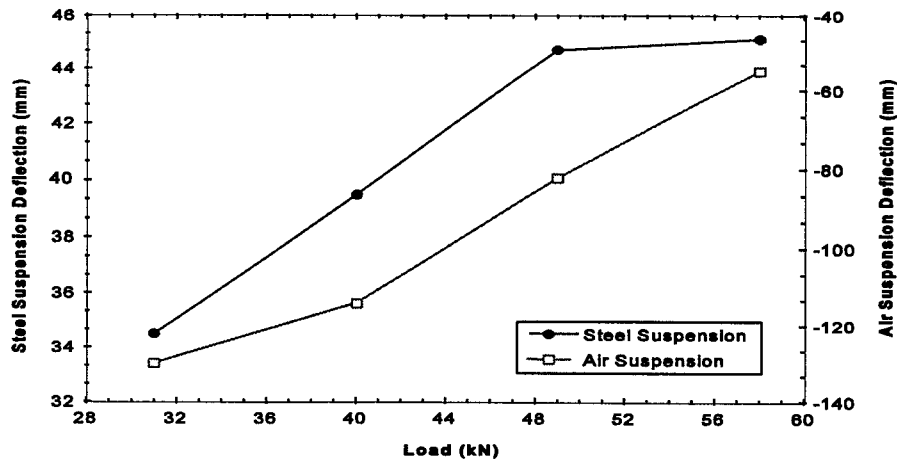
Figure 6.1. Stiffness of suspensions.

The wheel forces measured by the accelerometers were also monitored at the operating speeds when the steel springs become effectively locked. In this case, a natural frequency of 2.55 Hz was measured. Note that the natural frequency of a 5000-kg mass on a spring (wide-base single tire) with stiffness of 1.28 kN/mm is also 2.55 Hz. This indicates that during normal operation the steel-leaf spring is effectively locked and the vehicle bounces on its tire.

Pavement Primary Response

The pavement response to vehicle loads of 40, 49, and 58 kN at 45 km/h were measured. It was intended that these measurements be taken with each vehicle in its test wheelpath. Due to a misunderstanding these tests were conducted with the vehicles in the opposite wheelpaths. However, as the purpose of these tests is to determine the pavement response to changes in load and as the pavement is relatively uniform transversely, the measurements as presented fulfill their function. Again, the topic report presents a full description of the responses recorded.

Dynamic loads were induced by running the vehicles at 45 km/h over two bumps—a 300- by 25-mm bump, which induces axle hop response, and a 4000- by 25-mm bump, which induces body bounce response. The pavement responses to these loads were measured. The bumps were then moved by 500 mm and the tests repeated. As with the previous test, these tests were undertaken with the vehicles in the opposite wheelpath; however, these tests measure the pavement response to dynamic load as required.

Considerable difficulty was experienced in finding a satisfactory method of anchoring the "bumps" to the pavement in the CAPTIF environment where the vehicles traverse the bump every load cycle. The results of these measurements are presented in the report on this topic. The CAPTIF deflectometer, which is a modified Benkleman beam device, was used to measure pavement deflections in response to 49-kN vehicle loads. These can then be compared with FWD tests using the same load. These comparisons of peak FWD deflections with peak CAPTIF deflectometer deflections on both inner and outer wheelpaths showed that the CAPTIF

34

deflectometer appears to consistently measure deflections approximately 25 percent greater than the FWD.

6.2 MEASUREMENTS DURING TRAFFICKING

During trafficking of the test pavements, measurements were carried out to establish the nature and rate of any deterioration in the condition of the pavements, and any changes in the dynamic loading applied to the pavements brought about by deterioration in the roughness of the pavement.

Two types of measurements were collected during the tests: a complete data set and a reduced data set. The number of load cycles between measurements specified in the project brief was (in thousands) 20, 30, 40, 60, 80, 100, 150, 200, 250, 300, then at intervals of 100. To reduce the time and cost of collecting and processing the data, the complete set of measurements was to be collected every third measurement cycle, with a subset of the most critical data (reduced data set) collected every measurement cycle. Because the rate of pavement deterioration was slower than expected, the interval between measurements was increased to 100k load cycles from February 1995.

The complete data set includes:

Performance measurements. The longitudinal profile was measured in the center of each wheelpath and at 0.45 m on either side of each wheelpath using the Dipstick. These data were then processed to produce IRI values and power spectral density (PSD) functions for the longitudinal profiles.

The transverse profile was measured at each of the 58 stations around the track with use of the CAPTIF profilometer. The vertical surface deformation (VSD) and rut depth on each wheel track were then determined from the transverse profiles. The VSD is the relative surface elevation changes for a given point on the pavement after being trafficked, and the rut depth is the difference between the highest and lowest elevation points of the pavement surface along the transverse section for each wheelpath.

Pavement surface cracking was recorded using the method described previously in chapter 5.

Structural condition measurements. The structural condition of the pavement was measured using both the FWD and the CAPTIF deflectometer at each station in each wheelpath.

Pavement primary response measurements. To ensure data quality, all primary response gauges were first zeroed and calibrated using FWD tests. During the tests, all data from the gauges were reviewed to determine whether any data were in error or corrupted. The only discrepancy found was that the PDG data measured under the FWD during the zero measurements and after the first loading interval (20k loading cycles) were invalid. Thus, the FWD tests during zero measurements were used to calibrate all primary response gauges to the same zero except for the PDGs.

For the H-bar and Bison strain data, first the average value of each of six subsets (two wheelpaths and three layers) for the response under a 60-kN FWD load at 0 loading cycles was determined (the 50-kN FWD load tests done at 20k loading cycles were not used because the pavement responses and condition had changed by then), then strain at each of the stations in each wheelpath was divided by the average value for the respective subset. Error analysis showed that the measurement error was about 50 μm/m. Readings from the H-bar tensile strain gauges in the asphalt concrete were off-scale at 0 loading cycles, so the FWD 50-kN load tests at 20k cycles were used as the initial values.

During trafficking, once triggered by the moving vehicles, all sensors in an array were scanned every 30 mm of vehicle travel, and a continuous bowl of strain/displacement versus distance traveled were recorded.

Vehicle suspension measurements. Each of the loading vehicles was driven over the standard EC bump at crawl speed and its response monitored. The typical bump test response of the suspensions are plotted in figures 6.2 and 6.3. The bounce frequency and damping rates calculated from the test provided an indication of any changes in the suspension behavior. Where these were substantial (a change in either value of more than 20 percent), the suspension was inspected and/or serviced.

Wheel force measurements. The wheel forces generated by each vehicle were measured at three steady speeds, namely the mean operating speed (45 km/h) and the upper and lower limits of the variation used in testing, during zero measurements. The wheel forces arising on each vehicle were also measured at 45 km/h in the other vehicle's wheelpath to provide additional information on the relationship between pavement profile and dynamic response.

The reduced data set includes:

- Transverse profiles measured at every station in the 10-m section of track (stations 3 to 13), and at every sixth station over the remaining 48 m.

- Changes in cracking measured only in the 10-m section.

- No FWD but the CAPTIF deflectometer measurements.

- Wheel force bump tests at crawl speed; steady speed wheel force measurement at only one speed; pavement response measurements at only one speed.

- Longitudinal profiles only in the wheelpaths over the length of the track.

6.3 MEASUREMENTS AFTER TRAFFICKING

After about 1.7 million cumulative loading applications, the final set of pavement and vehicle measurements were completed. The pavement post-mortem tests were conducted in December 1995 and the laboratory tests were done in February/March 1996. A further series of moisture content tests were performed in May 1996. The purpose of these investigations was to establish, if possible, the sources of the observed deterioration of the pavements. The investigation

36

Bump Test Response for Air Suspension
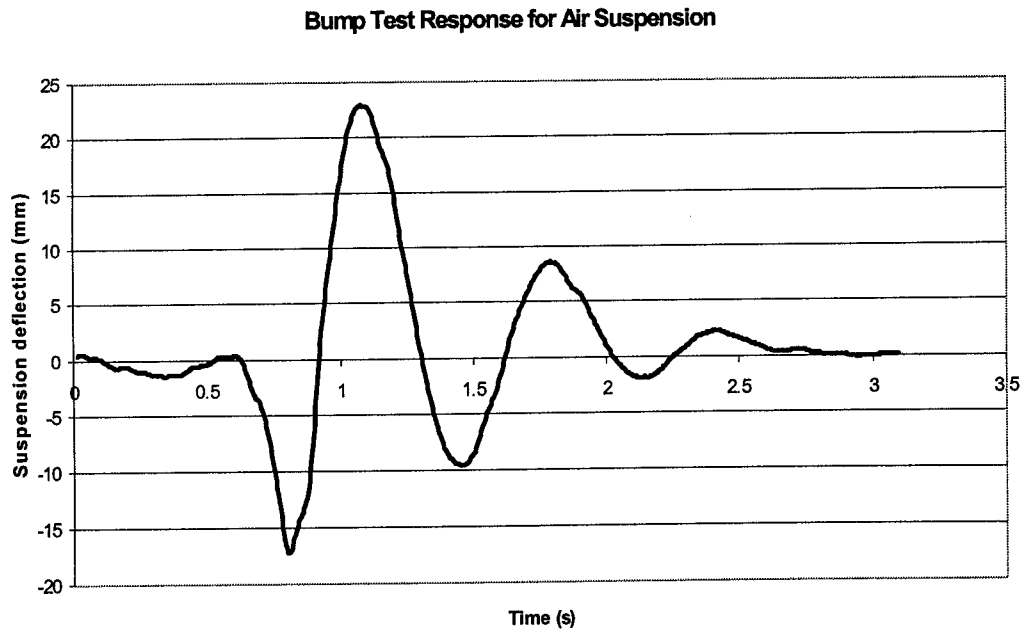
Figure 6.2. Bump test response of air suspension.

Bump Test Response for Steel Suspension
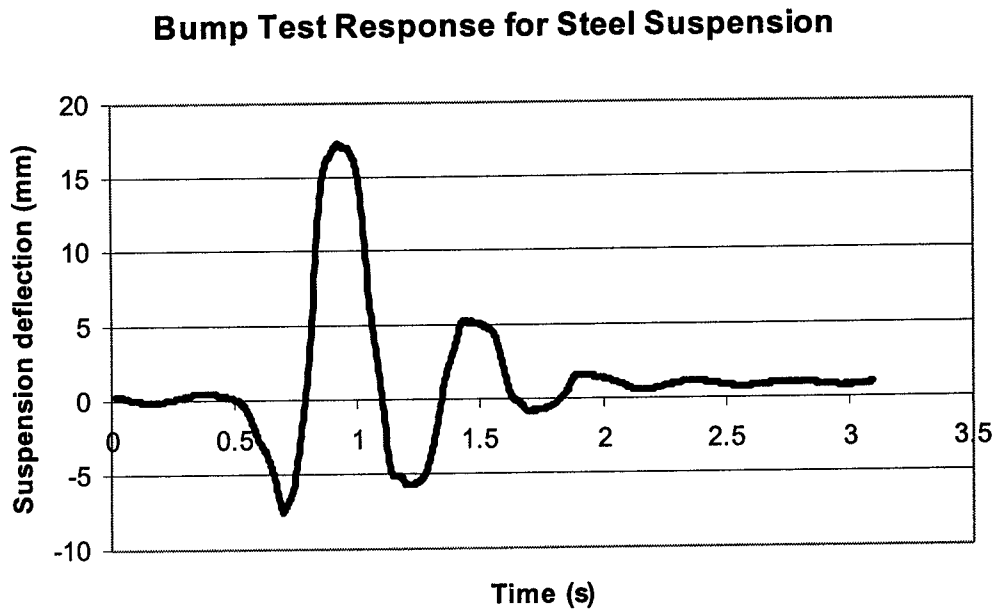
Figure 6.3. Bump test response of steel suspension.

included cutting cores from the asphaltic concrete for resilient modulus testing in the MATTA in the University of Canterbury Civil Engineering laboratories, excavating six transverse trenches through the asphalt and base course layers to measure the layer profiles and retrieve material samples for laboratory tests, and cutting six small holes through the layers to measure densities and carry out Loadman tests on the unbound base course and subgrade layers.

The Loadman consists of an aluminum tube (diameter 132 mm) containing a free-moving 10-kg steel weight. A circular loading plate of 132 mm diameter and an accelerometer are attached to the base of the tube, with control, electronics, and weight-supporting magnet positioned at the top of the tube. Prior to testing the Loadman is tilted upward so that the free-moving weight slides to and contacts the magnet near the top of the tube. The Loadman is operated by placing its base on the surface of the pavement or subgrade layers and then activating the electronics. An electro-magnet releases the weight and the onboard electronics records the response and computes the material modulus based on Boussinusq's theory.

The following vehicle/pavement tests were carried out:

- Transverse profiles at 58 stations.

- Longitudinal profiles with use of laser profiler and Dipstick on five wheelpaths (095, 135, 175, 215, and 255 cm).

- Pavement deflections with use of CAPTIF deflectometer and FWD, 58 stations on 2 wheelpaths.

- Crack measurements and photography.

- Bison strains and PDG deflections under 49-kN vehicle load at 20, 30, 40, and 45 km/h. 45-km/h vehicle speed under 49-, 40-, 30-, and 20-kN load. One wheelpath only.

- Dynamic wheel forces. 49 kN at 20, 30, 40, and 45 km/h. 45 km/h at 49, 40, 30, and 20 kN. Both normal and reverse wheelpaths.

Inspection Trenches

To evaluate the condition of the pavement, 6 full-width inspection trenches were excavated across the track and 12 potholes were excavated through the layers. The locations of trenches were selected on the basis of maximum, average, and minimum rut depths for each wheelpath. In all of the trenches, a diamond saw cut was made across the pavement at the station mark and 500 mm before the station mark. The asphaltic concrete was removed and samples of the base course were taken from the trafficked area below the wheelpath used for the selection of the trench. An additional base course sample was taken from an untrafficked area in the trench. The remainder of the base course was removed and the top of the subgrade was scraped clean. Profiles of the surface and each layer interface were taken with the manual profile beam and compared with the profiles taken during the pavement construction. The changes in pavement layer thickness are

38

Table 6.3. Changes in pavement layer thickness at the end of experiment (mm).

Inner Wheelpath						
Layer	Station					
	5	8	18	21	26	39
AC	4	5	4	-2	5	6
BC	13	10	1	9	5	2
SG	-6	-2	1	-1	1	1
Outer Wheelpath						
AC	0	5	5	2	4	6
BC	14	12	13	25	1	1
SG	-4	-4	-1	6	0	2

Positive values represent reduction in layer thickness.

shown in table 6.3. As can be seen in the table, the only station with any measurable compression in the subgrade was station 21. Stations 04 and 08 had an increase in the subgrade level due to the presence of the Bison coils when the final profiles were measured. The measured compaction in the asphaltic concrete layer under trafficking was consistent for most of the stations. The excavations revealed that most of the vertical deformation occurred in the unbound granular layer. The average maximum compaction within the asphaltic concrete in both the inner and outer wheelpaths was 4 mm; there was negligible compaction in the subgrade under both types of suspensions. The average maximum compaction within the unbound granular base course layer in the inner (airbag suspension) and outer (steel suspension) were 7 and 11 mm, respectively. The base course aggregate properties were the same in each wheelpath.

The 12 spot holes measured 0.7 m by 0.7 m and were excavated through the layers in order to measure densities and conduct Loadman tests on the unbound base course and subgrade. The 12 spot holes were 3 each from the cracked and uncracked areas of the pavement in both wheelpaths. Density and Loadman tests were performed on the base course and subgrade. The base course was also sampled for gradation, angularity, and moisture content measurements. During the excavation of the spot holes, the base course was carefully removed from the base course/subgrade interface. The result of this work showed that the base course had not penetrated into the subgrade and there was no measurable rutting of the subgrade; the single exception was that at station 21, the base course had punched into the subgrade by up to 5 mm.

Subgrade and Base Course

Nuclear density meter (NDM) tests were conducted on the base and subgrade in the spot holes. The technique used to excavate the trenches made the NDM tests unsuitable on the base course and subgrade in the trenches. Two sand replacement density tests were done on the base course

as a further check on the accuracy of the NDM. These results showed that the dry density results from the NDM are about 2 to 3 percent lower than the sand replacement densities. The measured base course densities were either less than 3 percent, or in the range of 7 to 18 percent below the target density of 2100 kg/m³. One possible reason for this variation is that when the asphaltic concrete slab was removed from the hole, the tack coat applied to the base course during construction removed part of the top layer of stones from the base course. This required removal of some additional material from the top of the base course in order to get a flat surface for the NDM. The NDM testing on the subgrade gave very consistent results with the results as constructed. The final dry density values were mostly within the range of 97 to 102 percent of the construction target density of 1870 kg/m³. A total of 13 of the 38 tests were greater than 110 percent of the target value, which shows that the subgrade density increased slightly due to the trafficking.

The Loadman was used on the base course in the spot holes, and for the subgrade it was used in the spot holes as well as post-mortem trenches. The Loadman results are reasonably consistent for both wheelpaths, with the exception of station 39 in the inner wheelpath. No reason can be given for such a high value, when compared with the other test results.

Because most of the rutting occurred in the unbound granular base course, extensive material tests have been conducted on the base course aggregate in the University of Canterbury Civil Engineering laboratories. Moisture content, broken faces (angularity), and sieve analyses of 23 samples were undertaken, representing various stations and both wheelpaths. All of the gradation results showed that the gradation still came within the material specification.

In May 1996, additional moisture content tests were done in the vicinity of the rutting near station 21. The holes that were excavated for the first series of tests limited the locations of further tests. Fifteen further base course and subgrade samples were removed for moisture content tests. When these results are combined with the first set of results, a comprehensive picture of the moisture content of the base course can be examined in the area of pavement distress. The results are shown in table 6.4. As it can be seen, the variation of the moisture contents is minor and previous laboratory tests have shown that base course density remains constant for moisture contents between 1.5 and 4.0 percent. From this it could be concluded that the extensive rutting in the base course around station 21 in the outer wheelpath was not due to excessive moisture in the base course.

Table 6.4. Moisture content in the base course and subgrade at the completion of test.

Station	Wheelpath	Moisture Content (percent)		Date Sampled
		Base Course	**Subgrade**	
5	215	2.2		08/12/95
5	255	1.4		08/12/95
8	095	1.3		08/12/95
8	135	1.4		08/12/95
12	215	1.5		08/12/95
14	135	1.6	10.7	14/05/96
14	175	1.6	10.7	14/05/96
14	215	1.5	10.9	14/05/96
16	135	1.5		08/12/95
17	215	1.7	11.1	14/05/96
18	095	1.8		08/12/95
18	135	1.3		08/12/95
20	175	1.8	12.1	14/05/96
20	135	1.6	11.3	14/05/96
20	215	1.9	11.9	14/05/96
21	215	2.7		08/12/95
21	255	2.5		08/12/95
22	135	1.6	9.8	14/05/96
22	175	1.7	10.2	14/05/96
22	215	1.6	10.9	14/05/96
24	135	1.5	10.2	14/05/96
25	215	2.0	11.0	14/05/96
26	215	1.6		08/12/95
26	255	1.6		08/12/95
28	135	1.6	10.5	14/05/96
28	175	1.6	11.0	14/05/96
28	215	1.6	11.8	14/05/96
29	135	1.6		08/12/95
29	215	2.1		08/12/95
34	135	1.4		08/12/95
34	215	1.2		08/12/95
39	095	1.7		08/12/95
39	135	1.6		08/12/95
41	215	1.6		08/12/95
46	135	1.2		08/12/95
48	215	1.6		08/12/95
55	135	1.6		08/12/95
56	215	1.9		08/12/95
Mean		1.66	10.94	
Standard Deviation		0.307	0.626	

Asphaltic Concrete

Three cores from each of the uncracked and cracked stations, in both wheelpaths (a total of 12 cores) were tested for resilient modulus (MR) in the MATTA. It was convenient that these cores were located adjacent to the full-width pavement trenches. The modulus tests were performed at three temperatures on each sample: the minimum, intermediate, and maximum asphaltic concrete loading temperature (6°C, 20°C, and 32°C). The results showed no clear distinction between the modulus values of the cracked and uncracked cores. A total of six cores were removed from the pavement where cracks went through the core. Due to the heat generated during the coring, any cracks that were present across the cut were not visible in the removed sample. This is possibly because the heat generated during the coring "mended" the cracks on the end of the sample. In an attempt to determine whether the cracks started at the top or the bottom of the asphaltic concrete layer, the samples were placed in the MATTA and an increasing (at the rate of 20 N/s) diametrical force was applied along the axis of the crack to induce a tensile stress perpendicular to the crack axis (the crack is vertical, so the vertical applied load creates a horizontal tensile stress in the cored specimen). The samples were loaded until the sample split open along the initial crack line. Observing the specimen during loading and inspecting the cracked specimens, the cracking commenced at the surface of the asphalt and spread downward to the bottom of the asphalt.

The pavement materials appear to have changed very little over the life of the pavement. The surface rutting occurred through densification of the asphaltic concrete and base course layers only. The modulus of the asphaltic concrete has increased in value, which could be due to the densification of the asphaltic concrete under loading. The base course layer showed the greatest consolidation under loading, but there was no significant difference in the gradation tests. From extensive testing on stations 14 to 28, it would appear that the high levels of rutting in the outer wheelpath were not caused by excessive moisture in the base course. The subgrade failed to show any significant signs of rutting and the subgrade properties remained constant throughout the project with the exception of the region around station 21.

Close examination of some cracks in the asphaltic concrete showed that the cracks have mostly originated from the surface and were not full-depth cracks.

6.4 DATA ARCHIVING

The task of collecting, storing, and distributing data was assigned to the University of Canterbury, Christchurch, New Zealand. During the CAPTIF tests, 24 sets of tests were completed and 182 Mb of raw data were collected. Raw data for each test interval were gathered on the HP Vectra. When the next loading interval began, the previous recorded raw data were copied. Initial processing of the ASCII data from the profilometer and deflectometer was performed to produce worksheets for later analysis. Once the initial data processing was complete, entire data for a loading interval (in laps, i.e., load repetitions) were archived.

Raw data were made available on the network for project engineers to analyze using various software programs. The programs included the dynamic wheel force analysis software from IRL; the Roadface, a data analysis software for Dipstick profiles; the ARRB laser profile analysis

software; and programs written by CAPTIF staff themselves. The data were then collated for dispatch via E-mail to IRL in Auckland.

All data collected during experimental phases were inspected and verified for soundness. Data in error or corrupted were rejected . All "good" data were then stored into files of agreed format that are clearly identified and marked with type, date of collection, treatments applied, etc. The data were saved in ASCII format, which will allow any competent computer user to import the data into either a data base or spreadsheet program to meet their needs.

The data were processed from the raw state to suitable units of measurement and only the processed data were distributed. The distributed data include: units of microstrain for the H-bars and Bison coils; units of millimeters for the partial-depth gauges, FWD, CAPTIF deflectometer, transverse profiles, Dipstick profiles, and ARRB laser profiles; units of kN for the wheel forces; units of degrees Celsius for the temperatures; and units of meters for cracking. All construction and post-mortem data were also included.

CHAPTER 7. DATA ANALYSIS

The data analysis conducted by DIVINE was designed specifically to use the data collected during the accelerated loading test in the most meaningful way and to provide detailed evaluation of these data. The intent is to compare the results obtained under the air suspension with those obtained under the steel suspension. Initially, selected DIVINE team members conducted seven analysis tasks: data verification/validation, analysis of structural variability, analysis of road roughness, analysis of dynamic wheel force, analysis of pavement cracking, analysis of rut depth, and analysis of pavement primary response. The data analyses evaluate those variables that could affect the comparison of steel versus air suspensions, such as variations in pavement construction, material properties, and pavement deterioration. Original data analyses task descriptions are given in appendix C. This chapter attempts to identify and compile the major findings of all of the conducted analyses to offer readers a clear perspective of the overall work accomplished. Many of the results have been presented elsewhere in this report. In addition, the results from other types of analysis, such as the analyses of scrubbing effect and tire footprint, are given in appendixes A and B.

7.1 PAVEMENT PRIMARY RESPONSE

Cross correlations were examined, in the space around the track, of: (1) the initial primary response (longitudinal, transverse, and vertical strains) in the pavement at the instrumented locations, and the temporal existence of rut depth, vertical deformation, and cracking; (2) horizontal and transverse strains; and (3) the dynamic loading and vertical strains in three layers. The partial depth gauges were not included because calibration to zero was not possible due to the invalid data produced at the time of the zero measurements. The calculated coefficients of correlation for those variable pairs are plotted in figures 7.1 to 7.6.

Correlation of vertical base course deformation and vertical compressive strains. Post-mortem excavations revealed that the vertical deformation occurred primarily in the unbound granular pavement layer. There is a good correlation (coefficient of correlation ranging between 0.70 and 0.95), after 100k cumulative loading cycles, between vertical compressive strains in the base course and the vertical deformation for the inner wheelpath (air suspension wheel load), which suggests that the vertical deformation in the inner wheelpath is due to the pavement condition, not loading. There is also a good correlation (0.92) between zeroed vertical strains and vertical deformation in the outer wheelpath (the steel suspension) at 100k loading cycles, implying that the pavement condition did produce the vertical deformation up until then. However, after that, the correlation diminishes substantially in a definite trend, to only 0.4 at 1.5×10^6 loading cycles. The correlation analysis results are plotted in figure 7.1.

Overall, there is substantial scatter in the data during the first 100k loading cycles, then the correlation in the inner wheelpath remains consistently high while the outer wheelpath drops off, again supporting the above statements.
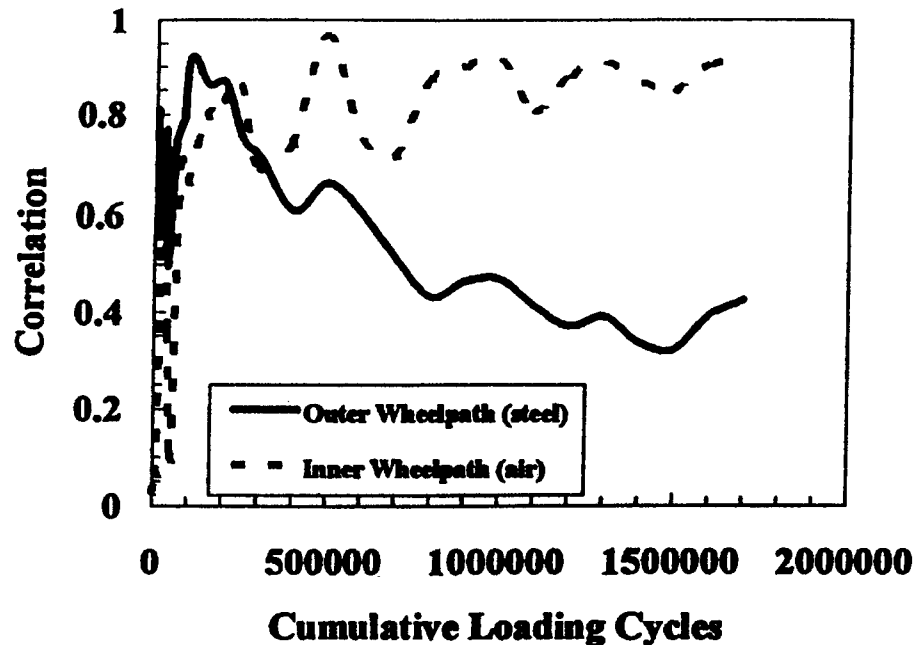
Figure 7.1. Cross correlation between vertical layer compressive strain and vertical deformation in base courses.

There is no correlation between the vertical compressive strain in the lowest subgrade strain gauge and vertical deformation for both wheelpaths. The correlations for the strains on the top of the subgrade in the inner and outer wheelpaths are 0.8 and 0.2, respectively.

Correlation of vertical AC deformation and horizontal tensile strains. There is a poor correlation between the horizontal tensile strains and the vertical deformation in both wheelpaths, except for the longitudinal strains in the inner wheelpath, which has a maximum coefficient of correlation of 0.9 at 100k cumulative loading cycles and then gradually reduces to 0.6 (see figure 7.2).

Correlation of cracking and vertical layer compressive strain. Generally, there is no correlation between surface cracking and the vertical compressive strains in the pavement and subgrade indicating that weaker base course and subgrade locations did not influence the occurrence of surface cracking. However, there is some correlation (coefficient of correlation of 0.77) between the vertical compressive strain in the lower subgrade and surface cracking in the inner wheelpath (see figure 7.3). This suggests that the surface cracking was influenced by higher deflections in the lower subgrade.

46
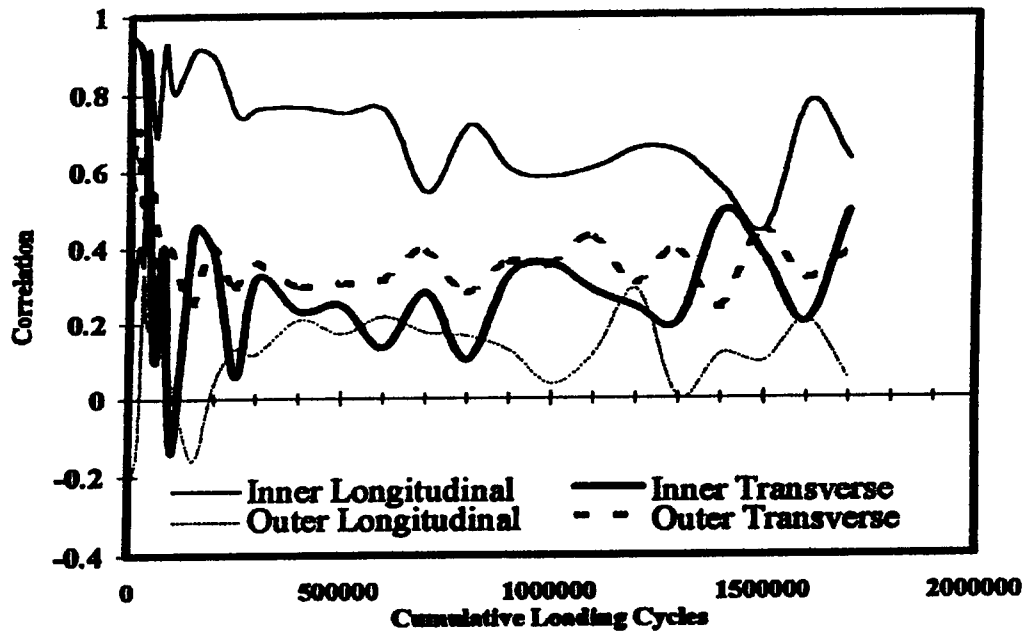
Figure 7.2. Cross correlation between horizontal tensile strain and vertical deformation in asphalt concrete.
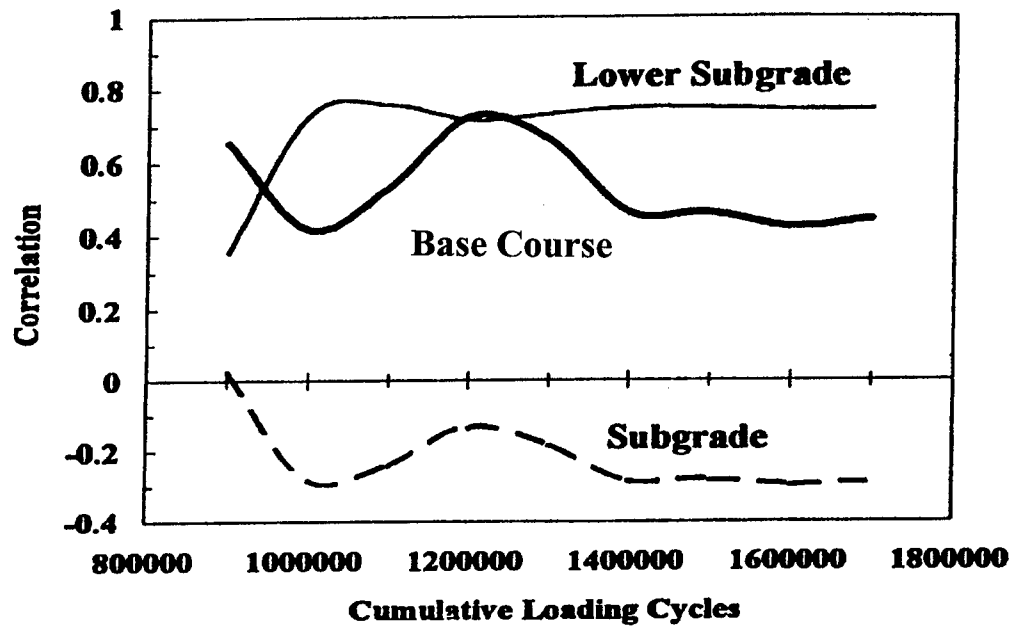
Figure 7.3. Cross correlation between vertical layer compressive strain and surface cracking.
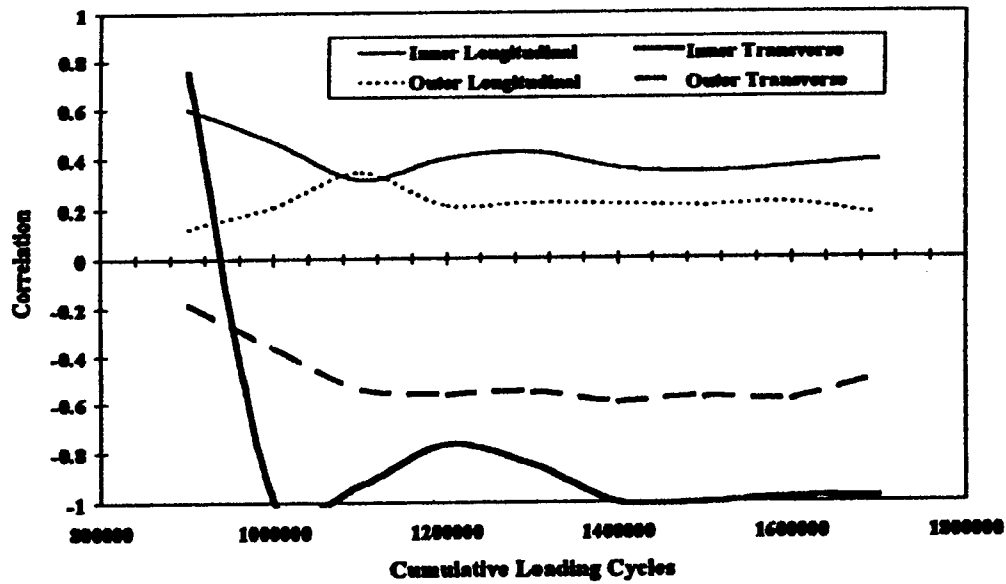
Figure 7.4. Cross correlation between horizontal AC tensile strain and surface cracking.

Correlation of cracking and horizontal AC strain. In the inner wheelpath, there is a poor correlation (coefficient of correlation of 0.4) between initial longitudinal strains and cracking, and a negative correlation between transverse strains and cracking. In the outer wheelpath, there is weak correlation between cracking and either transverse (-0.6) or longitudinal (0.2) tensile strains in the asphalt, indicating that the cracking was not caused by localized weak spots in the pavement. Coefficients of correlation of cracking and horizontal strain are plotted in figure 7.4.

Correlation of dynamic loads and vertical subgrade compressive strains and horizontal tensile strains. The analysis results are plotted in figures 7.5a and 7.5b. In the inner wheelpath, the coefficient of correlation between initial subgrade compressive strains and dynamic load is 0.6 during the first 900k loading cycles, and a better correlation (0.5 to 0.9) for the base course, initial pavement condition led to roughness, which, in turn, induced higher dynamic loads. In the outer wheelpath, there is no correlation between initial strains and dynamic loading (figure 7.5b).

In figure 7.5a, the coefficient of correlation between the transverse tensile strains and dynamic loading under the inner wheelpath varies greatly, from -1 to 0 to +1, whereas there is no correlation in the outer wheelpath (see figures 7.5a and 7.5b). Initially, there is no correlation between AC longitudinal strains and dynamic loading in the outer wheelpath, though the correlation does increase to 0.4 after 900k cumulative loading cycles. The correlation for the same factors in the inner wheelpath oscillates about 0, indicating very weak correlation.

48
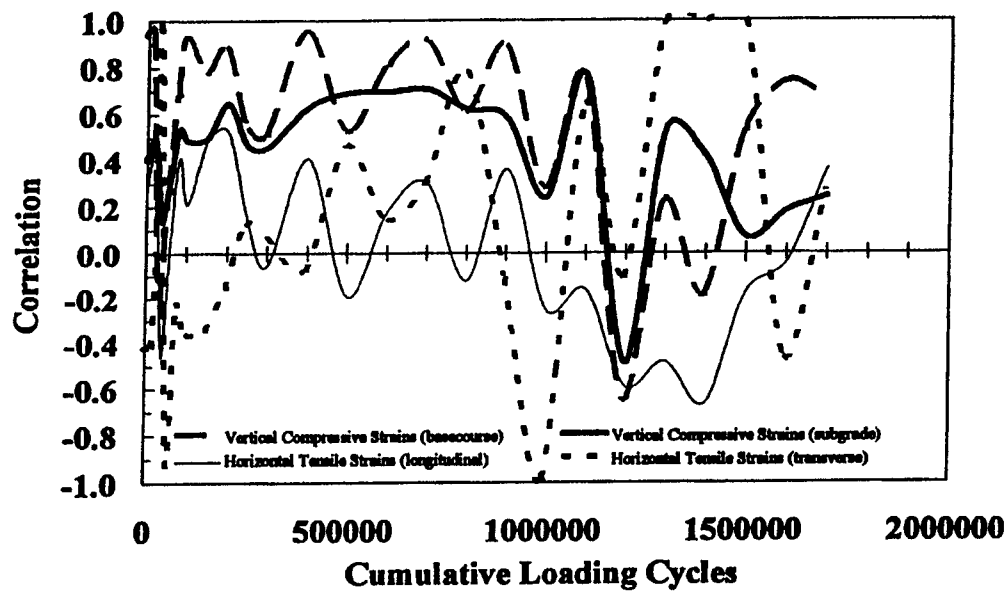
Figure 7.5a. Cross correlation between dynamic wheel forces and pavement strain responses, inner wheelpath, air suspension.
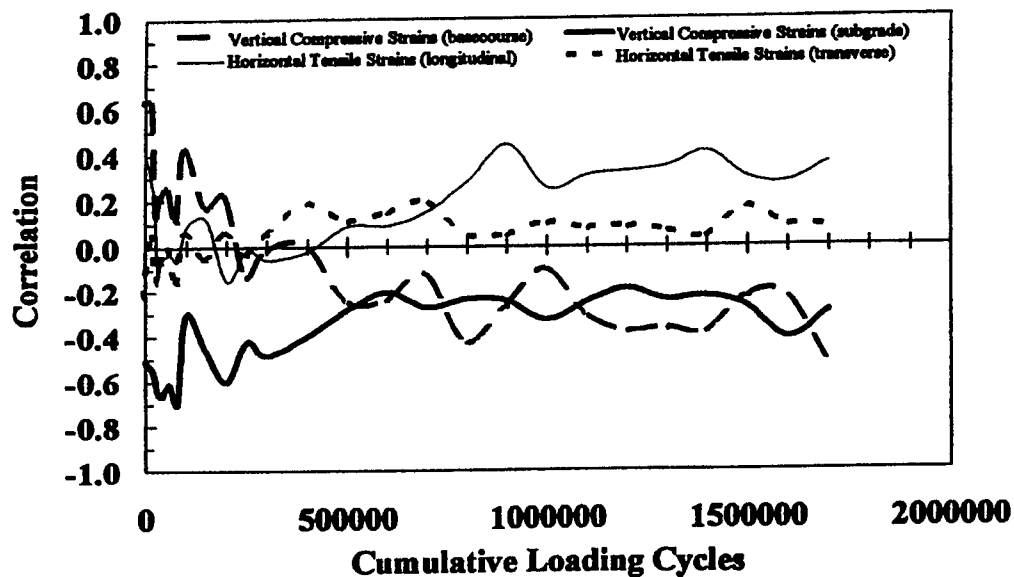
Figure 7.5b. Cross correlation between dynamic wheel forces and pavement strain responses, outer wheelpath, steel suspension.

49

7.2 DYNAMIC WHEEL FORCE

Between 27 October 1994 and 17 August 1995, the SLAVE applied 1.7 million 49-kN loads to each wheelpath of the DIVINE pavement, while traveling 98,000 km. Three sets of tires were used during the loading routine. Loading was interrupted to carry out the required pavement and vehicles testing specified in the project brief, and also when the wheel bearing failed in Vehicle A (steel suspension) after 1.4 million loading cycles. During the repair of the wheel bearing, it was found that some steel-leaf springs were broken. Since there was no noticeable change to the suspension's response during testing (either at steady speed or during the bump tests), the wheel and suspension were reassembled with a new wheel bearing, but with all of the original leaf springs.

Figure 7.6 shows the change in the DLC over time for each suspension type operating on both wheelpaths. Following the first 100k cycles of loading, DLCs generated by the steel suspension in the outer wheelpath (OWP) were much higher than the DLCs generated by the air in the inner wheelpath (IWP) and they increased more rapidly. It is also seen that when both suspensions are run in the OWP, the DLCs are higher than when both are run on the IWP. This would indicate a slightly higher roughness in the OWP.

Note that both suspensions show exactly the same trends on the two wheelpaths. At the start of the test both vehicles reacted very similarly to the two wheelpaths, indicating that after taking into account the speed differences, the two wheelpaths were statistically the same. After about 20k to 100k cycles, a large rut was formed in the outer track between stations 18 and 24, as seen in figures 7.7a and 7.7b. In the early part of the test there was a divergence between the two paths, with the outer path inducing greater response from the vehicles. This probably reflects the development of the rut in this wheelpath. However, even after this had stabilized the difference between the two wheelpaths continues to grow slowly.

To explain the mechanics of the formation of this localized "rut," intensive analysis of all available data has been carried out (the deformation occurred principally in the base course layer of the pavement). Following the first 20k cycles, which were taken up with pavement conditioning laps and zero measurements with each suspension operating in both wheelpaths for at least some of the time, the FWD test showed a local structural "weakness" centered on station 21 in the OWP (figures 7.8a and 7.8b). Indeed, it can be seen from figure 7.8b that the surface deflection in the OWP at station 21 was about 30 percent higher than the mean value along the entire wheelpath. However, there had been no evidence of this weakness in the pavement structure at construction; on the contrary: the base course thickness was relatively high at this location and the layer moduli and equivalent pavement stiffness were relatively high (this applied to both wheelpaths). While no totally satisfactory reason for the "weakness" at 20k cycles has become apparent, the FWD test showed clearly that it did exist.

50

Dynamic Wheel Forces vs. Applied Loads
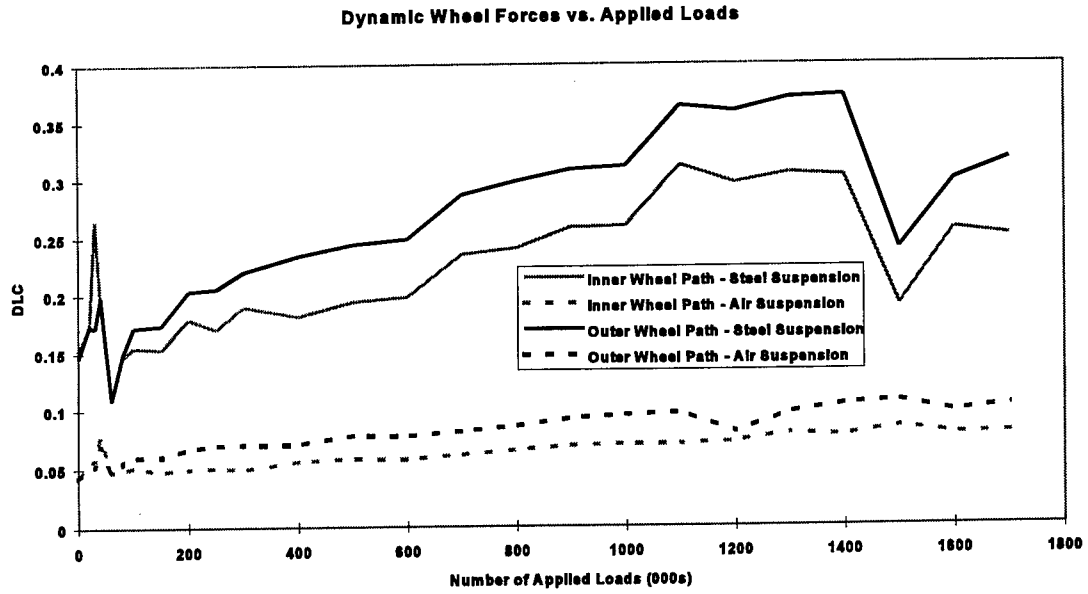
Figure 7.6. Trend of dynamic wheel forces in CAPTIF test.
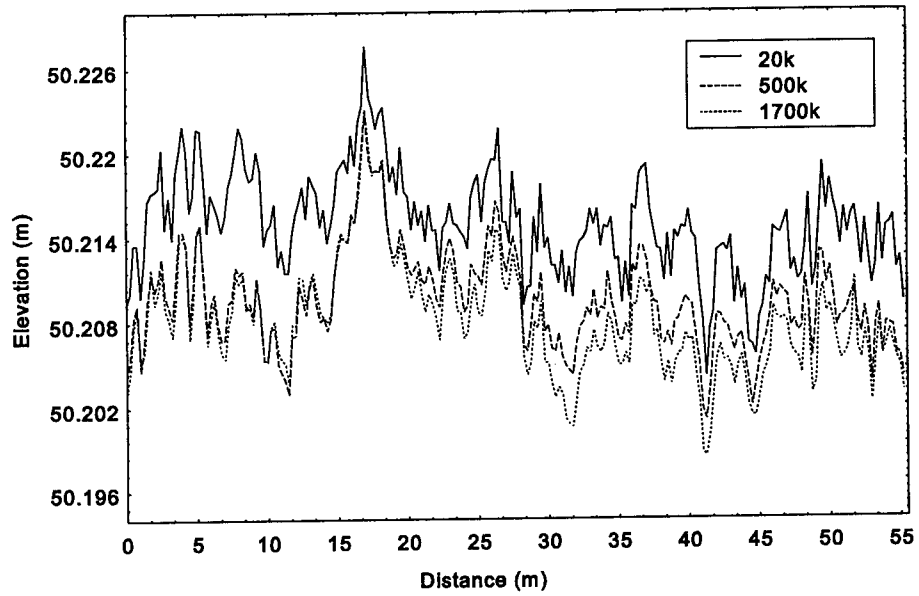
Figure 7.7a. Variation in wheelpath profiles with load repetitions (inner).
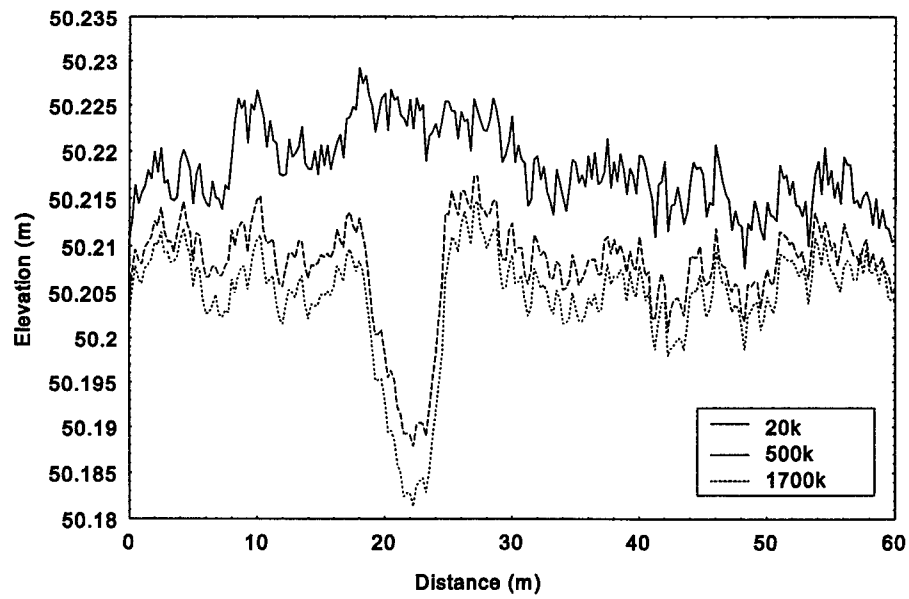
Figure 7.7b. Variation in wheelpath profiles with load repetitions (outer).
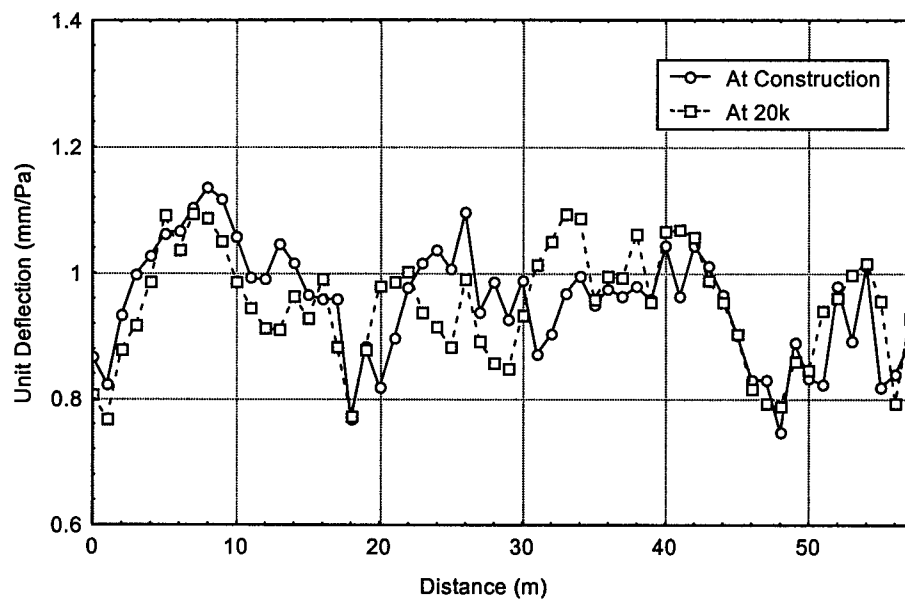
Figure 7.8a. FWD surface deflection, inner track.

52
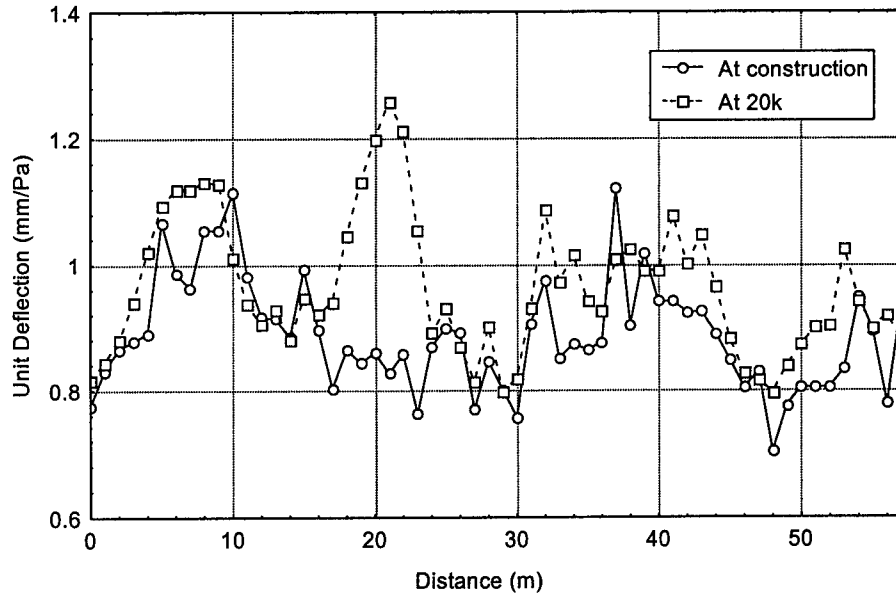
Figure 7.8b. FWD surface deflection, outer track.

It could be argued that the deformation failure was related to localized pavement factors, particularly in the base course layer, and not necessarily to dynamic loading. However, as shown in figure 7.9, the dynamic wheel loading pattern after 20k cycles was such that a dynamic peak was applied in the vicinity of station 21 (peak number 5), although this was not the highest dynamic load peak at that stage of the test. It is interesting to note, however, that the dynamic load peak at station 21, which was evident but relatively small at 20k cycles, grew significantly over time, and this is attributed to the growing "rut," both in extent and depth, causing an increase in dynamic loading. This is illustrated in figure 7.10, which shows the changes in dynamic load peaks around the test track throughout the test: at 100k cycles, there was a dynamic load impact factor (i.e., ration of dynamic load to static load of 50 kN) of 1.13 at station 21 and this grew to 1.41 by the end of the test. It is not clear, however, why the "rut" did not continue to grow rapidly with increased dynamic loading throughout the test.

On the basis of the FWD and wheel force data, therefore, it can be concluded that the formation of the large rut can be attributed to the interactive effects of a relative structural weakness and a changing, and worsening, pattern of dynamic wheel load.

The sudden reduction in wheel forces at 1400k loads occurred because a wheel bearing failure in this vehicle required the suspension to be disassembled and refitted. Although no modifications or repairs were undertaken, its performance improved substantially. The relative performance between the two wheelpaths was unaffected and this is discussed in the next section.

53
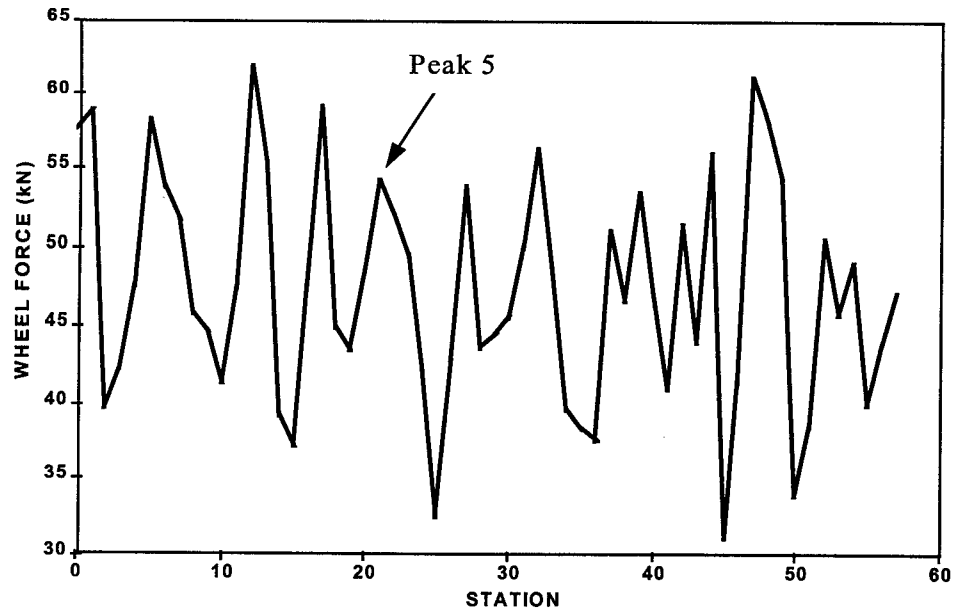
Figure 7.9. Dynamic wheel forces applied to OWP at 20k load cycles.
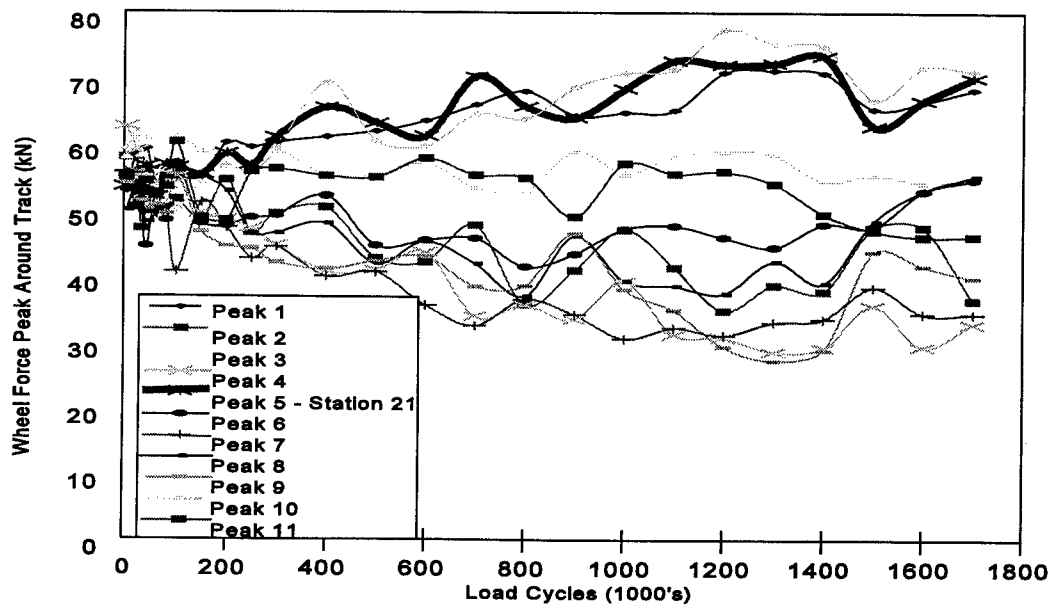
Figure 7.10. Changes in dynamic load peaks, steel suspension on OWP.

7.3 ROAD ROUGHNESS

Pavement management practices commonly use measures based on longitudinal profile as an indicator of pavement condition. In the past this was commonly done indirectly with some form of "response-type road roughness measurement system" (RTRRMS). More recently the

54

development of high-speed profilometers (usually laser-based) has enabled the actual profile to be measured. From these profiles various forms of statistics can be derived to give measures of roughness or unevenness.

During the DIVINE element 1 experiment at CAPTIF, road profiles were measured at regular intervals using a Dipstick profilometer. The Dipstick feet used were spaced at 250 mm, giving profile measurements at this interval. This is the maximum spacing allowed for a Class 1 method as defined in the International Road Roughness Experiment. Partway through the experiment a laser profilometer was fitted and profiles were subsequently measured using this device. This device provides profile readings at much closer intervals (50-mm spacing). The profiles measured by the two devices were substantially the same. For consistency, this analysis uses the Dipstick-measured profiles that were taken throughout the test. The Analysis of Structural Variability Task makes use of profiles taken from the measured transverse profiles.

Profile Changes With Number of Applied Loads

Road profiles on the centerlines of the two trafficked wheelpaths were recorded at each measurement interval. The absolute value of the profiles is determined by the measured transverse profile at the start point of the longitudinal profile measurement. This, in turn, is referenced to the known elevation of the concrete tank at this point.

Samples of recorded profiles on each of the two wheelpaths are shown in figures 7.7a and 7.7b in the previous section. On the inner wheelpath that was trafficked with the air suspension, the changes in profiles are relatively small. There was a general compaction of the pavement in that the absolute value of the elevation is decreasing and there appears to be a small increase in the amplitude of the unevenness. On the outer wheelpath that was tracked by the steel suspension, the development of the rut can be seen. From then on the magnitude of the changes in profile in the rutted area was similar to that in the rest of the wheelpath. Apart from this rut the pattern of changes in profile is similar to that in the inner path. From these two figures, it is not possible to identify a significant difference.

Spectral Analysis

Fourier transforms of the profiles were taken and PSD functions were calculated. These were smoothed using the algorithm defined in the draft International Organization for Standardization (ISO) standard ISO/DIS 8608. Samples of the PSDs are shown in figures 7.11a and 7.11b. The analyses show that most of the change appears to be occurring at the lower wave numbers, or the long wavelengths. On the outer wheelpath the formation of the rut around station 20 early in the test is clearly apparent with the large change in the PSD function at a wave number of about 0.1 cycles/m (10-m wavelength) between 20k load cycles and 100k load cycles. It also appears that the changes that occur at subsequent numbers of load cycles occur at different wave numbers for the two wheelpaths.
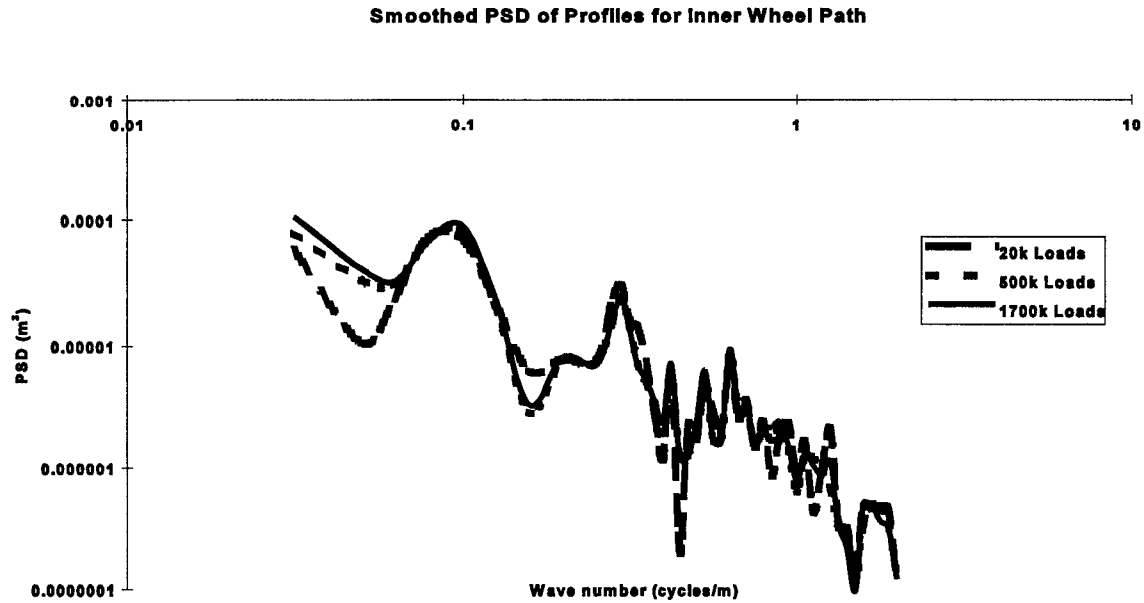
Figure 7.11a. Smoothed PSD of outer wheelpath profile.

Smoothed PSD of Profiles for Outer Wheel Path
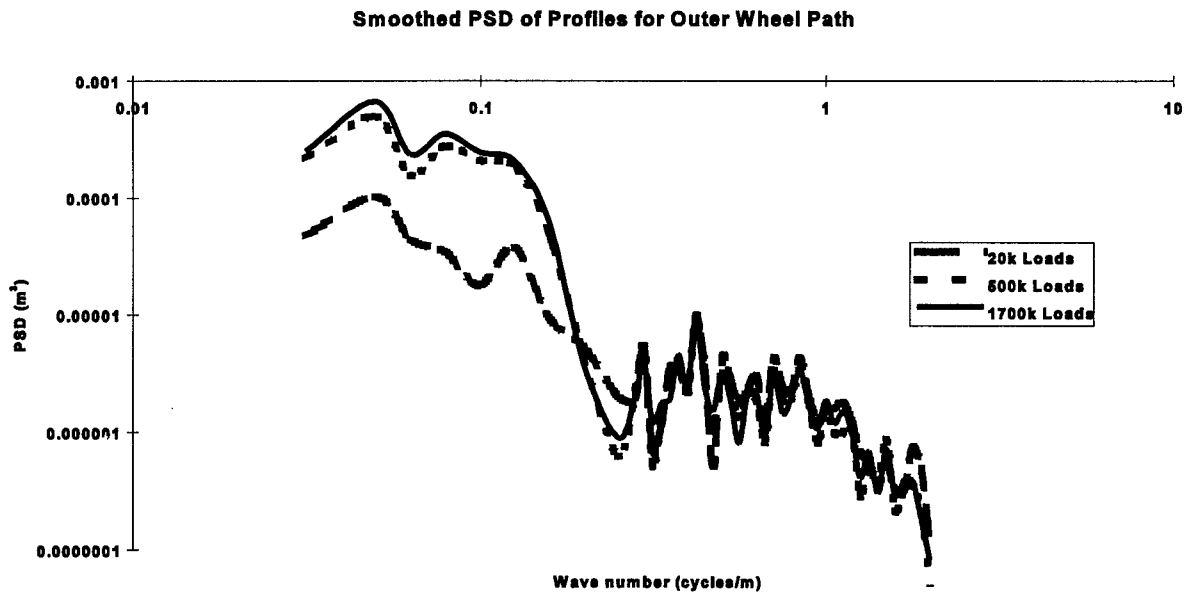
Figure 7.11b. Smoothed PSD of inner wheelpath profile.

Spectral Changes

By taking the Fourier transforms of elevation changes and calculating the PSD function, the differences in the frequency content of these changes was assessed. The PSD functions showed that for the inner wheelpath, there is a small bulge in the profile changes at a wave number of approximately 0.125 cycle/m. At the nominal test speed of 45 km/h, this corresponds to a

frequency of 1.5 Hz for the vehicle on the inner wheelpath, which is the natural frequency of the air suspension. For the outer wheelpath, this slight bulge occurs at a wave number of approximately 0.158 cycle/m, which corresponds to a frequency of 2.07 Hz, which, again, is the natural frequency of the steel suspension. These effects are not large enough to be conclusive, but they do support the proposition that the dynamic loading is a factor in inducing changes to the profiles.

International Roughness Index (IRI)

IRI is a pseudo-RTRRMS measure developed by the World Bank in 1982 as a mechanism for cross calibrating the various methods of measuring road roughness in use around the world. IRI is calculated from the accumulated suspension displacement of a linear dynamic quarter car model to the actual measured road profile traversed at 80 km/h. As the model is mathematical rather than physical its behavior is repeatable and predictable. The relative stiffness, damping, and mass characteristics of the model are similar to those of a North American passenger car of the 1960's and 1970's.

The magnitude of the frequency response function of the IRI shown in figure 7.12 illustrates how the IRI responds to the various frequency components in the pavement profile. The IRI value is the accumulated vehicle vertical displacement response divided by the distance traveled. Although there are two peaks reflecting the sprung mass resonance at about 1.2 Hz and the unsprung mass resonance at about 11 Hz, the damping is such that the model responds to all frequencies between about 0.5 and 20 Hz. The basis of the calculation is that the vehicle speed is 80 km/h, and thus these frequencies correspond to wavelengths between 1.1 m and 44.4 m. Limits of 1 m to 30 m are sometimes quoted. To accurately determine these longer wavelength components, a test length of 200 m or more is desirable. However, the track at CAPTIF is only 58 m long and thus the calculated IRI values fluctuate a little.

Figure 7.13 shows changes in pavement roughness (IRI) in both wheelpaths over time. The initial IRI values are high. It is thought that this is caused by high amplitude of the short wavelength components because of the hand-screening process used in construction. It is apparent that the OWP IRI, relative to that of the IWP, increased over the first 400k cycles of the test and then stabilized. The relative roughness of the steel suspension wheelpath increased by some 15 percent. It should also be noted that both wheelpaths became smoother during the first 100k cycles of trafficking as the initial load applications tended to even out the initially rough pavement profiles.
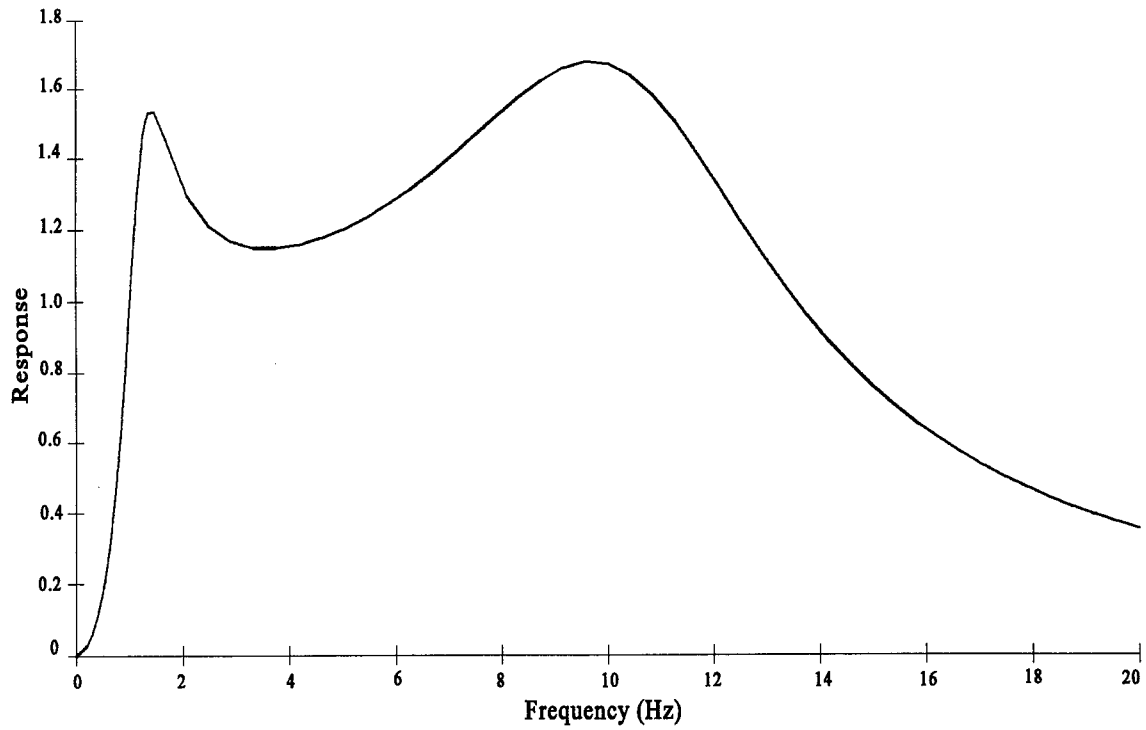
Figure 7.12. IRI frequency response function.
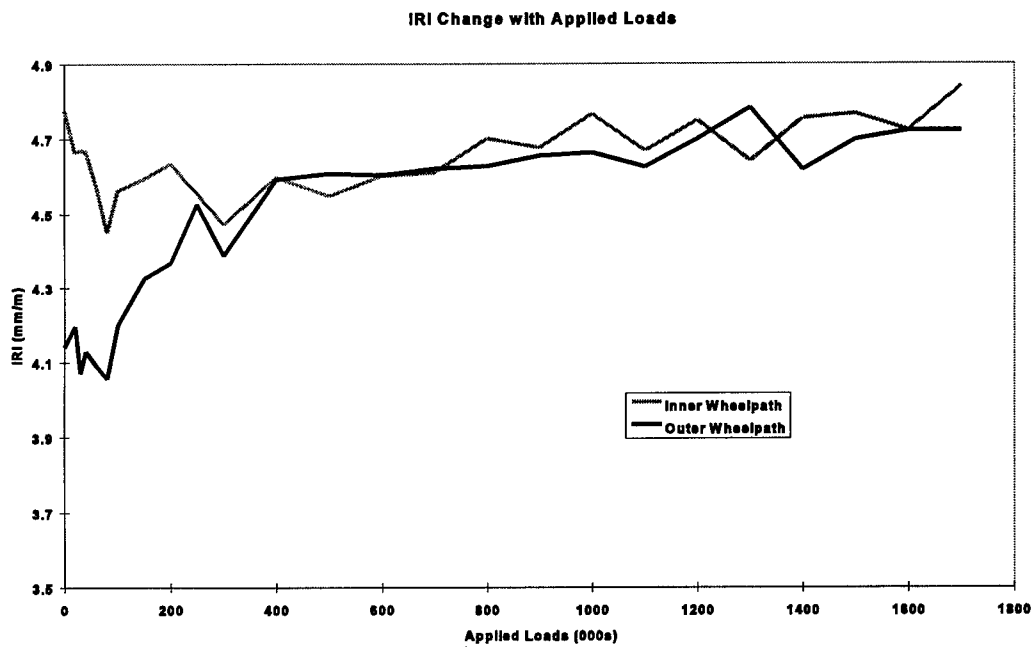
Figure 7.13. Trend of pavement roughness (IRI).

58

The initial IRI for the outer wheelpath appears to be lower than that of the inner wheelpath. The unevenness caused by radial screening has a shorter wavelength on the inner path than on the outer, which will generate a higher IRI value. However, this is offset by the differences in vehicle speed between the outer and inner wheelpath. When the dynamic wheel forces for the same vehicle on each of the two paths are compared, they were virtually identical at the start of the test. In both wheelpaths, the initial loading caused a smoothing of the pavement and a reduction in IRI. The rapid increase in IRI on the outer wheelpath in the early part of the test corresponds to the formation of the rut at station 20. Beyond this it is difficult to distinguish between the two trends. The relatively short test section means that the IRI value has a degree of uncertainty, as demonstrated by the waviness of the plots.

Pavement Serviceability Index (PSI)

The American Association of State Highway Officials (AASHO) road developed a method for relating the subjective pavement serviceability ratings to quantitative measures of pavement condition. This quantitative rating is known as the Pavement Serviceability Index (PSI). The full formulation is rather complex but it was found that a good estimate could be obtained using a much simplified equation:

$$PSI = 5.03 - 1.91 * \log(1+SV)$$

where SV = Slope variance in milliradians.

The characteristics of this function are the inverse of IRI, with a good pavement having high values and then declining as the pavement deteriorates. Applying the formula to the profile data showed that the initial trend is slightly different from the IRI in that there is an initial decline followed by an improvement. Using the PSI measure, there is no difference between the two profiles at the start of the test. The formation of the rut in the outer wheelpath has very little effect. It had a gentle entry and exit and presumably did not alter the pavement slope significantly.

ISO/DIS 8608 Standard Method

The draft ISO standard for reporting data on road surface profiles proposes a method using the PSD functions of the measured road profiles. This method calculates the PSDs, smooths and plots them on a log-log scale, then uses linear regression to extract two numbers from the data. These numbers are the slope of the regression (waviness, figure 7.14a) and the value of the regression line at the wave number of 0.1 cycles/m, which is called comparative density (see figure 7.14b). The standard also specifies that the test sections should be at least 1000 m and consequently the errors in applying this approach to the 58-m-long CAPTIF track are high. The linear regression is a poor fit primarily because of the short section of pavement analyzed, which leads to poor statistical accuracy and hence a high degree of variability in the trace. The magnitude of the slope of these PSDs (waviness) is at the low end of what is seen for typical road. That is, the amplitude of the short wavelength components is high relative to those of the longer wavelength components. Otherwise the general shape and magnitude is similar to that of a moderately smooth road. The effect of the development of the rut in the outer wheelpath early in
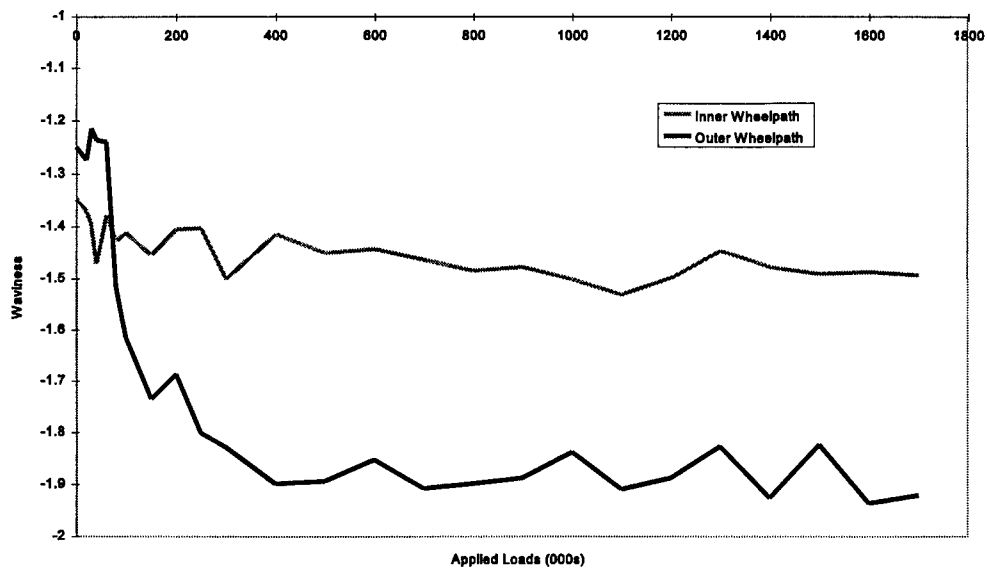
Figure 7.14a. Waviness changes vs. load cycles.
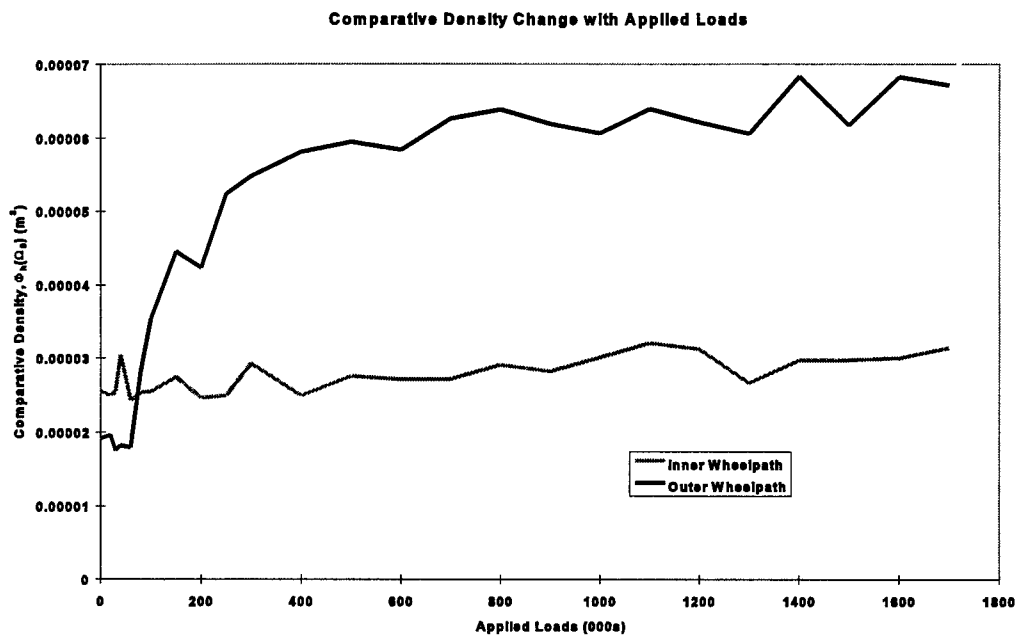
Figure 7.14b. Progression of pavement unevenness (comparative density).

the test was clearly visible based on the analysis results. The slope values remain relatively constant once they have settled. The larger (in absolute terms) value associated with the outer wheelpath is caused by the increased magnitude of the low-frequency components in the PSD.

Fitting a regression line to the waviness function from 400k loads onward showed that the outer wheelpath value increases at a rate of 80 percent greater than the inner. This trend did not show up in the IRI or PSI plots.

PSD-Based Statistics

Having calculated the PSD functions it is possible to derive any number of statistics by integrating between particular wavelengths and determining the root mean square (RMS) values. A logical approach in this test is to consider a low-frequency band RMS to reflect the sprung mass vibrations of the vehicles and a high-frequency band value to reflect the unsprung mass vibrations. The wave number limits chosen for the low-frequency statistic are 0.0702 to 0.2806 cycles/m. At the test speed these correspond to 0.9 to 3.5 Hz. For the high-frequency statistic the values used are 0.817 to 1.1554 cycles/m, which correspond to 10.2 to 14.4 Hz. The high-frequency band statistic was only slightly higher for the outer wheelpath, which remains totally consistent throughout the test. The low-frequency statistic clearly reflected the development of the rut in the outer wheelpath but even after this has stabilized it continues to increase more quickly in the outer wheelpath. Calculating the rate of growth by applying a linear regression from 400k loads to the end shows this outer wheelpath statistic increasing 3.8 times as rapidly as the inner.

7.4 PAVEMENT CRACKING

Because of time-consuming and logistically difficult processes, only transverse and longitudinal cracking was measured. The types of cracking that occurred tended to fall into these two categories and eventually the cracks joined to become block cracking. Any crack that lay within ±45° of the longitudinal axis of the track was classed as a longitudinal crack, and the same criteria were applied to transverse cracking.

The failure criterion for pavement cracking was set (by the DIVINE group) at 5 linear m of cracking per 1 m^2 of trafficked area, which will have occurred over 50 percent of the entire trafficked area. To produce a representative measure of the cracking that fitted in with the established referencing system used at CAPTIF, the linear length of cracking for the failure criteria was scaled to suit the area of trafficked pavement in a wheelpath for a 1-m section of track. This converted the 5 m/m^2 failure criterion to 2.5 linear m of cracking per station.

Development of Pavement Cracking

The first cracks in the pavement were noticed during a routine inspection at 840k laps in the outer wheelpath. Therefore measurement of the cracking commenced at the 900k testing interval. Subsequent measurements of cracking were made every 100k laps. Initially cracking developed rapidly over the first four measurements and then the rate of cracking increase decreased for the remaining intervals. The rubber from the SLAVE tires caused some difficulties when measuring the cracks. The rubber was deposited onto the track surface both as solid lumps, up to 80 mm in diameter and 10 mm high and as a thin film over the entire trafficked area. It was straightforward to interpolate the growth of a crack through/underneath a block of rubber, but the film of tire rubber tended to mask cracks until they were sufficiently wide enough to show through the rubber film. As a result of this, some cracks disappeared during subsequent loading as the

61

rubber built up faster than the crack was growing in width. The reader should refer to the discussion presented in chapter 2 and appendix A that addresses the "scrubbing" action of a tire in circulation.

Cracking in the inner wheelpath consisted mostly of a single crack along the centerline of the trafficked area with small isolated transverse branches coming off it. There were four distinct areas of block cracking by the completion of the project. These were at the following locations: stations 6 to 10, 11 and 12, 15 to 17, and 37 to 39. Fifty-two out of fifty-eight of the stations had developed cracks. The total length of cracking in the inner wheelpath was 64.112 m, with an average of 1.233 m of cracks per station that had commenced cracking. Longitudinal cracking totaled 41.571 m, or 64.8 percent of the total cracking. At the completion of loading, five stations had reached the pre-set failure level. The crack length in the 29th worst station (50 percent of the trafficked area) was 0.991 m.

Cracking in the outer wheelpath was a combination of centerline cracking as in the inner wheelpath, transverse cracks starting on the centerline crack, and transverse cracks linked up to become block cracking. The separate areas of block cracking were at stations 5 to 9, 12 and 13, 16 to 19, 20 to 24, 33 and 34, 37 to 39, and 40 to 42. Forty-eight out of fifty-eight stations developed cracks. The total length of cracking in the outer wheelpath was 86.96 m, with an average of 1.81 m of cracks per station that had commenced cracking. Longitudinal cracking totaled 48.58 m, or 55.9 percent of the total cracking. At the completion of loading, 13 stations had reached the factored failure level. The crack length in the 29th worst station (50 percent of the trafficked area) was 1.100 m. Table 7.1 summarizes the results of the crack measurements for both Select data (data set not containing the rut) and All data (data set containing the rut). From table 7.1, it can be seen that the failure criterion of 5 m/m^2 was exceeded (when All data are used) at 5 and 13 stations in the air suspension and steel suspension wheelpaths, respectively. The cracking in the air suspension wheelpath was fairly uniform, in terms of severity, around the track, while the cracking in the steel suspension wheelpath was quite severe in some locations and minimal in other locations. When the influence of the large rut in the outer wheelpath was excluded from the analysis, it became apparent that the total length of cracking, when corrected for the differing circumferences of the two wheelpaths, is similar. However, this comparison is complicated by the fact that there was significantly more transverse cracking in the OWP than the IWP and less longitudinal cracking.

Following the completion of trafficking, six cores were removed from the pavement, at locations where cracking extended across the top of the core, in an attempt to determine whether the cracking had been initiated at the surface or the bottom of the bituminous surface layer. Observations of the specimens during laboratory testing revealed that the cracking had commenced at the surface of the layer and spread downward toward the bottom of the layer.

The fact that the cracking was initiated at the surface of the bituminous layer rather than at the bottom suggests that there was no classic structural fatigue failure but rather a gradual disintegration of the bituminous surfacing under the continued application of vertical impact

Table 7.1. Results of cracking measurements (All/Select data).

Cracking Measurement (after 1.7 million cycles)	Air-Suspended Test Wheel (inner wheelpath)	Steel-Suspended Test Wheel (outer wheelpath)
Number of stations with cracking	52/46	48/41
Number of stations exceeding failure criterion	5/5	13/8
Total crack length (m)	64.1/59.6	87/58.3
Length of longitudinal cracks (m) % of total cracking	41.6/38.4 65%/64.5%	48.6/34.3 56%/58.8%
Length of transverse cracks (m) % of total cracking	22.5/21.2 35%/35.5%	38.4/34.3 44%/41.2%
Middle value of crack length (29th/26th) (m)	0.99/1.07	1.1/0.77

loads. The surfacing was composed of a conventional dense-graded bituminous mix containing a Class 170 (85/100 pen) binder rather than a fatigue-resistant mix containing, for example, a polymer-modified binder. Another explanation for the "top down" cracking may be the "scrubbing" effect, which is discussed in appendix A.

Quantitative comparison of cracking damage in the two wheelpaths is complex and is discussed further in the section on structural variability and also in the DIVINE Final Report.

Cracking Analyses

Spatial analysis of the cracking and the relationship of the cracking to the measured wheel forces was carried out by examining: (1) cracking intensity, (2) correlations between cracking and initial pavement structural condition, (3) localized maxima and minima of the wheel forces and the cracking densities in the associated areas, (4) correlation of the wheel forces and the levels of cracking density, and (5) the relationship between discrete sections of cracking around the track and the aggregated second power wheel forces.

Cracking intensity. Figure 7.15 plots the intensity of cracking for Select data. The figure shows that the cracking in the OWP (steel suspension) was higher in intensity and had a higher proportion of transverse cracks than that in the IWP (air suspension).

An analysis of the number of stations reaching certain levels of cracking intensity was carried out. This analysis was carried out for the Select data (i.e., excluding the influence of the large "rut") and was designed to show the influence of the more localized higher intensity cracking that occurred under the steel suspension. Figure 7.16 shows the progression of the percentage of

63

stations with total crack length exceeding a level of 2.5 m linear length of cracking per station. This level was selected to show the more rapid accumulation of stations with significant cracking distress under the steel suspension. Analysis of these curves showed that the number of test cycles required to produce 2.5 m linear length of cracking distress in 10 percent of stations was approximately 30 percent less for the steel suspension.

Correlation between cracking and pavement initial stiffness. Cross-correlation analysis was carried out to study the apparent causes of cracking. As shown in figures 7.17a, 7.17b, and 7.17c, there was a higher correlation between cracking and pavement initial structural stiffness (as represented by the FWD maximum deflection at the commencement of trafficking) in the OWP (steel suspension) than in the IWP (air suspension). There was also a higher correlation in the OWP (steel suspension) between the rut depth and cracking than in the IWP (air suspension). The influence of the localized rut near station 21 in the OWP contributed to the higher correlation coefficients in that wheelpath in both cases.

| Total Cracking | Longitudinal Cracking | Transverse Cracking |
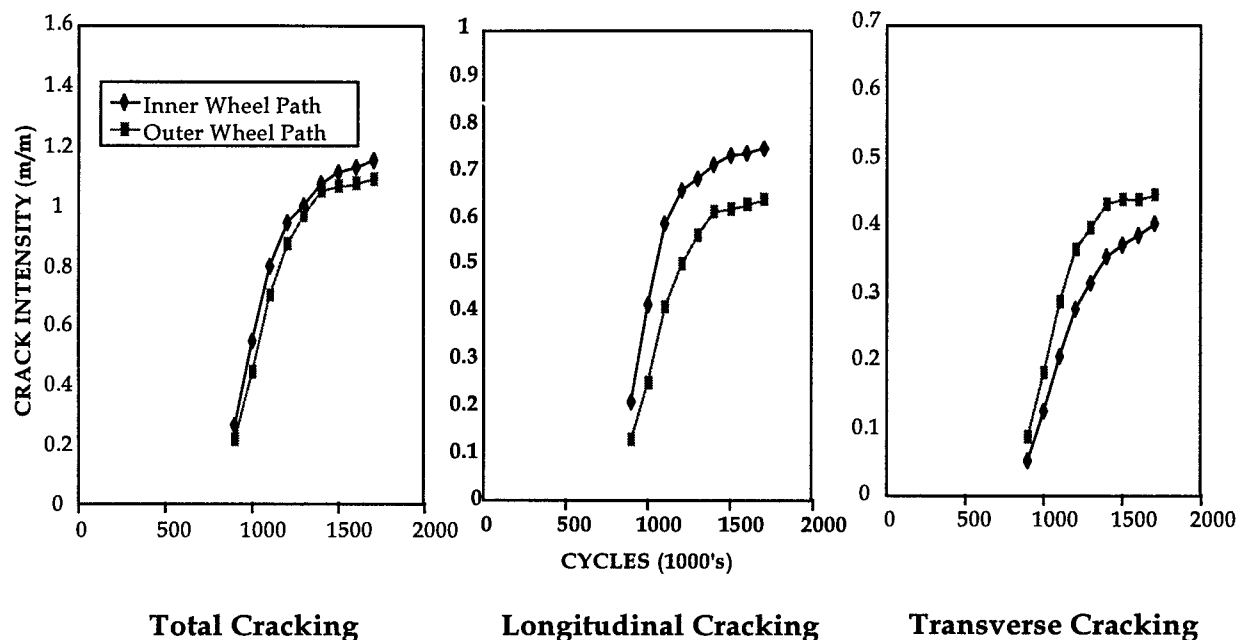
Figure 7.15. Cracking intensity versus trafficking, Select data.

STATIONS CRACKED TO 2.5 m - SELECT DATA
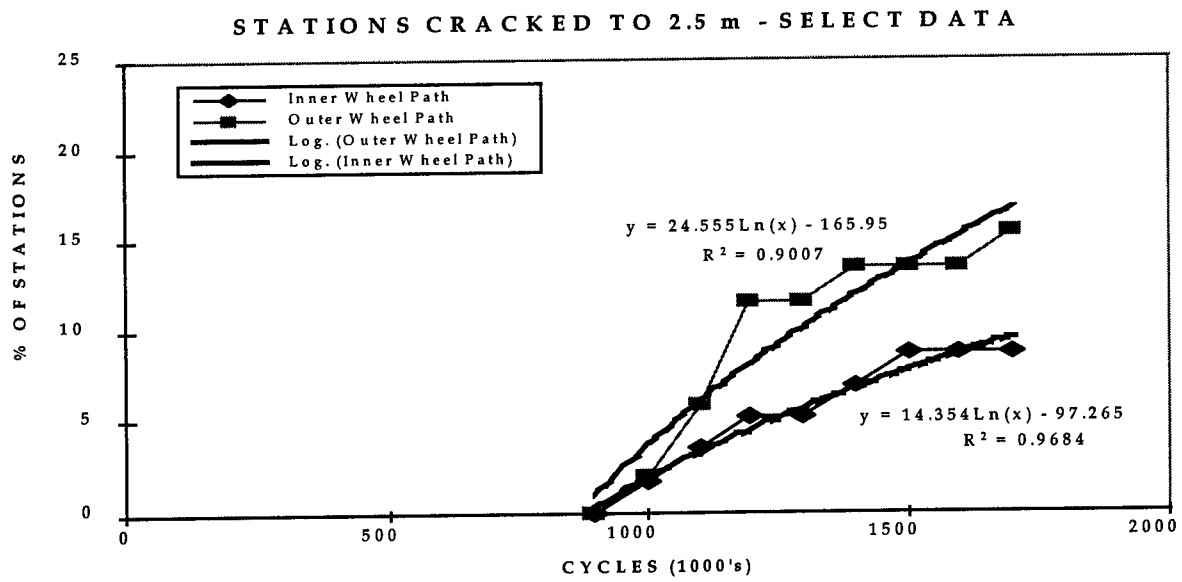
Figure 7.16. Progression of cracking damage.
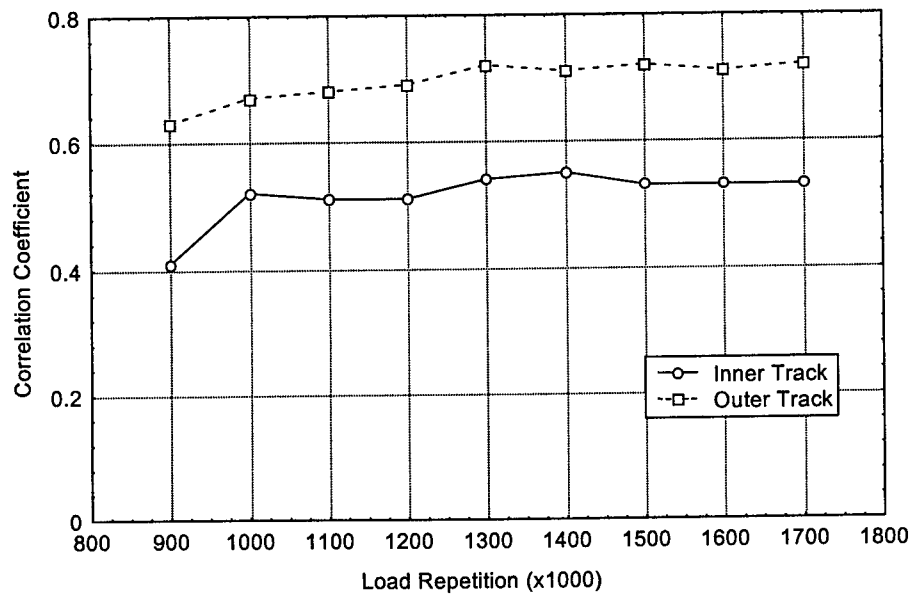
Figure 7.17a. Correlation between FWD maximum deflection at 20k cycles and cracking intensity — total linear cracking.
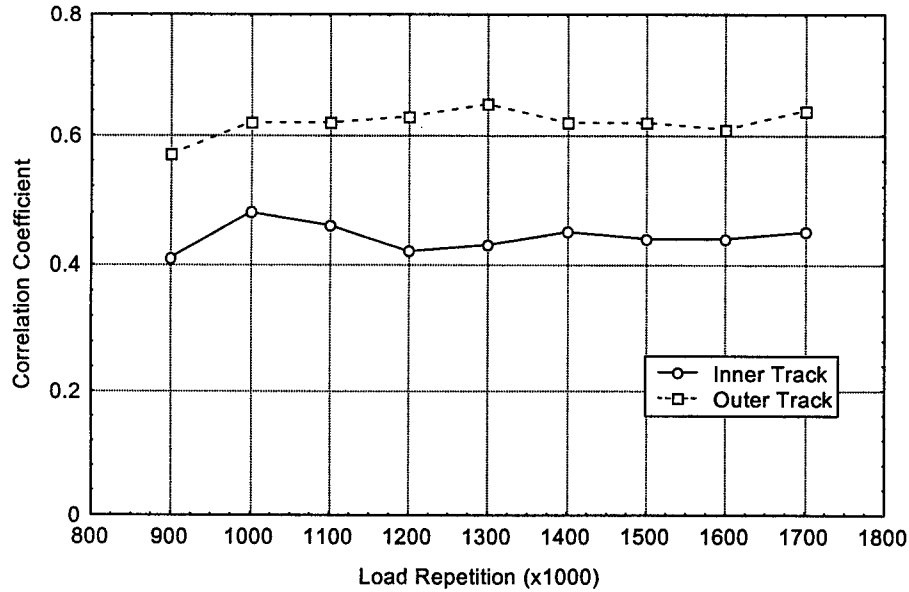
Figure 7.17b. Correlation between FWD maximum deflection at 20k cycles and cracking intensity — longitudinal linear cracking.
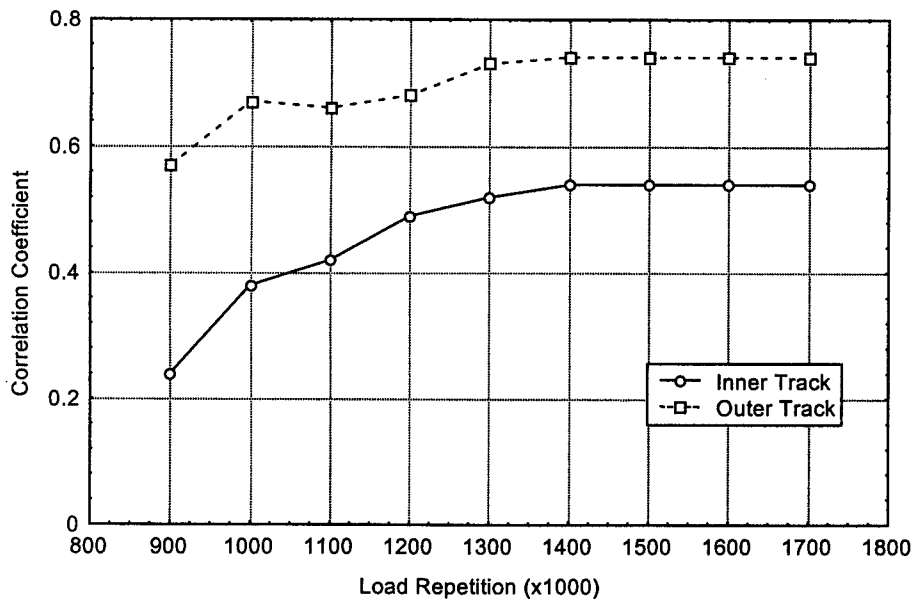
Figure 7.17c. Correlation between FWD maximum deflection at 20k cycles and cracking intensity — transverse linear cracking.

Localized maxima and minima of wheel forces and cracking density. This was done by looking at the low-frequency component of the wheel forces at the completion of the project and identifying the localized maxima and minima of the wheel forces. Once the localized maxima and minima of the wheel forces had been located, the crack length for the station in which the extreme wheel force was located and paired with the wheel force value. The ratio of crack length

66

for the adjacent local maxima and minima of the wheel forces was computed, along with the mean values. The values of n are calculated for the equation

$$\left(\frac{WF_{Mi}}{WF_{mi}}\right)^{n} = \frac{C_{Mi}}{C_{mi}}$$

where

i	=	location of maximum or minimum wheel force
n	=	factor based on pavement rigidity
WF_{M}	=	maximum wheel force
WF_{m}	=	minimum wheel force
C_{M}	=	cracking density at maximum wheel force
C_{m}	=	cracking density at minimum wheel force.

The calculated values of n can be compared to the exponent values used in the power law relationships between actual wheel forces, standard wheel forces, and pavement damage.

The wheel forces and corresponding maxima and minima for the inner wheelpath are shown in table 7.2. There were 11 paired values for the inner wheelpath. It was difficult to isolate the localized maxima or minima in some sections of the track because the performance characteristics of the suspension meant that the higher frequency response of the axle assembly influenced the overall response of the wheel forces. The ratio values for the localized values of the cracking varied from 0.35 to infinity (because zero length cracking was recorded in some sections of the wheelpath) and the average value was 0.935. It would be expected that this ratio would be greater than one if the cracking density was related to the wheel forces. The ratio values for the localized values of the wheel forces varied from 1.23 to 1.51 and the average value was 1.405. The calculated values of n vary from -3.940 to 3.358, with an average of -0.337 and a standard deviation of 2.444. The method of sampling could be contributing to this poor result: the wheel forces are measured with a longitudinal separation distance of 56 mm, while the cracking is measured over 1000 mm of the track. One other explanation for this result is that the pavement design and response are not very sensitive to the low variation of the dynamic wheel forces; the local maxima and minima of the wheel forces mostly lie within a ±10-kN envelope of the static axle weight.

The wheel forces and corresponding maxima and minima for the outer wheelpath are shown in table 7.3. There were nine paired values for the outer wheelpath. The local maxima and minima were very clearly isolated from each other. The ratio values for the localized values of the cracking varied from 0.65 to infinity and the average value was 6.105. The ratio values for the localized values of the wheel forces varied from 1.93 to 4.36 and the average value was 6.107. The calculated values of n vary from -0.277 to 1.490, with an average of 0.618 and a standard deviation of 0.811.

Correlation between the wheel forces and cracking. This method used a rank correlation test between wheel force and cracking density. For this test, the wheel force values were averaged to give a value that was representative of the same area covered by a crack density value. The rank

correlation coefficients for the inner and outer wheelpaths are 0.17 and 0.44, respectively. These results indicate that there was almost no correlation between wheel forces and cracking densities in the inner wheelpath and a moderate correlation for the outer wheelpath.

Table 7.2 Maximum and minimum wheel forces at inner wheelpath.

Location of Maximum Wheel Forces	Local Maximum Wheel Force (kN) WF_M	Cracking (lm/station) C_M	$\dfrac{C_M}{C_m}$	$\dfrac{WF_M}{WF_m}$	n
2.4	60.5	0.469	0.4	1.41	-2.632
7.1	58.7	4.285	1.87	1.51	1.522
10.6	58.2	1.488	0.35	1.46	-2.773
13.6	57.5	1.428	1.06	1.48	0.137
17.4	55.7	1.01	0.44	1.23	-3.940
24.3	59.2	0.932	2.31	1.51	2.034
32.4	56.8	0.944	∞	1.4	
40.4	55.2	1.512	1.07	1.39	0.203
43.1	57.4	0.971	0.8	1.27	-0.940
52.3	57.7	0.225	∞	1.42	
56.6	58	0.325	3.22	1.42	3.358

Location of minimum wheel forces	Local Minimum Wheel Force (kN) WF_m	Cracking (lm/station) C_m		
0.7	42.9	1.159	C_M	1.235
4	38.9	2.295	C_m	1.321
7.7	39.8	4.285	$\dfrac{C_M}{C_m}$	0.935
11.1	38.8	1.353		
15.8	45.2	2.301		
19	39.2	0.403	WF_M	57.700
28.6	40.6	0	WF_m	41.100
36.6	39.6	1.414	$\dfrac{WF_M}{WF_m}$	1.405
42.6	45.2	1.216		
46	40.6	0		
55	41	0.101		

Table 7.3. Maximum and minimum wheel forces at outer wheelpath.

Location of Maximum Wheel Forces	Local Maximum Wheel Force (kN) WF_M	Cracking (lm/station) C_M	$\dfrac{C_M}{C_m}$	$\dfrac{WF_M}{WF_m}$	n
1.2	86	1.611	5.28	4.36	1.130
7.6	88	3.975	14.56	2.15	1.490
13.8	74.8	0.391	0.66	1.89	-0.277
20.3	72.4	6.308	∞	2.13	
28.6	89.1	1.287	∞	1.93	
34.8	74.8	1.424	0.65	2.1	-0.213
41.2	74.4	3.613	41.53	2.44	0.958
46.8	82.4	0.774	∞	1.95	
53.3	75	1.644	∞	2.26	

Location of Minimum Wheel Forces	Local Minimum Wheel Force (kN) WF_m	Cracking (lm/station) C_m		
3.443	19.7	0.305	C_M	2.336
9.992	14.6	0.273	C_m	0.383
15.806	16.5	0.594	$\dfrac{C_M}{C_m}$	6.105
25.29	8.1	0		
32.911	22.7	0		
37.144	10	2.185	WF_M	79.700
44.201	1.5	0.087	WF_m	13.000
50.749	18.3	0	$\dfrac{WF_M}{WF_m}$	6.107
55.942	6	0		

Correlation between cracking and aggregated second power wheel force. This analysis investigated the relationship between discrete sections of cracking around the track and the aggregated powered wheel forces. Work by others (David Cebon) had influenced the research to calculate the aggregated wheel forces to the second power to establish a relationship between wheel force and pavement cracking. This method was used to determine the damaging effect of the wheel forces applied throughout the project with respect to the actual locations of pavement cracking. The average values of the aggregated wheel forces were similar to the equivalent static value, but the standard deviations were quite different (1.901 and 0.452 x 10^{15} N^2 for the inner and outer wheelpaths, respectively). The difference in centerline lengths of cracking between the inner and outer wheelpaths was 7 percent and just over half of the pavement was cracked for both wheelpaths. The threshold values for the 90th-percentile value of aggregated wheel force for the

cracking locations were similar for the two wheelpaths, 3.535 and 2.487 x 10^{15} N^2 for the inner and outer wheelpaths, respectively.

7.5 RUTTING

Apart from the large isolated rut in the outer wheelpath, rutting of the test pavement was relatively minor in both wheelpaths. Table 7.4 shows the mean rut depth and the standard deviation of the rut depth in both wheelpaths at the conclusion of the test. The mean rut depth in the OWP (steel suspension) was 6 percent less than that in the IWP (air suspension), while the variability in rut depth in the OWP was 12 to 18 percent greater than that in the IWP, depending on whether the standard deviation or coefficient of variation (ratio of standard deviation to mean) is used. The maximum rut depth under the steel suspension was 13 percent greater than that under the air suspension. Some care is needed in interpreting these rutting measurements, due to limitations in accuracy of rut depth measurement.

Figure 7.18 shows the ratio of the coefficients of variation (V) of the rutting in both wheelpaths. It can be seen that there was a gradual increase in the variability of the rutting in the OWP compared with that in the IWP, which can be attributed to the higher dynamic wheel forces induced by the steel suspension. It can also be seen that the V of the rut depth in the OWP at the end of testing was 19 percent greater than in the IWP.

The relatively high static wheel load in the CAPTIF test, combined with the use of wide single tires, and the relatively channelized trafficking in the wheelpaths should have accelerated the development of rutting. Nevertheless, general levels of rutting were small, except for the large "rut" near station 21 in the outer wheelpath, where the weakened base course was significantly deformed, coinciding with the application of a dynamic loading peak.

Table 7.4. Effect of suspension type on rut depth (Select data).

Rut Measurement (at 1.7 million cycles)	Air-Suspended Test Wheel (inner wheelpath)	Steel-Suspended Test Wheel (outer wheelpath)
Mean Rut Depth (mm)	8.94	8.44
SD (mm)	1.74	1.95
Min. Rut Depth (mm)	6	4
Max. Rut Depth (mm)	12.4	14
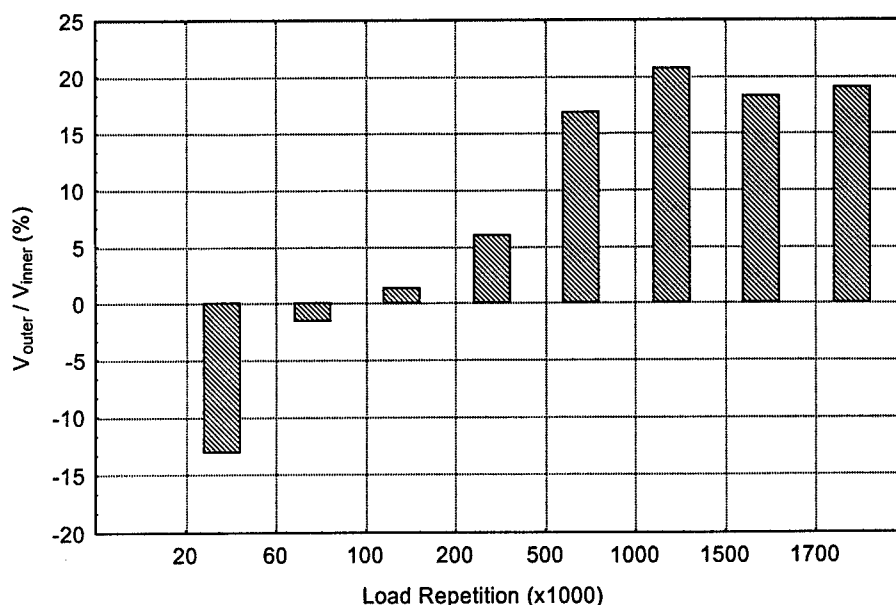
Figure 7.18. Comparison of rut depth variations in inner and outer wheelpaths (Select data).

Outer Wheelpath

$y = 2.4582Ln(x) - 4.0441$

$R^2 = 0.96$

Inner Wheelpath

$y = 1.8991Ln(x) - 1.3402$

$R^2 = 0.9823$
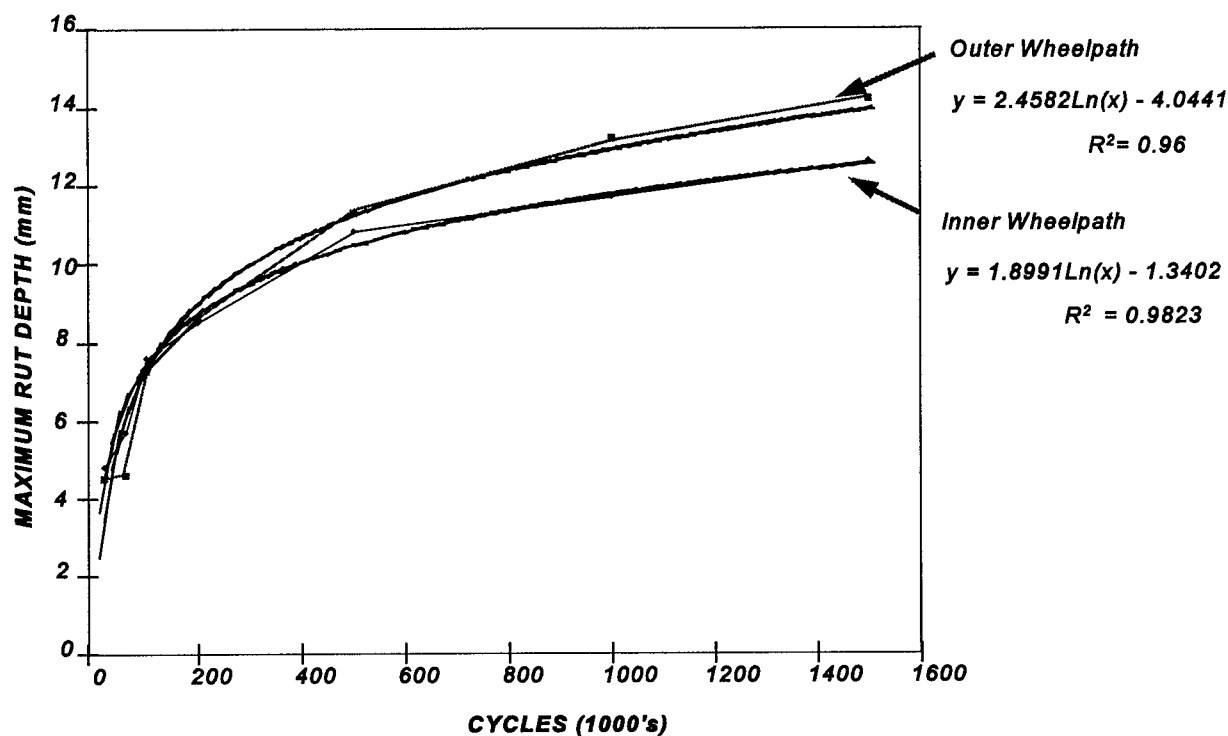
Figure 7.19. Maximum rut depth versus number of load cycles.

Despite the generally small degree of rutting evident in the test pavement in the CAPTIF indoor test, and the fact that the mean rut depths were the same, there were differences in maximum rut depths between the two wheelpaths, and the maximum rut depth under the steel suspension was

71

influenced by dynamic loading. The progression of maximum rut depth in the two wheelpaths, shown in figure 7.19, gives no sign of an accelerating damage trend that could be extrapolated to pavement "failure" to determine the relative pavement life under the two suspensions. However, if a maximum rut depth in the range of 11 to 12 mm is taken as a criterion level, analysis of the rutting curves shows that the air suspension would achieve 45 to 65 percent more load cycles than the steel suspension to produce the same rutting distress; a similar analysis of the standard deviation of rut depth indicates that the air suspension would achieve 35 to 55 percent more load cycles. The significance of this result is tempered by the small amount of rutting distress that occurred, the accuracy of the rutting measurements, and the fact that the variability in rut depth was used, rather than the mean value.

7.6 COMPARATIVE SUSPENSION EFFECTS

Table 7.5 is an attempt to summarize the effects of the two suspensions on pavement performance.

7.7 ANALYSIS OF STRUCTURAL VARIABILITY

The initial structural variability of the CAPTIF pavement is investigated in terms of two known measured variables, thickness and initial FWD center deflection. FWD center deflection was selected to represent the combined effect of material variability existing in the subgrade, base, and AC surface for both the inner and outer tracks. Basic statistics of selected parameters measured during construction were performed and correlations between these initial measures and the selected performance measures were calculated.[11]

Type of Analysis

Three types of data analysis were performed: (1) variations defining initial pavement conditions, (2) variations of selected variables at different load repetitions, and (3) cross correlations of selected variables taken at different load repetitions. To carry out the analyses, first the statistics of the selected variables were calculated so as to detect the existence of differences in the structural capacity of the inner and outer track before trafficking; then, a check was made to see if and how any of these variables may have changed during trafficking; finally, cross correlations were performed to check the relative influence of initial pavement condition (thickness, strength, roughness, etc.) on pavement performance. Actual test trafficking was started after the pavement had received approximately 20k repetitions of mixed loadings over the whole pavement. These loadings can be considered as conditioning cycles.

Table 7.5. Comparative pavement effects of the two suspension systems.

Measured Characteristic	Air-Suspended Test Wheel (inner wheelpath)	Steel-Suspended Test Wheel (outer wheelpath)	Comparison of Pavement Effects
Pavement Profile IRI	Initially 4.8; fluctuated slightly through test, but did not exceed 4.8	Initially 4.1; increased throughout test, up to 4.8	Relatively, steel suspension increased IRI by 15 percent
PSD	Profile changes found to correspond with suspension frequency	Profile changes found to correspond with suspension frequency	Difficult to compare relative magnitudes
Waviness 10-m wavelength	Very little change	Significant change throughout test	Steel suspension effect 80 times higher
VSD correlations	$VSD = c * FWD^{1.1}$ $r = 0.53$	$VSD = c * FWD^{3.2}$ $*WF^{1.8}$ $r = 7.6$	Pavement deformation was primarily related to: FWD under air and product of FWD & wheel force under steel
Pavement Serviceability PSI	Some reduction through test	Slightly more deterioration through test	Some evidence of greater deterioration under steel suspension
Rutting (Select data) mean (mm)	8.94	8.44	Steel suspension produced 6 percent less average rut depth
std. (mm)	1.74	1.95	Steel suspension produced 12-18 percent more variability in rut depth
cov	0.195	0.231	
max. (mm)	12.4	14	12 percent greater under steel suspension
Rutting (All data) mean (mm)	8.75	10.5	Steel suspension produced 20 percent more average rut depth
max. (mm)	12.4	36.9	Structural weakness of 30 percent and impact factor of 1.13-1.4 under steel suspension produced 200 percent greater max rut depth
Cracking Total extent (m)	64	87	Steel suspension produced 36 percent more cracking (All data)
Intensity (29th worst station, m per station)	0.99	1.10	On average, steel suspension produced 10 percent more local cracking

73

Variations Defining Initial Conditions

Spatial variations of parameters associated with the pavement's structural integrity at construction were calculated so as to detect the existence of differences in the structural capacity of the inner and outer track prior to the actual trafficking of the pavements after 20k preload repetitions. The analyses included:

- Spatial variation of layer thickness at construction.

- Spatial variation of FWD layer deflection at construction.

- Spatial variation of layer moduli at construction.

- Spatial variation of initial equivalent stiffness at construction.

- Spatial variation of FWD deflection at beginning of test (after preloading).

- Correlation between FWD surface deflections at beginning of test. Study of the test pavement's initial thickness (many of the results were presented in section 3.4) showed that the mean thicknesses of the AC and base layers of the two tracks were almost identical, and the variation in layer thickness for the top two layers in both paths is very small, between 4.3 percent and 7.7 percent (see figures 3.1 and 3.2, table 3.1).

In addition, cross correlations conducted between base and AC layer thickness in each wheelpath around the track yielded coefficients of cross correlation of -0.803 for the inner and -0.789 for the outer wheelpaths.

Plots of unit load FWD deflection for all layers in both wheelpaths are given in figures 3.3 and 3.4 and the basic statistics are given in table 3.2. The data show that the variation of unit deflection for all layers in both tracks is about 10 percent. Although mean deflection on top of the AC layer of the outer path is about 7 percent less than that of the inner path (outer is slightly stiffer), mean deflections at the top of base and subgrade for the inner and outer wheelpaths are about the same, indicating that at construction, the inner path was structurally similar to the outer path.

Layer moduli of the AC, base, and subgrade layers at 1-m intervals in each wheelpath around the track were given in figures 3.5, 3.6, and table 3.4, and indicated that the moduli of the layers of the two tracks were similar. Although not shown, combined equivalent stiffness of the base and AC layers was calculated and presented in reference 11. The data also indicated similar trends.

After the 20k conditioning cycles, the mean values of surface deflection indicate that generally the structural integrity of the inner and outer pavements are still very similar, but the coefficients of variation differ slightly: 9.4 percent for the inner track (before any loading it was 9.3) and 11.5 percent for outer track with the use of All data (before any loading it was 10.1 percent). This small difference is largely due to the fact that at station 21, the surface deflection of the outer

track is about 30 percent higher than its mean value (maximum is about 15 percent more than its mean at some other location in the pavement), indicating that the outer pavement is relatively weaker than the inner track around station 21.

Cross-correlation analysis showed that, between the inner and outer wheelpaths, the coefficients of correlation were 0.61 using the deflections at all 58 stations around the tracks (All data), and 0.81 using these data less the deflections occurring between stations 18 and 24 (Select data). This indicates that the two tracks are very similar even after preloading (20k cycles) if not considering the "rut."

Variations of Selected Variables at Different Load Repetitions

Variations of selected variables at different load repetitions during trafficking were calculated. The variables are:

- DLC and IRI.
- Profiles.
- Vertical Surface Deformation (VSD).
- Rut depth.

Typical profile, VSD, and rut depth data used in the analyses are given in tables 7.6, 7.7, and 7.8. Summary of profile, VSD, and rut depth changes is given in table 7.9.

The data in table 7.6 show that using All data, the mean profile changed 8 mm for the inner track and 15 mm for the outer track between 20k and 1700k load cycles, or the change in mean profile on the outer track is about 88 percent greater than that on the inner track; if using Select data, then this change becomes 7 mm for the inner and 13 mm for the outer track, or the outer is about 86 percent more than the inner. Since the tires on the inner and outer tracks are under the same static load, the change in mean profile should be the same for any value of dynamic loading considering that the two wheelpaths were very similar. The fact that the mean elevation changes are not the same in both tracks may be due to the errors induced by using the Dipstick measurement technique.

The profile data using the Dipstick show no change in the variation (standard deviation) of the profile elevations from beginning to end for the inner track. The standard deviation actually decreased from 0.004 to 0.003 using Select data from the outer track, but increased from 0.004 to 0.006 (50 percent) using All data, due to the strong influence of the rut.

The data in table 7.7 show that the change in mean VSD between 20k and 1700k repetitions on the outer track is about 12 percent greater but 12 percent less than the change on the inner track, using All data and Select data, respectively. Considering that the "rut" occurring on the outer track cannot represent normal road condition, the data should give us an indication that the dynamic loading had no effect on the accumulation of mean surface deformation, contrary to the finding for mean profile change above.

The VSD data also showed that the change in the standard deviation of VSD on the outer track is about 27 percent greater than that on the inner track if using Select data. Since the variation of

Table 7.6. Statistics of pavement elevation (profile, m).

Load Repetition	Track	Data Set	Mean	Minimum	Maximum	std.	V	V_{outer}/V_{inner}
20k	Inner	All Data	50.216	50.208	50.228	0.004	0.00007	
		Select Data	50.215	50.208	50.228	0.004	0.00008	
	Outer	All Data	50.219	50.211	50.229	0.004	0.00009	1.146
		Select Data	50.219	50.211	50.227	0.004	0.00007	0.960
60k	Inner	All Data	50.215	50.208	50.228	0.004	0.00007	
		Select Data	50.215	50.208	50.228	0.004	0.00008	
	Outer	All Data	50.213	50.207	50.220	0.003	0.00006	0.861
		Select Data	50.214	50.208	50.220	0.003	0.00006	0.781
100k	Inner	All Data	50.213	50.206	50.227	0.004	0.00008	
		Select Data	50.213	50.206	50.227	0.004	0.00008	
	Outer	All Data	50.211	50.198	50.218	0.004	0.00008	1.103
		Select Data	50.212	50.206	50.218	0.003	0.00006	0.766
200k	Inner	All Data	50.212	50.205	50.225	0.004	0.00007	
		Select Data	50.212	50.205	50.225	0.004	0.00007	
	Outer	All Data	50.211	50.195	50.219	0.005	0.00010	1.361
		Select Data	50.213	50.207	50.219	0.003	0.00006	0.817
500k	Inner	All Data	50.209	50.202	50.223	0.004	0.00008	
		Select Data	50.209	50.202	50.223	0.004	0.00007	
	Outer	All Data	50.208	50.189	50.217	0.006	0.00011	1.501
		Select Data	50.209	50.202	50.217	0.003	0.00007	0.908
1000k	Inner	All Data	50.208	50.199	50.222	0.004	0.00008	
		Select Data	50.208	50.199	50.222	0.004	0.00008	
	Outer	All Data	50.207	50.187	50.217	0.006	0.00012	1.511
		Select Data	50.208	50.202	50.217	0.003	0.00007	0.863
1500k	Inner	All Data	50.209	50.199	50.223	0.004	0.00008	
		Select Data	50.208	50.199	50.223	0.004	0.00008	
	Outer	All Data	50.205	50.184	50.215	0.006	0.00012	1.518
		Select Data	50.207	50.200	50.215	0.003	0.00007	0.817
1700k	Inner	All Data	50.208	50.223	50.198	0.004	0.00008	
		Select Data	50.208	50.223	50.198	0.004	0.00008	
	Outer	All Data	50.204	50.215	50.181	0.006	0.00012	1.530
		Select Data	50.206	50.215	50.198	0.003	0.00006	0.827

Table 7.7. Statistics of pavement vertical surface deformation (VSD, mm).

Load Repetition	Track	Data Set	Mean	Minimum	Maximum	std.	V	V_{outer}/V_{inner}
20k	Inner	All Data	0.710	-0.7	3.0	0.715	1.006	
		Select Data	0.754	-1.0	3.0	0.736	0.976	
	Outer	All Data	0.750	-0.7	3.0	0.714	0.952	0.946
		Select Data	0.781	-1.0	3.0	0.718	0.920	0.942
60k	Inner	All Data	2.760	1.0	5.0	0.722	0.262	
		Select Data	2.821	1.0	5.0	0.683	0.242	
	Outer	All Data	3.197	1.0	13.1	2.515	0.787	3.007
		Select Data	2.440	1.0	5.0	0.798	0.327	1.350
100k	Inner	All Data	5.078	3.0	7.0	1.129	0.222	
		Select Data	5.196	3.0	7.0	1.072	0.206	
	Outer	All Data	5.748	2.0	22.3	4.188	0.729	3.276
		Select Data	4.473	2.0	7.0	1.220	0.273	1.322
200k	Inner	All Data	6.128	4.0	9.0	1.252	0.204	
		Select Data	6.285	4.0	9.0	1.196	0.190	
	Outer	All Data	7.157	3.0	27.5	5.058	0.707	3.459
		Select Data	5.614	3.0	9.0	1.196	0.213	1.119
500k	Inner	All Data	8.366	5.3	11.7	1.528	0.183	
		Select Data	8.564	5.0	11.7	1.470	0.172	
	Outer	All Data	9.407	4.0	32.0	5.864	0.623	3.413
		Select Data	7.614	4.0	11.2	1.627	0.214	1.245
1000k	Inner	All Data	8.857	5.6	12.8	1.775	0.200	
		Select Data	9.087	6.0	12.8	1.711	0.188	
	Outer	All Data	10.157	4.4	34.0	6.174	0.608	3.034
		Select Data	8.275	4.0	12.7	1.846	0.223	1.185
1500k	Inner	All Data	9.557	5.9	13.4	1.843	0.193	
		Select Data	9.762	6.0	13.4	1.807	0.185	
	Outer	All Data	10.971	5.3	35.8	6.456	0.588	3.052
		Select Data	9.010	5.0	13.6	1.972	0.219	1.183
1700k	Inner	All Data	9.688	6.2	13.7	1.879	0.194	
		Select Data	9.915	7.0	13.7	1.814	0.183	
	Outer	All Data	10.835	4.7	35.9	6.500	0.600	3.093
		Select Data	8.887	5.0	14.0	2.076	0.234	1.277

Table 7.8 Statistics of pavement rut depth (mm).

Load Repetition	Track	Data Set	Mean	Minimum	Maximum	std.	V	V_{outer}/V_{inner}
20k	Inner	All Data	1.428	0.0	4.8	1.139	0.798	
		Select Data	1.385	0.0	4.8	1.102	0.796	
	Outer	All Data	1.433	-0.6	4.5	0.967	0.675	0.846
		Select Data	1.398	-1.0	4.5	0.968	0.692	0.870
60k	Inner	All Data	2.929	1.0	5.7	1.108	0.378	
		Select Data	2.983	1.0	5.7	1.069	0.358	
	Outer	All Data	3.388	1.0	13.8	2.537	0.749	1.980
		Select Data	2.640	1.0	4.6	0.932	0.353	0.985
100k	Inner	All Data	4.993	3.0	7.6	1.211	0.243	
		Select Data	5.110	3.0	7.6	1.169	0.229	
	Outer	All Data	5.966	3.0	23.8	4.243	0.711	2.932
		Select Data	4.662	3.0	7.3	1.081	0.232	1.013
200k	Inner	All Data	5.871	3.0	8.5	1.299	0.221	
		Select Data	6.008	4.0	8.5	1.237	0.206	
	Outer	All Data	7.269	3.1	29.0	5.344	0.735	3.322
		Select Data	5.614	3.0	8.6	1.226	0.218	1.060
500k	Inner	All Data	7.712	4.2	10.8	1.528	0.198	
		Select Data	7.898	5.0	10.8	1.428	0.181	
	Outer	All Data	9.279	3.5	33.2	6.005	0.647	3.266
		Select Data	7.433	4.0	11.3	1.570	0.211	1.169
1000k	Inner	All Data	8.214	4.7	11.7	1.752	0.213	
		Select Data	8.423	5.0	11.7	1.660	0.197	
	Outer	All Data	9.805	3.5	35.2	6.384	0.651	3.053
		Select Data	7.852	4.0	13.2	1.868	0.238	1.208
1500k	Inner	All Data	8.650	5.1	12.6	1.883	0.218	
		Select Data	8.814	5.0	12.6	1.842	0.209	
	Outer	All Data	10.419	3.6	37.1	6.770	0.650	2.985
		Select Data	8.350	4.0	14.2	2.064	0.247	1.183
1700k	Inner	All Data	8.753	5.2	12.4	1.817	0.208	
		Select Data	8.935	6.0	12.4	1.738	0.195	
	Outer	All Data	10.459	3.7	36.9	6.623	0.633	3.050
		Select Data	8.439	4.0	14.0	1.953	0.231	1.190

Table 7.9. Summary of pavement deformation changes (mm).

From Beginning to the End of Test (20k to 1.7 million cycles)	All Data		Select Data	
	Outer Track	Inner Track	Outer Track	Inner Track
Change of Mean Rut Depth	9.0	7.3	7.0	7.6
Change of Mean VSD	10.1	9.0	8.1	9.2
Change of Mean Profile	15.0	8.0	13.0	7.0
Change of STD of Rut Depth	5.7	0.7	1.0	0.6
Change of STD of VSD	5.8	1.2	1.4	1.1
Change of STD of Profile	2.0	0.0	-1.0	0.0

VSD is also a measurement of the fluctuation of the pavement surface, one could infer that the steel suspension caused more roughness to the pavement than the air suspension.

The data in table 7.8 show that the change in mean rut depth, from beginning to end, on the outer track is about 23 percent greater but 8 percent less than the change on the inner track, using All data and Select data, respectively. This should confirm that dynamic loading had no influence on mean rut depth change.

The rut depth data also showed that the change in the standard deviation of rut depth on the outer track is about 67 percent greater than that on the inner track if using Select data. Since the variation of rut depth also reflects the fluctuation of pavement surface, one could infer that the steel suspension caused more roughness to the pavement than the air suspension.

Cross Correlation

Linear and nonlinear cross correlations at different load repetitions among the variables, FWD surface deflection, profile elevation, VSD, rut depth, cracking, and wheel force were calculated in an attempt to determine the degree of correlation among these variables and the possibility of the existence of a relationship among these variables. A more complete picture of the effects of dynamic loading and variability on pavement performance can thus be attained using these techniques. This analysis included:

- Linear cross correlations between initial variability and performance measures.

    1. FWD Surface Deflection and VSD.
    2. FWD Surface Deflection and Rutting.
    3. FWD Surface Deflection and Cracking.

- Linear cross correlations between wheel force and other variables.

   1. Wheel Force and FWD Surface Deflection.
   2. Wheel Force and VSD.
   3. Wheel Force and Surface Cracking.

- Linear cross correlation between cracking and rut depth.

- Linear cross correlation between final (1700k) profile and profiles at other load repetitions.

- Pseudo-nonlinear cross correlations between VSD and other variables.

   1. VSD and Wheel Force* Surface Deflection.
   2. VSD and Wheel Force/Surface Deflection.

- Pseudo-nonlinear cross correlation between wheel force and other variables.

   1. Wheel Force and VSD^m/FWD Surface Deflection.
   2. Wheel Force and VSD/FWD^3.

- Pseudo-nonlinear cross correlation between performance measures and other variables.

Cross correlation between FWD surface deflection at 20k repetitions and VSD (figure 7.20) showed that the VSDs are mainly explained by the FWD deflections at 20k repetitions such that initially weaker pavement portions generate higher VSDs. The poor correlation for the outer track suggests that factors other than pavement variability must play a bigger role in explaining VSD for the outer track.

The higher correlation (see figure 7.21) between cracking and pavement initial structural condition obtained for the outer track (outer coefficient = 0.7) suggests that cracking on the outer track is mainly explained by pavement variability and that the poor correlation on the inner track indicates that other factors, such as shearing stresses, nonlinearity, etc., may have a greater effect on cracking for the inner track.

No significant linear correlation between wheel force and any of the other variables under study was obtained.[11] For instance, the coefficient of correlation between wheel force and VSD at different load repetitions is less than 0.3 (see figure 7.22). However, a somewhat more significant relationship involving wheel force and VSD was found through the following expressions:

$$VSD = c*FWD^{P1}*WF^{P2}$$

which yielded coefficients of correlation of 0.54 for the inner track (with P1 = 1.005 and P2 = 0.225) and 0.759 for the outer track (with P1 = 3.222 and P2 = 1.781).
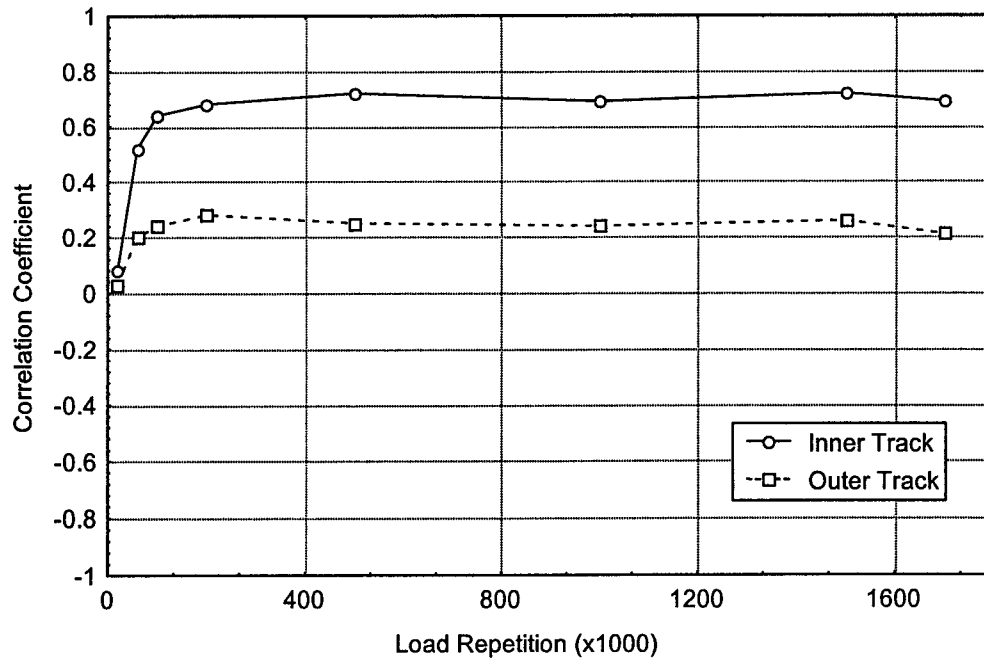
Figure 7.20. Cross correlation between FWD surface deflection at 20k and VSD.
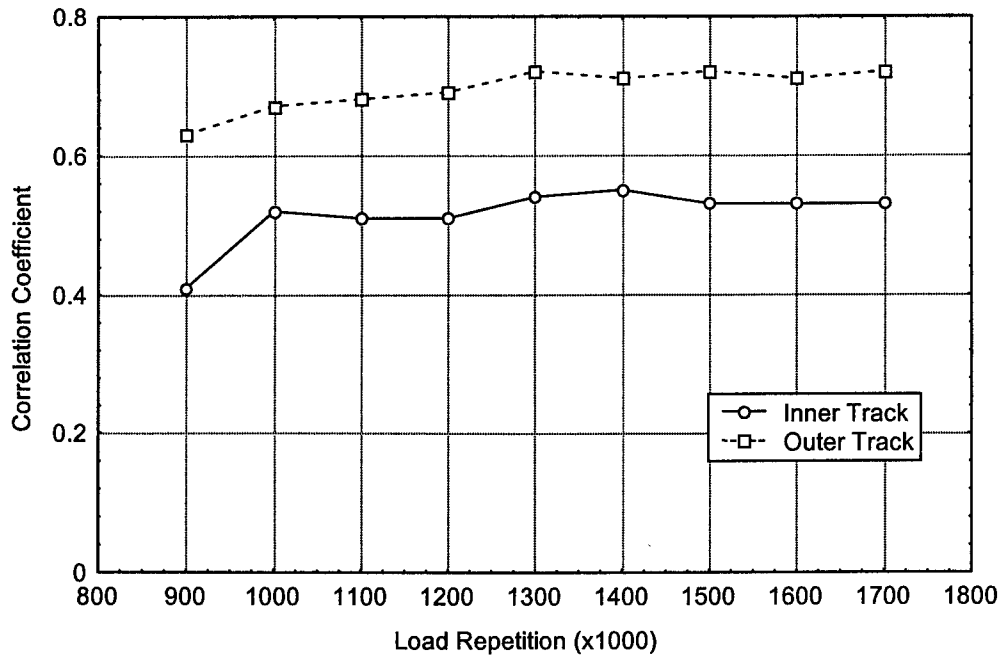

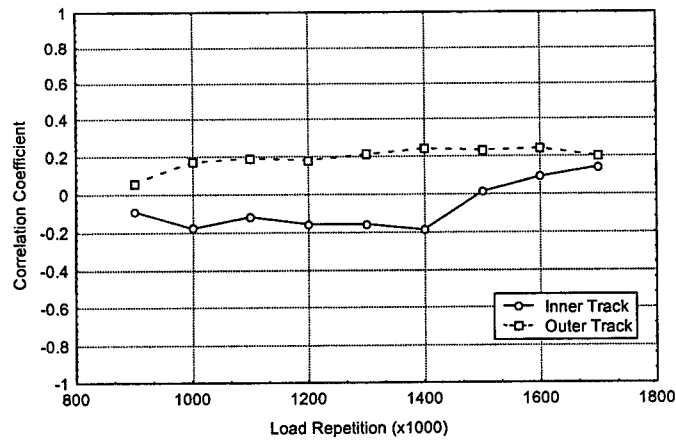**Figure 7.21. Correlation between FWD deflection at 20k and total linear cracking.**

Figure 7.22. Cross correlation between wheel force and VSD.
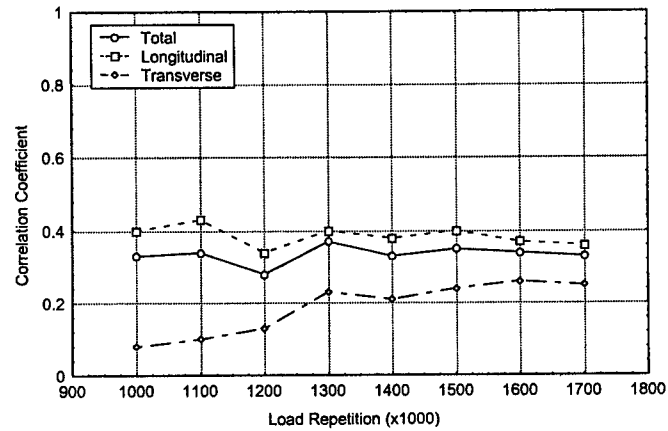

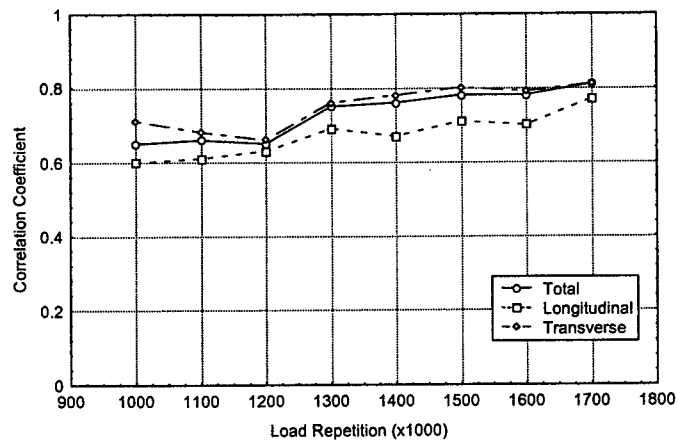**Figure 7.23a. Cross correlation between rut depth and surface cracking, inner track.**

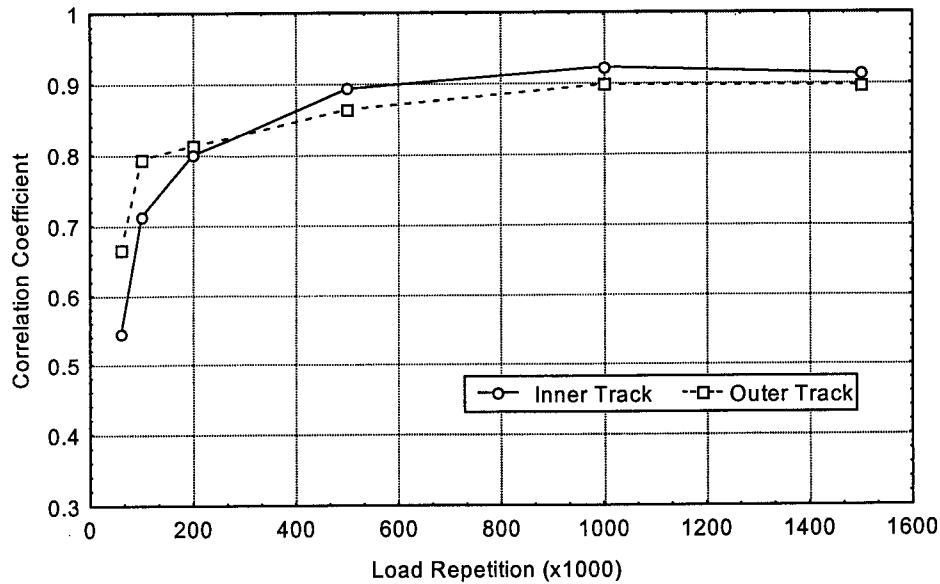**Figure 7.23b. Cross correlation between rut depth and surface cracking, outer track.**

82

Figure 7.24. Correlation between profile at 1700k and profiles at other load repetitions.

Likewise, for profile, the expression:

$$Profile = b*FWD^{P1} + a*WF^{P2} + c*FWD^{P1}*WF^{P2}$$

yielded coefficients of correlation of 0.639 for the inner track (with P1 = 0.502 and P2 = 1.079) and 0.667 for the outer track (with P1 = 0.011 and P2 = 2.967).

Linear cross-correlation analysis between surface cracking and rut depth yielded coefficients of correlation of about 0.8 for the outer and about 0.4 for the inner tracks (see figures 7.23a and 7.23b). The moderate correlation for the outer track indicates that more cracking damage is associated with the location where rutting is more severe.

A high coefficient of correlation (e.g., 0.9, see figure 7.24) between road profiles at higher load cycles (500k+), and a low coefficient of correlation between initial and final profiles indicate that initial road profile had little influence on profile changes.

It is felt that using VSD in pavement permanent deformation analysis (not necessarily rutting damage) may be more proper than using profile and rut depth on the basis of the following arguments:

- The VSD data determined from CAPTIF test were based on measured vertical deformation on each station along the transverse section. The method used in this measurement avoided accumulated elevation error, as the Dipstick method does when measuring profile during the test.

- VSD is the pure elevation change at a given point on the pavement surface during certain load repetitions; therefore, it directly relates to the pavement stiffness and the load

83

applied, while the rut depth is actually determined by surface vertical deformation at a given point and surface deformation around that point.

CHAPTER 8. SUMMARY AND CONCLUSIONS

The DIVINE Element 1 project investigated the effects of two different suspensions, an air and a steel suspension, on the performance of a full-scale flexible pavement with focus on:

- Change in layer thickness and material properties subjected to accelerated loading.
- Primary pavement response.
- Rates of damage progression subjected to accelerated loadings.
- Effect of initial pavement structural variability and dynamic loading on pavement performance.

The results showed that:

1. The high negative correlation between the constructed thickness of the AC layer and base layer of the pavement is probably because of the intent to make the pavement surface flat and smooth.

2. Based on FWD surface deflections at construction, there was little difference in the structural integrity for both wheelpaths; however, an increase in the FWD surface deflections around station 21 (between stations 18 and 24) on the outer track just prior to trafficking at 20k repetitions is an indication that the pavement had weakened in that area:

    - A rut was generated on the outer track (steel suspension) between stations 18 and 24 during the initial stages of trafficking. Because of the high FWD deflections at 20k load cycles, the rut in that area is believed to be due to dynamic loading and to the fact that the pavement weakened in that area.

    - Because of the occurrence of the rut between stations 18 and 24, two sets of data—Select data (data set not containing the rut) and All data (data set containing the rut)—were used in the analysis. In most cases, Select data were used for the outside track analyses whereas for the inner track both All data and Select data were used since the inner track contained no obvious localized weakened area.

3. The pavement materials appear to have changed only slightly over the life of the pavement:

    - The modulus of the asphalt concrete has increased somewhat.

    - The rut that occurred around station 21 is attributed to both dynamic loading and consolidation of the base course layer, and it was the base course layer that experienced the greatest consolidation overall. There was no significant difference in the before and after gradation tests. The high levels of rutting in the outer wheelpath around station 21 were not caused by excessive moisture in the base course.

- The subgrade failed to show any significant signs of rutting (except the region around station 21 on the outer track) and the subgrade properties remained constant throughout the project.

- Densification of the asphalt concrete and basecourse layers is mainly responsible for observed surface rutting overall.

4.   The cross-correlation analysis conducted for primary responses showed that there were some good correlations for vertical layer deformation, dynamic loading, and initial primary responses in the pavement and subgrade for the inner wheelpath.

5.   The outer wheelpath was subjected to significantly greater dynamic load and had larger increase in roughness than the inner. This is the case even after the rut stabilized.

Various statistic measures of the track profiles with load repetitions were used to assess profile unevenness (roughness). In general those based on the PSD of the profiles provided the most insight, though the wheel force response of the test vehicles was also a useful indicator. However, the measure of the IRI is questionable (use of the word "profile" in this report implies that it was calculated directly from Dipstick measurement).

Spectral analysis of the profile changes showed a match between the wavelengths of the changes and the natural frequencies of the vehicle suspensions, particularly on the outer wheelpath. This indicates that dynamic wheel forces do contribute to profile changes.

The IRI was shown to have some limitations as a measure of roughness in the CAPTIF environment where the track length is relatively short and vehicle speeds are significantly lower than the IRI standard speed of 80 km/h.

At the end of testing, no measurable difference in the variation of the profile elevations between the two tracks was detected. Again, the errors associated with measurement taken using the Dipstick are deemed responsible for the lack of roughness difference between the two tracks.

6.   The change in mean VSD and mean rut depth on both tracks was similar with use of Select data, confirming theoretical assumptions that dynamic loading had no effect on the accumulation of mean surface deformation. (Similar conclusions could not be drawn from profile measurements that used the Dipstick. There is little chance of any induced error associated with VSD and rut depth measurements, whereas it is most likely that error was induced using the Dipstick technique.)

7.   Comparison of pavement surface roughness change of the two tracks.

Since variation is a measurement of how values of a variable fluctuate around its mean, the variations of VSD, rut depth, and profile are an indication of how the surface

86

elevation fluctuates around their means along the pavement. This fluctuation can also be seen as an indicator of road roughness. Based on this argument, the authors observed that:

- At the end of testing, the coefficient of variation of VSD on the outer track was about 28 percent greater than that on the inner track if using Select data for both tracks. Because the coefficient of variation of the FWD deflections (representing pavement variability) on the outer track is 4 percent greater than that on the inner track, it can be inferred that the steel suspension could be responsible for 24 percent (28 percent - 4.0 percent) more roughness damage on the outer track.

  Note: Subtracting coefficient of variation of FWD deflection from the coefficient of variation of VSD is based on the following arguments: (a) The cross-correlation analysis showed that the VSD is closely correlated with the FWD deflection; (b) Coefficient of correlation is unitless, and it presents the degree of variation of a variable relative to its mean; (c) Considering (a) and (b), the subtraction, the authors believe, can separate the effect of initial structural variation from the VSD performance, allowing a better comparison.

- At the end of testing, the coefficient of variation of rut depth on the outer track was 19 percent greater than that on the inner track if using Select data for both tracks. It could be inferred that the steel suspension was responsible for 15 percent (19 percent - 4 percent) more surface roughness damage on the outer track based on rut depth measurements.

  Note: The same argument presented in the note directly above applies here also.

8. Based on cross-correlation analysis, the initial profile had little influence on the final profile in the two different tracks regardless of the type of suspension.

9. Linear and nonlinear relationships (cross correlations) at different load repetitions among the variables, FWD surface deflection, profile elevation, VSD, rut depth, cracking, and wheel force were determined:

- The coefficient of correlation between VSD and FWD surface deflection for the inner track is about 0.75 and for the outer track is about 0.30. The stronger correlation on the inner track indicates that pavement variability played a more dominant role in explaining the occurrence of VSD on the inner track. The poorer correlation on the outer track indicates that factors other than pavement variability, such as load, played a bigger role in explaining VSD on the outer track.

- The coefficients of correlation between rut depth and FWD surface deflection for both tracks are similar at around 0.6.

- The coefficient of correlation between wheel force and VSD normalized by FWD surface deflection for the inner track is about -0.2 and for the outer track is about

0.4. The stronger correlation for the outer track indicates that wheel force plays a stronger role in explaining VSD on the outer track.

Note: In reference 11, the authors suggested an interpretation that 40 percent of the VSD could be considered attributable to the dynamic wheel force generated by the steel suspension and that the dynamic wheel force generated by the air suspension had little influence on VSD. Although this assumption, especially the quantity, may not necessary be justified, if we consider that the coefficient of correlation is the measurement of linear relationship between two variables, and the squared coefficient of correlation can be viewed as the R^2 value in a linear regression model relating the dependent variable to an independent variable, then, a higher coefficient of correlation indicates that there is more possibility that the change of one variable will cause the other variable to change accordingly, or that one variable has a stronger influence on the other variable.

- The coefficient of correlation between wheel force and the cubic root of VSD normalized by FWD is about 0.1 for inner track and 0.5 for outer track. The stronger correlation for the outer track indicates that wheel force plays a stronger role in explaining VSD on the outer track.

Note: Based on the same argument presented in the note directly above, in reference 11, the authors suggested an interpretation that 50 percent of the powered VSD is attributed to the steel suspension-induced dynamic wheel force and that the air suspension-induced dynamic force had very little or no influence on VSD.

- The coefficient of correlation between wheel force and VSD normalized by FWD to the power of 3 showed similar results as above—about 0.6 for the steel suspension and 0.2 for the air suspension.

Note: Based on the same argument presented in the note directly above, in reference 11, the authors suggested an interpretation that about 60 percent of the VSD on the outer track can be explained by the steel suspension-induced dynamic wheel force and that the dynamic wheel force induced by air suspension has little or no influence on VSD.

- Other nonlinear correlation analyses among the variables, profile, VSD, wheel force, and surface deflection were also conducted; however, lower coefficients of correlation were obtained.

10. The cracks that occurred in the asphaltic concrete mostly originated from the surface and were not full-depth cracks. The cracks that did occur also provided a indicator as to the difference in performance of the two suspension types:

- Cracking in the outer wheelpath (steel suspension) was 36 percent greater than that in the inner wheelpath (air suspension). The cracking here is the total measured length of cracks around the track.

- Cracking was more localized in the outer wheelpath, with more than twice as many stations reaching the cracking failure criterion.

- Cracking in the outer wheelpath was strongly related to profile changes and to rut depth, while the relationships in the inner wheelpath were much weaker.

- If using Select data, the differences in cracking performance between the two tracks is insignificant.

11. Cross correlation between surface cracking and rutting yielded coefficients of correlation of 0.8 for the outer and 0.4 for the inner track. Given that the mean rut depths of the two tracks are similar, the greater variation of rut depth on the outer track indicates the existence of more locations with more rutting around the track; the higher correlation between cracking and rutting for the outer track indicates that surface cracking started when rutting reached a certain level of severity. Therefore, it may be concluded that the steel suspension-induced wheel force caused more localized rutting damage and more localized cracking.

APPENDIX A. SCRUBBING EFFECT ON CIRCULAR TRACK
(Contributed by David Cebon)

Figure A.1 shows a schematic view of the CAPTIF experiment. The wheel is of radius r and rolls around the center of the facility on the arm of radius R. The forward speed of the wheel is V. As a consequence, the angular velocity of the arm relative to the ground is $\Omega = V/R$, and the angular velocity of the wheel relative to the arm is $\omega = V/r$.

Angular velocities are vector quantities that can be added vectorially like linear velocities. Thus, the total angular velocity is the vector sum of Ω and ω. The vector construction is shown in figure A.2. Using Pythagoras, the total angular velocity of the wheel Ω_{tot} is:

$$\Omega_{tot} = (\omega^2 + \Omega^2)^{\frac{1}{2}} \tag{A.1}$$

The total angular vector is inclined to the horizontal (contact plane), at an angle of:

$$\gamma = \tan^{-1}(\Omega/\omega) = \tan^{-1}(r/R) \tag{A.2}$$

For the CAPTIF experiment,

$r \approx 0.5$ m, $R_{inner} = 8.8$ m, $R_{outer} = 9.6$ m, $r/R_{inner} \approx 0.057$ m with $\gamma_{inner} \approx 3.3°$, and

$r/R_{outer} \approx 0.052$ m with $\gamma_{outer} \approx 3.0°$.

The effect of inclining the angular velocity vector to the horizontal is exactly the same as inclining the axle to the horizontal (i.e., setting a camber angle) for a wheel in a straight-line motion. It generates a *camber thrust*—a side force—due to "spin creep" (i.e., due to the "spin" component of the angular velocity about the tire/road contact patch—Ω). (See [17] for further information.) The magnitude of the camber thrust is:

$$F\gamma = C_\gamma\gamma \tag{A.3}$$

where $C\gamma$ is a property of the tire that depends on the tire structure, inflation pressure, tread pattern, etc., but not speed.

For a wide single truck tire, $C\gamma$ might be expected to be about 1 kN/deg, so using equations A.2 and A.3, the steady-state radial forces between the two SLAVE types and the road surface would be on the order of (rough estimates - within a factor of 2):

$F_{inner} \approx 3.3$ kN (740 lbf) $F_{outer} \approx 3.0$ kN (670 lbf)
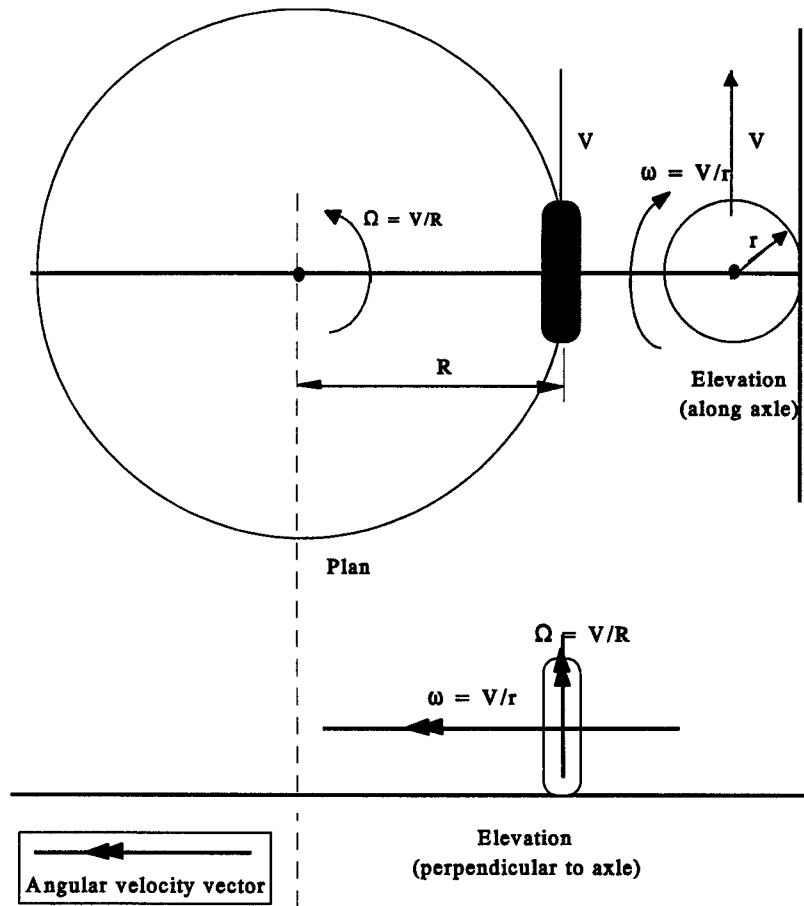
Figure A.1. Schematic of angular velocity, CAPTIF experiment.
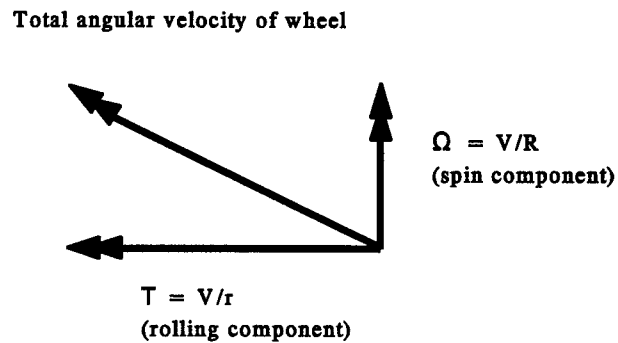

Figure A.2. Angular velocity components.

These radial "scrubbing" forces were applied to the road surface (in the outward direction) by the tires, continuously throughout the experiment. Since the fatigue properties of asphalt are very

92

sensitive to stress level, the experiment result will be affected because the scrubbing force: (1) would change the stress state in the pavement surface; (2) would act as initiation sites for secondary, circumferential, and radial cracks; and (3) would decrease the stiffness (load-carrying capacity) of the asphalt layer, which would accelerate the formation of ruts in the granular layers.

A solution to this problem is to align the total angular velocity vector to be parallel with the contact plane (road surface). This can be achieved either by cambering the wheel *inward* by angle γ or by cambering the track *outward* by angle γ. (The camber angle on the inner wheel track should, therefore, be greater than the camber angle on the outer wheel track.)

APPENDIX B. FOOTPRINT EFFECT ON PROPORTIONALITY

Certain of the results of the Element 2 tests on pavement primary response are pertinent to this discussion and, therefore, those aspects of the Element 2 research are summarized herein. In the Element 2 tests it was demonstrated[16] that after viscoelastic effects of the pavement are minimized (vehicle speeds above 25 km/h), the thicker pavements tested in both the United States and Finland behaved in a linear elastic manner. In other words, the strains measured at the bottom of the AC layer (FHWA and VTT [Technical Research Centre of Finland]) and at the top of the AC layer (FHWA) were generally in close proportion to the applied dynamic load.

In reference 16, the abbreviation DSC (dynamic strain coefficient) is introduced to represent the coefficient of variation of the elastic dynamic strain data that occurred at a point in the pavement as a dynamic load moved along the surface of the pavement (the load is moving sufficiently fast to have minimized viscoelastic pavement effects). The ratio of DSC/DLC, where DLC is the dynamic load coefficient of the dynamic load data, is then introduced in order to obtain a mathematical measure of the degree of linear elastic behavior of the pavement under dynamic loading. Linear elasticity is defined classically to mean that the dynamic stress is proportional to the dynamic strain. The report further defines a DSC/DLC ratio of 1.00 to reflect a completely proportional linear elastic relationship so that for any given percent increase in dynamic load, there is an identical percent increase in dynamic strain. A value greater or smaller than 1.00 is deviation from linear elasticity. For instance, if the pavement is in the viscoelastic state because loading is applied very slowly (slow speed) or if pavement temperature is high, or both occur, then the DSC/DLC ratio would be much higher than 1.00. This was the case for the FHWA Element 2 tests at speeds below 25 km/h. On the other hand a ratio less than 1.00 would imply deviation from linear elasticity in terms of a nonlinear concave downward strain-load plot (concave upward load-strain plot).

For the FHWA Element 2 tests, the DSC/DLC ratios were calculated for the 152-mm-thick pavement for all vehicle speeds. The thickness of 152 mm is considered as a thick pavement in a comparative sense with the 88-mm-thick AC layer at CAPTIF. A bump of about 3 m in length (long bump) was used to induce vehicle dynamics so as to exaggerate dynamic wheel loadings. The DSC/DLC ratios calculated for both top-side and bottom-side AC layer strain ranged between 1.00 and 1.23 for all speeds above 25 km/h. At slower speeds, of course, viscoelastic effects dominated, causing these ratios to be much higher.

An average DSC/DLC ratio for bottom-side AC layer strain was also calculated by the authors for use in this report for the 150-mm-thick AC Element 2 tests conducted in Finland that used a similar bump and 45-km/h test speeds. The ratio estimated from the Finnish data (18) was about 0.80. Finnish tests using a shorter bump were estimated to be around 1.27 (quite in line with the FHWA values).

Quite contrary to the above findings, however, are the Finnish results at 45 km/h for an 80-mm-thick AC-layered pavement (thin pavement). For this pavement the range in ratios was estimated by the authors from the Finnish bottom-side AC strain data for this report as being between 0.20 and 0.22. There is considerable speculation as to why the strains did not respond to the dynamic loading for the thinner pavement. It has been reasoned that error existed in strain gauge calibrations, or that there was inaccurate tracking of the wheels over the gauges rather than

nonlinearity, or that some of this discrepancy could be due to the phenomena of the footprint effect on proportionality described below.

To investigate the Finish findings for the thin pavement on a more theoretical basis, the VESYS computer program was called on to simulate pavement strain response to pavements of varying AC layer thickness when they are subjected to both a low load and a high load wherein the tire-pavement footprint is increased for the larger load, thus reducing the strains occurring in the pavement. The premise here is that for thick AC-layered pavements, the reduction in strain on the bottom of the pavement because of increased footprint area will be much less than the reduction in strain that would have occurred at the underside of a thinner pavement because of increased footprint area.

The curves in figure B.1 illustrate the change of contact area with load for a wide-base single and dual tire set. The load-area data presented here were collected at the University of Michigan Transportation Research Institute (UMTRI) and FHWA for the wide-base single and dual tires, respectively. The single diamond represents the contact patch measured for the CAPTIF wide-base single tire at the test load and is seen to be quite in line with the UMTRI curve.

For the VESYS runs, a pavement was selected that had the same elastic moduli material properties as those calculated for the CAPTIF pavement layers:[11] 1034 MPa (150,000 psi) for the AC layer, 227.6 MPa (33,000 psi) for the aggregate base layer, and 103 MPa (15,000 psi) for
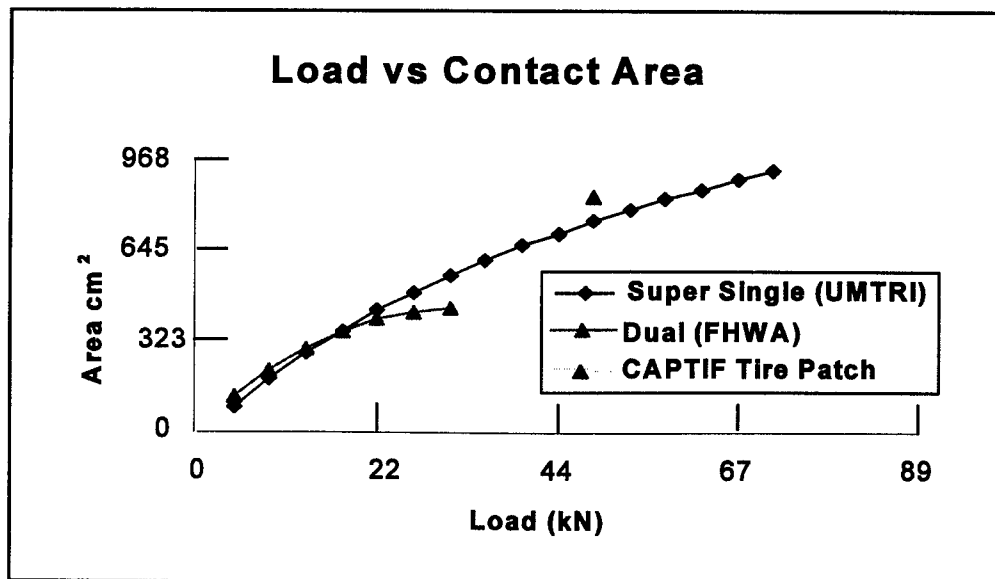

Figure B.1. Tire load vs. contact area.

the subgrade. AC layer thicknesses used were 80, 102, 152, and 203 mm (3.14, 4, 6, and 8 in). The 80-mm AC thickness would present thin pavements similar to those at Finland and CAPTIF, and the 152-mm-thick pavement would be representative of the pavements for the U.S. DIVINE Element 2 study and for the thick Finnish DIVINE Element 2 study. The contact area load curves previously mentioned in figure B.1 were then used to determine the input radii and pressures

96

representing three load levels: 35.6 kN (8 kips), 42.7 kN (9 kips), and 71.1 kN (16 kips), corresponding to loading pressures of 620 kPa, 660 kPa, and 1100 kPa, respectively.

Table B.1 and figure B.2 summarize the results obtained from the VESYS simulation in terms of normalized ratios. In table B.1, the R_{Strain} is the ratio of pavement strain response under given load to strain response under a load of 35.6 kN (8 kips); and R_{Load} is the ratio of given load to load of 35.6 kN. One can refer the ratio of R_{Strain} / R_{Load} to the measured dynamic DSC/DLC ratios, as discussed in reference 16.

The results show that for dual tires, the ratios of R_{Strain} / R_{Load} for thin pavement are higher than those reported from Finnish tests, while the ratios for thick pavement appear to be more in line with those measured in Finland and the United States.

It also shows that the effect of nonlinearity is greater for wide-base single tires than that for dual tires because of the larger contact area. This does not mean, however, that strains are smaller for thin pavements, it only suggests that the rate of change of strain is reduced compared with the change of dynamic loading. This reduction takes place at a much higher level of strain in thin pavement than what would have taken place in a thicker pavement.

Table B.1. Ratio of strain change to load change for wide-base single and dual tires.

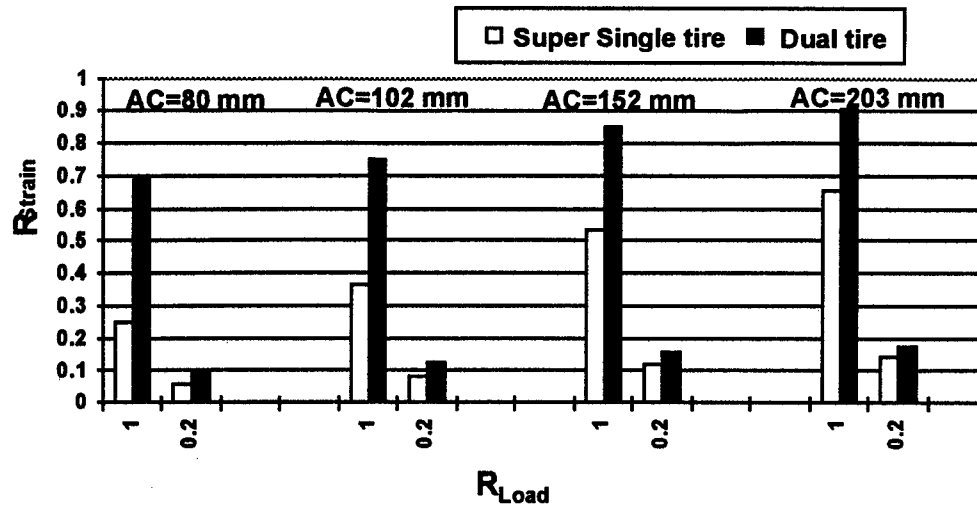| AC Layer (mm)	Load Pressure (kPa)	R_{Strain} / R_{Load}	
		Single	Dual
80	660 (R_{Load}= 0.2)	0.30	0.51
	1100 (R_{Load}= 1.0)	0.25	0.68
102	660	0.42	0.62
	1100	0.36	0.75
152	660	0.59	0.85
	1100	0.53	0.78
203	660	0.71	0.86
	1100	0.65	0.91

Figure B.2. R_{Strain} vs. R_{Load} for wide-base single and dual tires.

APPENDIX C. ORIGINAL ELEMENT 1 DATA ANALYSIS TASKS

The seven initial analysis tasks were: data verification/validation, analysis of structural variability, analysis of road roughness, analysis of dynamic wheel force, analysis of pavement cracking, analysis of rut depth, and analysis of pavement primary response. During the course of the experiment, analyses of scrubbing and tire footprint effects were also included. The analysis of rut depth was incorporated with the pavement primary response and variability analyses. The reader should refer to the individual reports by the authors listed in the references. A brief description of the original tasks is given below:

Pavement Primary Response

Establish relationships or develop cross correlations between initial primary response existing in the pavement at the gauged locations and the dynamic load, rut depth, and cracking of the pavement produced during the tests. Typical primary response parameters include longitudinal and transverse tensile strains at the bottom of the AC layer, and vertical compressive strain at the top of each layer.

Dynamic Wheel Force

Analyze dynamic wheel force and the change in dynamic wheel force as load repetitions are applied. Establish whether or not a "feedback" relationship exists between change in dynamic wheel force and growth of roughness. For example, do the wheel forces increase (frequencies increase or decrease) as roughness increases and vice versa? Are they applied in a spatially repeatable pattern or they are applied randomly? The analyses should consider different representations of dynamic loads such as spatial trace, peak loads, frequency distribution of loads, DLC, RMS, and PSD.

Road Roughness

Analyze wheel track profile and the change in profile as load repetitions are applied. This change in profile should be correlated to selected variables such as dynamic wheel force, rut depth, etc. The analysis should consider all possible indicators of profile such as spatial elevation, slope variance, IRI, frequency domain RMS, PSI, slope PSD, and amplitude PSD. Draw conclusions on: (1) the most meaningful representation of roughness and (2) the parameters controlling roughness growth.

Pavement Cracking

Examine the progress of pavement area and/or lineal surface cracking (longitudinal and transverse) globally, then analyze subsections around the track separately. The subsections should be of sufficient length to encompass a "complete definition" of cracking and of the existing modes of dynamic loading. Determine the distribution of cracking, e.g., is the cracking distributed spatially (is the load distributed spatially) or is the cracking distributed randomly (cracking does not follow the load)? The subsection analyses should examine the causative nature of the cracking, e.g., identify cracking solely due to dynamic loading (assuming that the pavement has zero structural variability,

or homogeneous pavement) as opposed to cracking due to a nondynamic moving load (constant moving load) given the current state of structural variability.

Analysis of Structural Variability

Determine the extent of the structural variability of the pavement in terms of the variability of the initial stiffness and constructional uniformness of the pavement. Consideration should also be given to variations in pavement layer thicknesses, modulus, and moisture contents. The cross-correlation analysis between pavement initial stiffness and pavement profile, vertical permanent deformation, rut depth, and cracking will give measurement of the influence of the structural variability on pavement performance. The results of the analysis will be used to establish correction factors for structural variability.

REFERENCES

1. Steven, B.D.; Fussell, A.W.; and Pidwerbesky, B.D. (1996). *DIVINE Element 1 Construction Report*. Civil Engineering Research Report CERR96-8, University of Canterbury, Christchurch, New Zealand.

2. Steven, B.D.; Fussell, A.W.; and Pidwerbesky, B.D. (1996). *DIVINE Element 1 Pavement Post-Mortem Report*. Civil Engineering Research Report CERR96-9, University of Canterbury, Christchurch, New Zealand.

3. Sharp, K.G. and Moffatt, M.A. (1996). *Analysis of Performance Data Collected During Trafficking of Test Pavement by CAPTIF: Element 1 of OECD IR6 Project*. ARRB Transport Research Contract Report CR RI905/3, Melbourne, Australia. April 1996.

4. Sharp, K.G. (1996). *Resilient Modulus and Dynamic Creep Testing of Asphalt*. CR R1905/1; ARRB Transport Research Limited. Melbourne, Australia.

5. Sharp, K.; Jameson, G.; and Yeo, R. (1996). *Analysis of FWD Data Collected on All Layers at Construction*. CR R1905/2; ARRB Transport Research Limited. Melbourne, Australia.

6. Fussell, A.; Steven, B.; and Pidwerbesky, B. (1996). *OECD DIVINE Element 1: Loading Report*; Civil Engineering Research Report CERR96-5. University of Canterbury. Christchurch, New Zealand.

7. De Pont, J. (1994). *Report on Zero Measurements for DIVINE Element 1: Accelerated Pavement Testing*. Industrial Research Ltd. Auckland, New Zealand.

8. De Pont, J. (1997). *OECD DIVINE Project - Element 1. Longitudinal Pavement Profiles*, ISBN 0-473-04475-7, Industrial Research Ltd. Auckland, New Zealand.

9. Devine, J. and Pidwerbesky, B. (1995). *Resilient Modulus and Rutting Tests on Pavement and Subgrade Materials: DIVINE Element 1*. University of Canterbury. Christchurch, New Zealand.

10. Pidwerbesky, B. (1996). *DIVINE Element 1 Analysis Plan Task 7 - Correlations With Pavement Primary Response*. Civil Engineering Research Report CERR96-7, University of Canterbury. Christchurch, New Zealand.

11. Kenis, W. and Wang, W. (1997). *Analysis of Pavement Structural Variability*. Report No. FHWA-RD-97-072, Federal Highway Administration. Washington, DC.

12. OECD Road Transport Research Programme (1992). *Dynamic Loading of Pavements*. Report prepared by OECD Scientific Expert Group IR2. OECD, Paris.

13.   Steven, B. and Pidwerbesky, B. (1996). *DIVINE Element 1 Analysis Plan Task 5 - Correlations With Pavement Cracking*. Civil Engineering Research Report CERR96-6. University of Canterbury. Christchurch, New Zealand.

14.   Standards Australia (1994). *Determination of the Resilient Modulus of Asphalt*. Draft AS2891.13.1, Version 6. June.

15.   Standards Australia (1994). *Determination of the Accumulated Compressive Strain Characteristics of Asphalt by the Dynamic Creep Test*. Draft AS2891.12.1, April.

16.   Kenis, W.; George, D.; and Hammouda, J. (1997). *Pavement Primary Response to Dynamic Loading*. Report No. FHWA-RD-97-073, Federal Highway Administration. Washington, DC.

17.   Johnson, K.L. (1986). *Contact Mechanics*. Cambridge University Press.

18.   Huhtala, M.; Pihlajamaki, J.; and Halonen, P. (1997). *Pavement Response Due to Dynamic Loads*. Technical Research Centre of Finland, Espoo.